5-2023

On the Micro-Mechanical Property Characterization and Bulk-Volume Behavior Prediction of Additively Manufactured 17-4 PH Stainless Steels

David González-Niño
University of Arkansas-Fayetteville

On the Micro-Mechanical Property Characterization and Bulk-Volume Behavior Prediction of Additively Manufactured 17-4 PH Stainless Steels

A dissertation submitted in partial fulfillment
of the requirements for the degree of
Doctor of Philosophy in Engineering

by

David González-Niño
University of Puerto Rico at Mayagüez
Bachelor of Science in Mechanical Engineering, 2013
University of Puerto Rico at Mayagüez
Master of Science in Mechanical Engineering, 2017

May 2023
University of Arkansas

This dissertation is approved for recommendation to the Graduate Council.

_____
Gary Prinz, Ph.D.
Dissertation Chair

_____
Cameron Murray, Ph.D.
Committee Member

_____
Micah Hale, Ph.D.
Committee Member

_____
Robert D. Moser Ph.D.
Committee Member

_____
Pedro Quintero, Ph.D
Committee Member

Abstract

Selective laser melting is an additive manufacturing technology that opens the possibility to manufacture components with complex geometries that are difficult with traditional manufacturing techniques which could benefit engineering applications such as aviation or structural engineering. However, the lack of a reliable universal predictive model for selective laser melting components could impede the full implementation in industrial applications. Therefore, this dissertation investigates the mechanical behavior of selective laser melting 17-4 PH stainless steel under ultra-low cycle fatigue regime and propose a novel micro-mechanical based modeling using statistical and representative volume element.

The first phase of this project examined the mechanical behavior of selective laser melting 17-4 PH stainless steel at macro-scale by tensile test and ultra-low cycle fatigue testing ($\Delta\varepsilon/2$ = 2%, 3% and 4%), and were compared to its wrought counterpart. Results showed that selective laser melting components underperform by 62% and 65%, compared to its wrought counterpart, when subjected to cyclic load with amplitudes of ($\Delta\varepsilon/2$ = 3% and 4%) respectively. Further examination in the fracture surface revealed the presence of voids within selective laser melting samples. This shows the detrimental effect that fabrication induced defects have over the fatigue life in selective laser melting. Also, Coffin-mason universal slope over predicts the performance of additively manufactured steel by 119% and 213% on strain amplitudes of 3% and 4%. Thus, a predictive model based on micro-mechanical testing is studied.

The second part of this project describes a methodology to improve the micro-tensile sample fabrication throughput. This methodology consists in the pre-fabrication of micro-columns by photolithography and wet-etching. During wet-etching, excess of bulk material is removed, reducing the material re-deposition during the focused ion beam milling and easing the

maneuverability of the grip by fabricating samples above bulk surface. Possible challenges during testing were commented on along recommendation on how to perform micro-tensile tests.

Once the methodology was developed, selective laser melting 17-4 PH stainless steel was characterized via small scale mechanical testing such as nanoindentation, micro-compression and micro-tensile. An elastic modulus of 187.6 GPa was measured using nanoindendation with a Berkovich indenter. From the micro-compression, a yield stress of 759 MPa ± 207 MPa was measured. Also, a strain-hardening behavior was seen. An increase of 47% in the yield stress (1115 MPa) in micro-tensile test was seen, when compared to micro-compression. When micro- and macro- tensile test are compared, micro-tensile specimen shows an ultimate tensile strength of 1359 MPa, ~21% higher than the bulk specimen (1115 MPa). Also, the pronounced strain hardening behavior in macro-specimen was not shown during micro-specimen, suggesting different failure mechanisms.

Lastly, this project proposes a framework for a predictive model based on micro-mechanical testing using statistical and representative volume elements. For this, a methodology was suggested, using representative volume element, to up-scale micro-mechanical properties. Then, using statistical volume elements, the effects of voids were studied. Although the model predicts mechanical behavior with low accuracy, suggestions as performing mechanical testing at the meso-scale and combining characterization techniques with micro-mechanical testing were done.

Acknowledgements

I would like to thank my advisor, Dr. Prinz, for his support and mentorship during this process. I am also grateful for the advice and support provided by the committee members Dr. Murray, Dr. Hale, Dr. Moser and Dr. Quintero.

Also, I would like to express my greatest thanks to my family and friends for their incredible support. To my partner, María España, who has been very supportive and always finds the words of encouragement that I need.

Big thanks to all my colleagues, Fernando Benitez, Jose Transito, Charissa Puttbach, Callie Clark, Hossein Kashefizadeh, Paul Chabaud, Gavin Briggs, Lane Edwards, Adam Kirchner, Rilye Dillard, and Elizabeth Poblete. Also, I would like show appreciation to my colleagues from Dr. Zou's lab, Mahyar Afshar Mohajer and Julia Hoskins for their incredible help in the lab.

Finally, I would like to acknowledge the Counseling & Psychological Services (CAPS) of University of Arkansas, who were really helpful during this stressful time.

Table of Contents

List of Figures

List of Tables

List of Published Papers

Chapter 1: Introduction and Study Motivation

1.1 Motivation for the Proposed Study

Many structural systems rely on inelastic material behavior to dissipate energy under extreme loads (i.e. building seismic force resisting systems, impact components in vehicles, blast energy absorption devices, etc.). Due to the economics and limitations associated with conventional manufacturing technologies, performance optimization of these components is often limited. Additionally, such components are often limited by ultra low-cycle fatigue (ULCF) induced fractures, resulting from large repeated inelastic demands. To optimize performance, complex geometry fabrication technologies and improved material behavior understanding (ULCF control) is needed. Figure 1 shows two recent attempts at seismic ductile fuse improvement using material casting fabrication methods [1,2]; however, it is important to note that geometry control, and therefore optimization, is still limited in such applications.

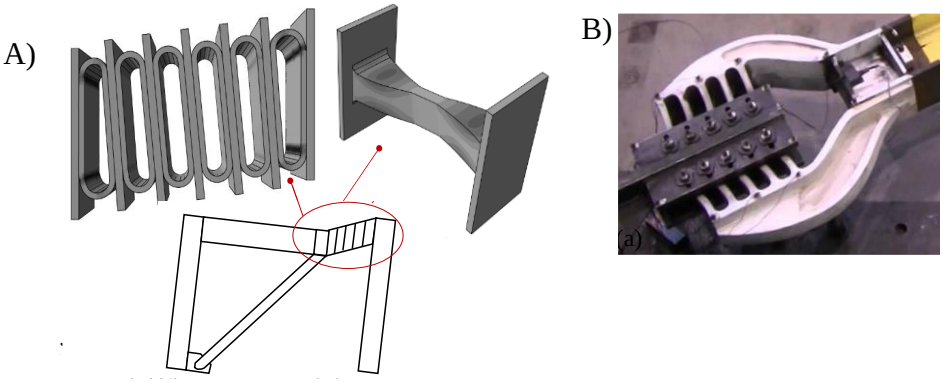

Figure 1: Examples of recent effort of fabricating dissipating seismic force using cast components. A) Designs of replaceable EBF link [1] and B) Castconnex scorpion yielding brace connection [2].

Additive manufacturing (AM) technologies (such as selective laser melting or SLM) are promising for component optimization as they can accommodate highly irregular designs through highly controlled geometry creation not practically achieved using traditional manufacturing techniques. As the name suggests, the SLM fabrication process forms three-dimensional material geometries by melting sequential layers of metal powder using localized heat from lasers. Tradeoffs exist however, as the layer-by-layer SLM fabrication process can result in a heterogeneous material microstructure as well as volume-dependent interior void defects (see Figure 2). As such, characterization and ductile fracture prediction models for SLM materials may differ from those used in traditional wrought materials. The research discussed herein aims to understand the inelastic micro-mechanical fracture processes in SLM metals and develop scalable material characterization methods.

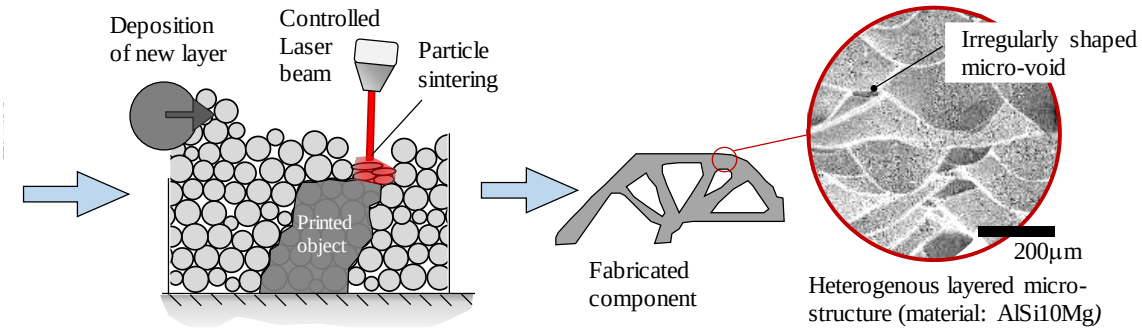

Figure 2: Selective laser melting additive manufacturing process illustration.

Materials created through SLM processes are subjected to complex thermal histories resulting in irregular microstructures and inconsistent material behavior. SLM material thermal histories are defined by heating and cooling cycles and are affected by several parameters: laser power, scanning strategy, fabrication volume, etc [3]. These parameters can all contribute to variations in microstructure and uncertainty in the resulting mechanical properties [3,4] even though the final geometry and input constitutive powders are held constant.

Microstructure-based modelling approaches may be useful to predict mechanical behavior of AM metal components fabricated through SLM processes. Microstructural-based models can account for differences in microstructure features, such as grain size, defect size, and defect distribution, to predict material mechanical behavior. Different approaches have been successfully used to predict various mechanical behavior for AM materials. Yadollahi et al [5] predicted an upper and lower bound of tensile properties of LENS^{TM} 316L SS using an internal state variable plasticity-damage model; Torries et al. [6]used a microstructure-sensitive fatigue model to predict the fatigue behavior of LENS Ti-6Al-4V, and Pei et al. [7] used a damage evolution model based on microstructural characteristics to predict tensile and cyclic mechanical performance of SLM Inconel 718 (IN718). However, the inherent randomness due to process related defects pose a challenge to these deterministic models. Although these models were successful in predicting mechanical behavior of AM parts, calibrations of these models could be a tedious task. Also, these models were tested on standard laboratory specimens where defect statistics could differ between commercial designed parts. As it was mentioned before, fabrication parameters (or even a design) can influence in AM part's microstructure [3,4,8]. Therefore, the use of statistical volume element (SVE) or representative volume element (RVE) to build a stochastic model, where the inherent randomness of AM part behavior can be integrated, is proposed in this project.

Representative Volume Element is a common homogenization method that can predict mechanical behavior of heterogeneous materials such as composite materials, using a small volume to represent the behavior of the whole. Usually, a component or material volume is sectioned into smaller areas, wherein mechanical properties of the volume are estimated by the microstructure contained in the sectioned area. This area is increased until mechanical properties are independent from the size of the area, which means that this area became representative of the

whole. However, this process would eliminate the known anisotropy and heterogeneity of AM parts. Therefore, in order to capture heterogeneities in material, SVEs are typically used. An SVE is a smaller version of a RVE, where homogenization is still not achieved. This approach has been used to predict different types of heterogeneous materials such as brain white matter [9], fiber reinforced polymer [10], porous steel [11] to name a few. Statistical volume elements can be used to create a microstructure-based model to predict mechanical behavior and heterogeneity of AM parts. In order to calibrate the SVE model, micro mechanical testing can be performed in order to obtain the variability of mechanical properties within microstructure.

Micro-mechanical testing has been gaining popularity in applications such as micro-electromechanical systems (MEMS), where material properties at the micro level do not necessarily relate to material bulk properties. Often inferring mechanical properties from the bulk-scale to micro-scale is not feasible since materials at micro level show significantly higher strength [12]. Thus, the ability to perform mechanical testing at this scale would give the ability to determine the material properties at the scale that would be used. In AM application, the testing at this level allows the comprehensive understanding of the microstructure mechanical properties (i.e. phase, grain), isolating the effect that a defect, such as a void, could have on the bulk mechanical property. By complementing the micro-tensile testing with other characterization techniques, such as electron backscatter diffraction (EBSD) and energy-dispersive x-ray spectroscopy (EDS), it is possible to link a mechanical property with a specific microstructure (i.e. phase) contained in AM materials. Therefore, if the phase composition and distribution along with defect statistics are known, it could be possible to predict AM part mechanical behavior by creating a stochastic model based on the mechanical properties of the microstructure itself.

1.2 Scope, Objectives and Research Approach

This research program makes a necessary transformative leap towards the application of AM technologies in the optimized performance of our civil infrastructure and pave the way for a hybrid analysis-AM framework applicable to a broad range of engineering industries (aerospace, automotive, nuclear, etc.). The objective of the proposed research is to test the hypothesis that microscale measurements of material morphology and toughness can be scaled to accurately predict macroscale ductile fracture in steel alloys created through common AM processes such as selective laser melting (SLM). Figure 3 shows the flowchart of the tasks for this research.

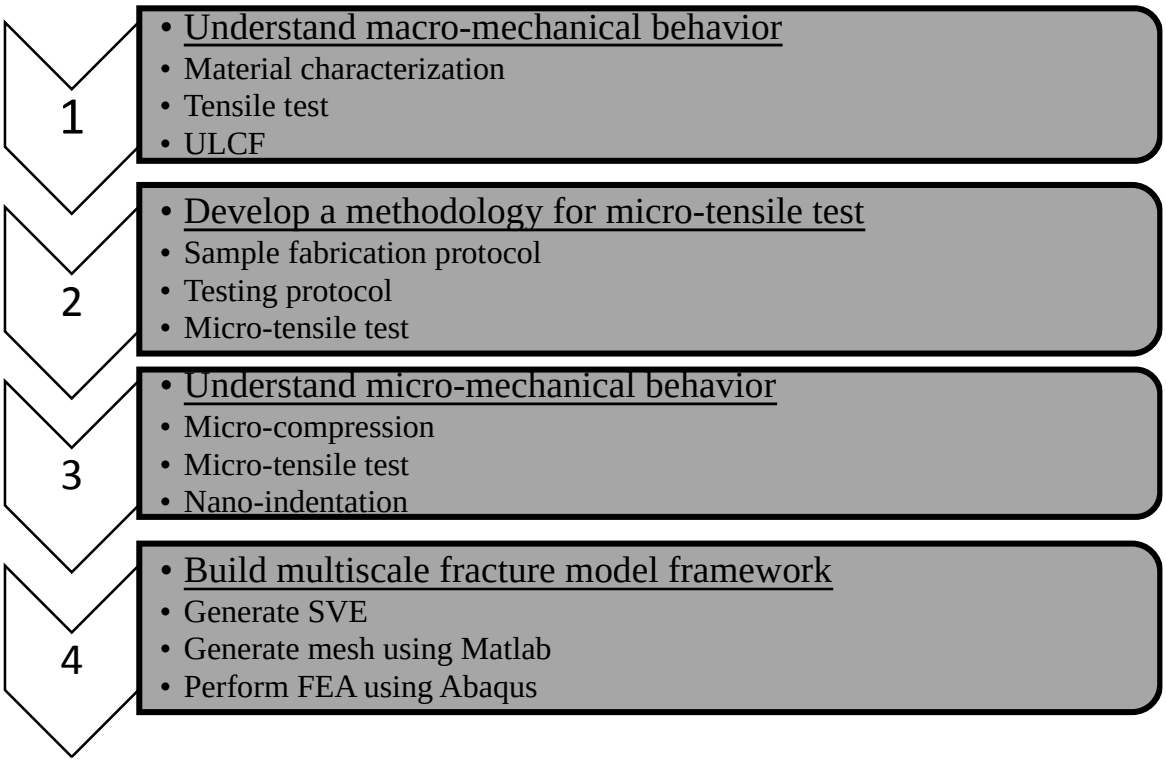

Figure 3: Flow chart of the research tasks.

1.2.1 Understanding the fatigue behavior of SLM 17-4 PH steel under ULCF.

Chapter 2 covers investigations into the mechanical ULCF performance of AM 17-4 PH materials. Monotonic ductile fracture, high cycle fatigue (HCF), and low cycle fatigue (LCF), have been investigated in recent research studies [4,13–15]; however, limited investigations exist for the ultra-low cycle fatigue (ULCF) regime, where materials are subjected to extreme inelastic strain deformations, such as those imposed during earthquakes. The objective for this task has the purpose of providing new data that is currently unavailable in literature and comparing AM materials with materials fabricated with traditional manufacturing techniques. For this task, two sets of AM 17-4 PH specimens and two sets of rolled 17-4 PH steel specimens were considered. For the AM materials, one set was tested as it was built and the second one was subjected to an annealing heat treatment. For the rolled steel, one set was used as received and the second one was subjected to an annealing heat treatment. To complete this objective, all samples were subjected to a series of material characterization testing such as Vicker micro-hardness, tensile test, x-ray diffraction (XRD) and micrography. Then, samples were subjected to a strain-controlled fatigue testing at strain levels of 2%, 3% and 4%. After fatigue testing, fractured surfaces were subjected to a fractography using a Scanning Electron Microscope (SEM). This task established a baseline which was used to compare with the final fracture model.

1.2.2 Understanding the Micro-tensile and micro-fatigue properties of AM 17-4 PH steel.

One of the major drawbacks of SLM is the quantity and size of voids. The presence of voids makes it difficult to predict the mechanical behavior of AM parts. Therefore, the testing of tensile and fatigue behavior, at the micro scale, helps to understand the properties of 17-4 PH steel without such defects. The objective of this task is to obtain data of the mechanical properties at

this level, which is scarce or inexistent in the literature, and compare the performance of AM parts with its wrought counterpart. To achieve this objective, micro-tensile dog-bones were fabricated using Focused Ion Beam (FIB). A Bruker's Pico-indenter PI-88 was used to perform the micro-testing. Since the sample fabrication is time-consuming, a guided methodology was developed. The data acquired in this task was used to construct the SVE model in ABAQUS.

1.2.3 Developing an up-scaling fracture model framework based on micro- and macro-mechanical testing.

Defects size and distribution, along with grain alignment, contribute to the anisotropy and heterogeneity of AM parts, which scatter the mechanical properties' data. Fracture modeling based on microstructure has been proposed and used to have a better prediction of AM parts behavior. However, the inherent randomness and heterogeneity in AM parts, pose a challenge to calibrate these deterministic models. The objective of this task is to create a stochastic model by creating SVE's model based on direct mechanical testing on microstructure, taking consideration the natural heterogeneity of AM parts.

1.3 References

1. Tan, K.G.; Christopoulos, C. Development of Replaceable Cast Steel Links for Eccentrically Braced Frames. *Journal of Structural Engineering* **2016**, *142*, doi:10.1061/(asce)st.1943-541x.0001550.
2. Gray, M.G.; Christopoulos, C.; Packer, J.A.; Lignos, D.G.; Candidate, P.D. *Development, Validation and Modeling of the New Cast Steel Yielding Brace System*; 2012;
3. Yadollahi, A.; Shamsaei, N. Additive Manufacturing of Fatigue Resistant Materials: Challenges and Opportunities. *Int J Fatigue* **2017**, *98*, doi:10.1016/j.ijfatigue.2017.01.001.
4. Mahmoudi, M.; Elwany, A.; Yadollahi, A.; Thompson, S.M.; Bian, L.; Shamsaei, N. Mechanical Properties and Microstructural Characterization of Selective Laser Melted 17-4 PH Stainless Steel. *Rapid Prototyp J* **2017**, *23*, doi:10.1108/RPJ-12-2015-0192.

5. Yadollahi, A.; Shamsaei, N.; Hammi, Y.; Horstemeyer, M.F. Quantification of Tensile Damage Evolution in Additive Manufactured Austenitic Stainless Steels. *Materials Science and Engineering A* **2016**, *657*, 399–405, doi:10.1016/j.msea.2016.01.067.

6. Torries, B.; Sterling, A.J.; Shamsaei, N.; Thompson, S.M.; Daniewicz, S.R. Utilization of a Microstructure Sensitive Fatigue Model for Additively Manufactured Ti-6Al-4V. In Proceedings of the Rapid Prototyping Journal; Emerald Group Publishing Ltd., 2016; Vol. 22, pp. 817–825.

7. Pei, C.; Zeng, W.; Yuan, H. A Damage Evolution Model Based on Micro-Structural Characteristics for an Additive Manufactured Superalloy under Monotonic and Cyclic Loading Conditions. *Int J Fatigue* **2020**, *131*, doi:10.1016/j.ijfatigue.2019.105279.

8. Carlton, H.D.; Haboub, A.; Gallegos, G.F.; Parkinson, D.Y.; MacDowell, A.A. Damage Evolution and Failure Mechanisms in Additively Manufactured Stainless Steel. *Materials Science and Engineering: A* **2016**, *651*, 406–414, doi:https://doi.org/10.1016/j.msea.2015.10.073.

9. Hoursan, H.; Farahmand, F.; Ahmadian, M.T. A Three-Dimensional Statistical Volume Element for Histology Informed Micromechanical Modeling of Brain White Matter. *Ann Biomed Eng* **2020**, *48*, 1337–1353, doi:10.1007/s10439-020-02458-4.

10. Sanei, S.H.R.; Fertig, R.S. Uncorrelated Volume Element for Stochastic Modeling of Microstructures Based on Local Fiber Volume Fraction Variation. *Compos Sci Technol* **2015**, *117*, 191–198, doi:10.1016/j.compscitech.2015.06.010.

11. Yin, X.; Chen, W.; To, A.; McVeigh, C.; Liu, W.K. Statistical Volume Element Method for Predicting Microstructure-Constitutive Property Relations. *Comput Methods Appl Mech Eng* **2008**, *197*, 3516–3529, doi:10.1016/j.cma.2008.01.008.

12. Greer, J.R.; Kim, J.-Y.; Burek, M.J. The In-Situ Mechanical Testing of Nanoscale Single-Crystalline Nanopillars. *The Journal of The Minerals, Metals & Materials Society* **2009**, *61*, 19–25, doi:https://doi.org/10.1007/s11837-009-0174-8.

13. LeBrun, T.; Nakamoto, T.; Horikawa, K.; Kobayashi, H. Effect of Retained Austenite on Subsequent Thermal Processing and Resultant Mechanical Properties of Selective Laser Melted 17–4 PH Stainless Steel. *Mater Des* **2015**, *81*, doi:10.1016/j.matdes.2015.05.026.

14. Liverani, E.; Toschi, S.; Ceschini, L.; Fortunato, A. Effect of Selective Laser Melting (SLM) Process Parameters on Microstructure and Mechanical Properties of 316L Austenitic Stainless Steel. *J Mater Process Technol* **2017**, *249*, doi:10.1016/j.jmatprotec.2017.05.042.

15. Mower, T.M.; Long, M.J. Mechanical Behavior of Additive Manufactured, Powder-Bed Laser-Fused Materials. *Materials Science and Engineering: A* **2016**, *651*, doi:10.1016/j.msea.2015.10.068.

Chapter 2: Ultra Low-Cycle Fatigue Behavior Comparison between Additively Manufactured and Rolled 17-4 PH (AISI 630) Stainless Steels

2.1 Research Objective Summary and Findings from Completed Work

This research objective aims to investigate the mechanical behavior of AM 17-4 PH (AISI 630) stainless steels to aid future developments in AM seismic structural fuse design. Ultra low-cycle fatigue (ULCF) driven fractures are a common performance limitation of existing seismic systems, and improved understanding of ULCF behavior in AM metal materials may help future developments in seismic fuse geometry optimization. To understand parameters affecting AM 17-4 PH ULCF behavior, both AM and traditionally produced (wrought) material samples are fatigue tested under fully reversed (R= -1) strain controlled (2 – 4% strain) loading and characterized using micro-hardness, XRD, and fractography methods. Results indicate decreased fatigue life for AM specimens as compared to wrought 17-4 PH specimens due to fabrication porosity and un-melted particle defect regions which provide a premature mechanism for internal fracture initiation. Heat treatment processes performed to both the AM and wrought specimens had no observable effect on ULCF behavior. Result comparisons with an existing fatigue prediction model (the Coffin-Manson universal slopes equation) demonstrated consistent over-prediction of fatigue life at applied strain amplitudes greater than 3%, likely due to inherent AM fabrication defects. An alternative empirical ULCF capacity equation is proposed herein to aid in future seismic fuse optimization using AM 17-4 PH stainless steel materials.

2.2 Introduction and Background

Current approaches to the seismic resistant design of steel structures rely on ductile energy dissipation mechanisms that are only optimized at a crude level due to the economics and

limitations of traditional fabrication technologies (e.g. eccentrically braced frame links, reduced beam-section moment connections, etc.). Researchers often seek better control and optimization within these ductile mechanisms to improve global seismic performance and create economic savings throughout the structural system. Additive manufacturing (AM) through selective laser melting (SLM) of metal powders is a novel fabrication solution for seismic structural fuse components having optimized geometries too complex for traditional fabrication methods, including casting.

One potential drawback of AM SLM is the creation of material voids during fabrication, caused by un-melted particles and gas entrapment, which can negatively affect mechanical performance [1–8]. Figure 4 shows an illustration of the SLM fabrication procedure, where metal powders are deposited and then melted in layers to form three-dimensional parts. While some research on the mechanical behavior of AM metal parts under monotonic loading, high-cycle fatigue (HCF) and low-cycle fatigue (LCF) have been conducted [2,9–13], little is understood about the mechanical performance under ultra low-cycle fatigue (ULCF) conditions ($N_f < 100$ cycles) such as those produced during design-level seismic events. Ultra low-cycle fatigue (ULCF) driven fractures are a common performance limitation of existing seismic systems and improved understanding of ULCF behavior in AM metal materials may help future developments in seismic fuse geometry optimization.

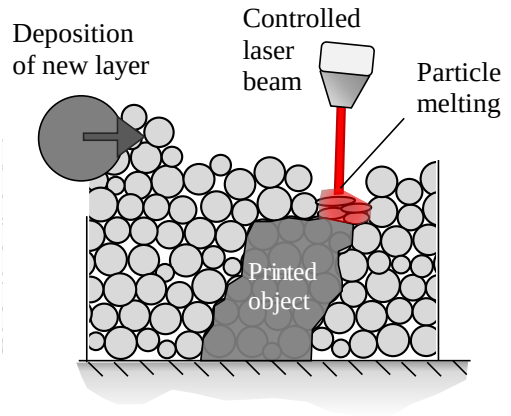

Figure 4: Selective laser melting additive manufacturing process illustration.

Because AM SLM components are created by melting sequential particle layers, material build orientation can lead to anisotropic behavior and the formation of internal voids. Research by Yadollahi et. al [14], identified voids resembling both a slit and a sphere within AM SLM metals resulting from un-melted particles and gas entrapment respectively. Internal material void formations oriented perpendicular to the intended loading direction have been shown to exhibit lower mechanical performance than void formations oriented parallel to the loading direction [1,2,10]. Additionally, sequential powder melting can form elongated grains in the build direction, deflecting crack propagation when loaded parallel to the build orientation, prolonging the time to failure [11,15].

Heat treatment has been shown to affect the strength and HCF performance of AM SLM metal parts. Several studies have successfully used solution annealing and peak-age heat treatment (Condition A and H900) to achieve comparable yield and ultimate strengths in AM 17-4 PH steels compared to wrought counterparts [9,11,14]. These improvements are due to the fine chromium-nickel-copper precipitation in the AM steel, which prevent dislocation movement and increase hardness, yield, and ultimate strength [9,11,14]; however, heat treated samples often have higher amounts of martensite, a stronger and more brittle material phase than austenite, which can result

in a low elongation-to-failure [9,11] possibly affecting ULCF performance under large inelastic strains. Because retained austenite in non-heat-treated samples can improve material fracture toughness due to strain-martensite phase transformation [16,17], it is unclear how heat treatment will affect the ULCF behavior of 17-4 PH stainless steels. In [14], Yadollahi et. al. investigated the HCF behavior of heat treated (solution annealing and peak aging) and non-heat treated AM 17-4 PH samples, and found the non-heat treated samples outperformed the heat-treated samples. While multiple studies have investigated the fatigue strength of AM parts in HCF and LCF regimes, investigations into ULCF behavior of 17-4 PH steels are lacking.

Understanding the mechanical performance of AM 17-4 PH steel components in ULCF is needed for the development of optimized energy dissipative components subjected to large repeated strains (such as yielding dampers and structural fuse elements in buildings during seismic loading) [18]. ULCF fracture processes are fundamentally different than those in the HCF regime as they form through a process of micro-void growth and coalescence during material yielding [19–23]. Komotori et al. [21] studied the effect of low ductility metal (cast iron) grain size under ULCF, where internal fractures were driven by micro-void coalescence via detachment of the matrix from the interstitial carbon inclusions. Additionally, the strain-magnitude and ratio of the ULCF loading can alter internal void shape formation leading to flattened void shapes and increased stress concentrations at void boundaries, resulting in shortened fatigue life [19,22].

This work aims to improve the understanding of AM 17-4 PH stainless steels during ULCF loading and develop predictive tools for estimating ULCF life in structural components subject to inelastic strains. Ductile fracture behavior from tensile testing will provide a performance baseline, with strain controlled (2 – 4% strain amplitude) fatigue testing used to characterize cyclic performance parameters. Micro-hardness, X-ray diffraction (XRD), and scanning electron

microscopy (SEM) are used to study phase composition and fracture surface features. The following section describes the detailed experimental procedure, including sample fabrication and testing approach. Next, results from the mechanical characterizations are described, and ULCF prediction approaches for AM 17-4 PH steels are proposed. Following that, conclusions regarding AM 17-4 PH stainless steel behavior in ULCF are presented.

2.3 Sample fabrication, Mechanical Testing and Material Characterization Procedures

A total of nine AM samples were fabricated by the National Institute of Standards and Technology (NIST) and a private industry partner using an EOSINT M270 direct metal laser-sintering system using EOS standard fabrication parameters which deposit material in 20 μm thick layers in a checkerboard pattern (providing rotation between layers). Current high costs associated with AM metal fabrication prohibited the testing of multiple replicate specimens. The chemical composition of the metal powder used to fabricate the specimens is shown in Table 1. Half of the samples were subjected to a heat treatment (650°C for 1h), as recommended by EOS, while the other half were left in the "as-built" condition. To limit surface roughness effects resulting from AM fabrication, and to provide a consistent surface condition with the wrought materials, all AM specimens were machined to ASTM sample specifications as shown in Figure 5 after being heat treated. Wrought samples were machined from a hot-rolled 17-4 PH steel plate. A set of wrought samples were tested as received (W-AR), while another set of wrought samples were heat treated at 650°C for 4 hours and cooled overnight in the furnace.

Table 1: Metal powder chemical composition.

	Cr (wt%)	Ni (wt%)	Cu (wt%)	Mn (wt%)	Si (wt%)	Mo (wt%)	Nb (wt%)	C (wt%)
Nominal Values	15 - 17.5	3 - 5	3 – 5	Max. 1	Max. 1	Max. 0.5	0.15 – 0.45	Max 0.07

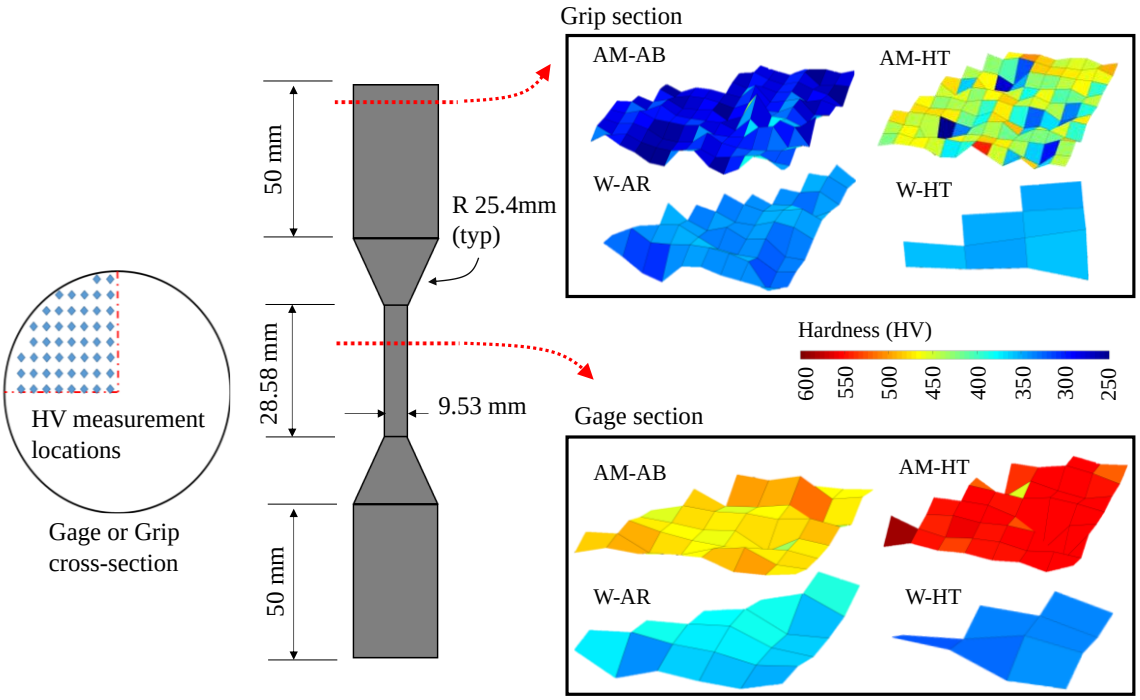

Figure 5: Micro-hardness test measurements from gauge and grip locations.

Displacement controlled tensile ductile fracture and ULCF tests were performed in accordance with ASTM E606/E606M-12 [24] using a Walter+Bai Servohydraulic Biaxial Fatigue Testing Machine. The experimental set-up is shown in Figure 6. In all ULCF testing, specimens were subjected to strain-controlled fully reversed (R= -1) uni-axial cyclic strains at constant strain-amplitudes ($\Delta\varepsilon/2$) of 0.02, 0.03 and 0.04 respectively. All AM specimens were fabricated in the horizontal build orientation and loaded perpendicular to the layer build direction as shown in Figure 7.

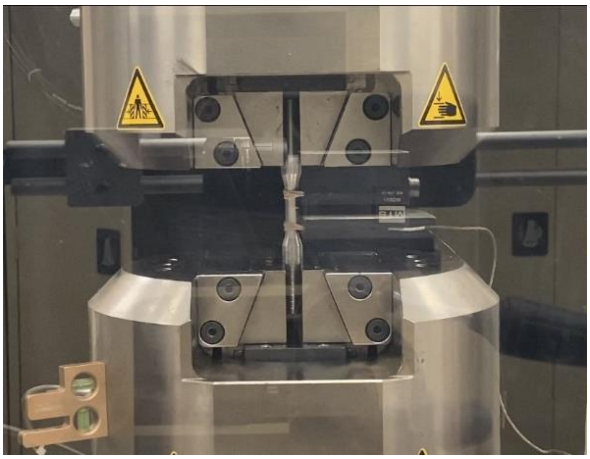

Figure 6: Experimental set-up.

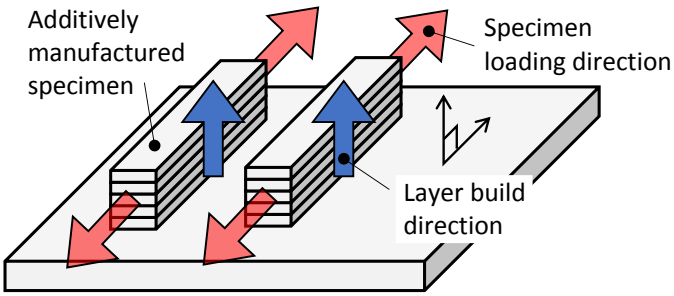

Figure 7: Illustration of specimen build direction relative to the applied loading direction.

To help identify the ULCF mechanisms leading to fracture, each sample was investigated using SEM, micro-hardness testing, and XRD. All SEM images were taken using a Tescan Vega 3 SEM. Vicker's micro-hardness surface testing was performed using a Pace Technologies (model HV-1000Z) micro-hardness tester, applying a load of 0.098 N (100-gf) over a dwell time of 15 s. Multiple micro-hardness measurements were taken from a quadrant of the gage and grip area of each sample (see Figure 5). X-ray diffraction (XRD) measurements from the grip cross-section of each fatigue specimen were taken using a PANalytical X'Pert MRD diffractometer with Cu Kα1 radiation (λ=1.540598 Å) at an operating voltage and current of 45 kV and 40 mA, respectively.

Additionally, metallographic investigations of the specimen surfaces were conducted following polishing and etching with Fry's reagent to reveal the microstructure.

2.4 Results and Discussion

2.4.1 Effect of Heat Treatment Processes on Tensile Behavior

Because post-yield material behavior can control ULCF crack initiation (i.e. void initiation, growth, and coalescence), understanding post-yield mechanical behavior in the heat-treated and non-heat-treated AM specimens may provide insight into material ULCF performance. Results from monotonic tensile testing indicate that heat treatment following the AM SLM fabrication process results in reduced ductility and early initiation of yield. Table 2 shows the tensile mechanical properties for the AM and wrought specimens, showing a nearly 19% reduction in yield stress and 19% decrease in fracture strain between the AM as-built (AM-AB) and AM heat-treated (AM-HT) specimens. Post-yield tensile behavior indicates that the heat treatment increases the ultimate tensile strength (UTS) leading to a larger strain-hardening ratio for the AM materials. From Table 2, the UTS of the AM-HT specimens increased by nearly 31% compared to the AM-AB specimens. This post-yield strain-hardening behavior differs from observations in the wrought materials, where heat treatment in the wrought (W-HT) samples results in a UTS reduction. It should be noted that the lower yield strength of the AM specimens will result in a slight increase in plastic strain demand; however, this plastic train demand increase will be very small and will diminish within the first few loading cycles due to strain hardening.

Table 2: Tension and micro-hardness material characterization results.

Sample Description	Material Type	Fracture Strain [ε_f]	Yield Stress [$\sigma_{y\,(0.2\%)}$] (MPa)	Ultimate Stress [σ_u] (MPa)	Vickers Hardness (HV)	
					Grip	Gage
Wrought – as received	W-AR	0.153	881	1060	335	356
Wrought – heat treated	W-HT	0.152	882	1017	356	333
AM – as built	AM-AB	0.190	630	1025	294	475
AM – heat treated	AM-HT	0.153	512	1495	432	535

2.4.2 Results from Micro-hardness Investigations

Micro-hardness testing throughout the specimen cross-sections suggests microstructure and phase changes during loading for the AM-AB and AM-HT samples, specifically in martensite and austenite content. Figure 5 shows the micro-hardness measurement contours within the gauge and grip regions for the AM and wrought steel specimens (for both heat-treated and non-heat-treated conditions). Hardness measurement comparisons between the strained gauge region and unstrained grip region indicate increased strain hardening for the AM steel specimens (as compared to the wrought steel specimens). This AM steel increase in hardness is due to strain-induced martensite formation within the gage length during plastic deformation. Grip and gauge region hardness measurements from the wrought samples were similar, suggesting an already martensite dominated grain structure prior to loading. Hardness measurements between the grip and gauge regions for the AM-AB samples increased by 51.2% while the AM-HT specimens increased by 29.5%. It is important to note however, that both microstructure and material phase affect hardness. Rapid solidification during the AM steel fabrication process resulted in finer microstructural features as compared with those in the wrought steels and resulted in initial

hardness values that were similar to those in the wrought steels (note the grip region hardness values in Table 2), even though the AM materials had increased austenite content.

2.4.3 Results from XRD Phase Analysis

Results from XRD analyses confirm microstructural phase differences between the AM and wrought steel specimens. Results from the XRD phase analysis show the presence of both martensite and austenite phases within the AM microstructure, and mostly martensite (near no presence of austenite phase) within the wrought steel microstructure. Figure 8 shows the XRD spectra for the AM and wrought specimens, with the austenite peaks within the AM steels clearly visible. Also evident from Figure 8 heat treatment slightly increased the austenite phase peak for the W-HT samples. Increased austenite phase for the AM-AB specimens explains the higher elongation to failure and lower material hardness within the grip area for the AM-HT specimens during monotonic tension testing. The heat treatment resulted in an increased martensite phase, which helps explain the reduction in elongation at failure and the increase UTS shown in Table 2. Micrographs also shown in Figure 8 indicate a difference in microstructure.

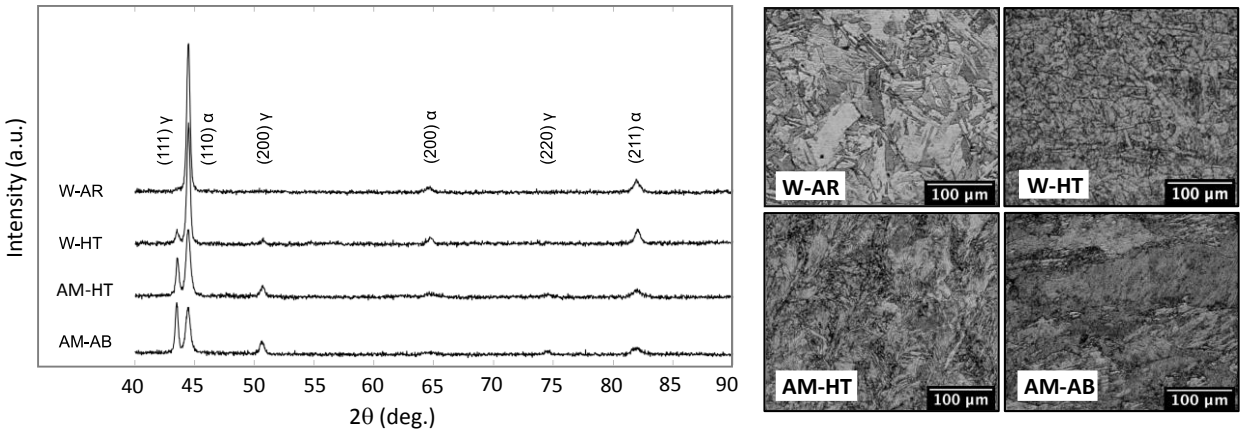

Figure 8: XRD spectra and micrograph from within the un-strained grip location.

2.4.4 Observations from Fatigue Testing and Effect of Heat Treatment on ULCF Performance

Table 3 shows the ULCF results for both the AM and wrought 17-4 PH stainless steel specimens (with and without heat treatment) and Figure 6 shows the resulting fatigue-life curves. From Table 3 (shown graphically in Figure 9) the wrought specimens consistently achieved a higher fatigue life when compared with the AM counterparts. For the high strain amplitude cycles, a fatigue-life reduction of nearly 65% on average was observed for the AM fabricated steel. At lower strain amplitudes (3% strain), the observed decrease in fatigue life due to AM fabrication was 62% on average. For the lowest considered strain amplitude which entered into the LCF regime (resulting in fatigue lives greater than 100 cycles), fatigue performance of the AM and wrought specimens were similar.

Table 3: Ultra low-cycle fatigue test results.

Material Type	Specimen No.	Strain Amplitude [$\Delta\varepsilon/2$] (%)	N_f (cycles)
W-AR	1	2	384
	2	2	337
	3	3	79
	4	3	105
	5	4	35
	6	4	50
W-HT	7	2	575
	8	2	471
	9	3	118

	10	3	151
	11	4	41
	12	4	32
AM-AB	13	2	515
	14	3	47
	15	4	14
	16	4	15
AM-HT	17	2	462
	18	3	44
	19	3	37
	20	4	14
	21	4	12

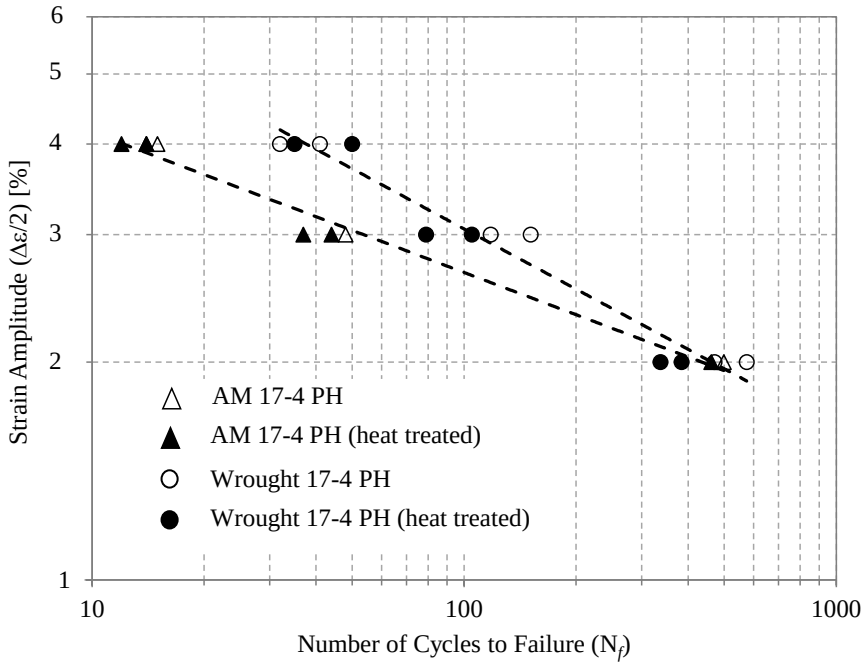

Figure 9: Fully reversed (R=-1) strain-life fatigue curves for 17-PH AM-AB, AM-HT, W-AR, and W-HT steels.

Reductions in ULCF performance for the AM 17-4 PH steel can be attributed to fabrication defects resulting from the powder SLM process. Scanning electron microscopy investigations of the sample fracture surfaces found AM fabrication defects (likely due to gas entrapment and un-melted particles) of between 150 – 200 μm as shown in Figure 10a. Figure 10b shows a computerized tomography (CT) scan image of the unstrained AM-AB grip region having distributed void defects of up to 115 μm (in volume equivalent sphere diameter). Material defects in the wrought specimen resulting from inclusions were measured to be between 20 – 30 μm in size, as shown in Figure 11. Because ULCF fracture processes initiate from internal void growth and linking, the larger internal defects observed in the AM samples could be expected to grow and coalesce into micro-cracks within fewer fatigue cycles than the wrought counterparts. At the lower applied strain ranges (around the 2% strain amplitude loading), data suggest that there may be a failure mechanism transition wherein AM fabrication defects play a reduced role in fracture formation (over other processes wherein conditions between he AM and wrought microstructure conditions are similar).

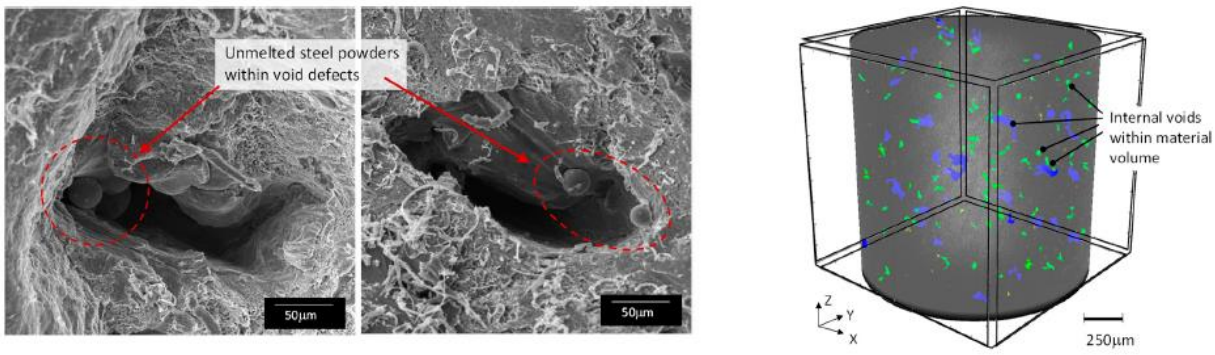

Figure 10: Voids due to un-melted metal powder in an AM-AB specimen: (a) SEM fractograph, and (b) CT scan of unstrained area.

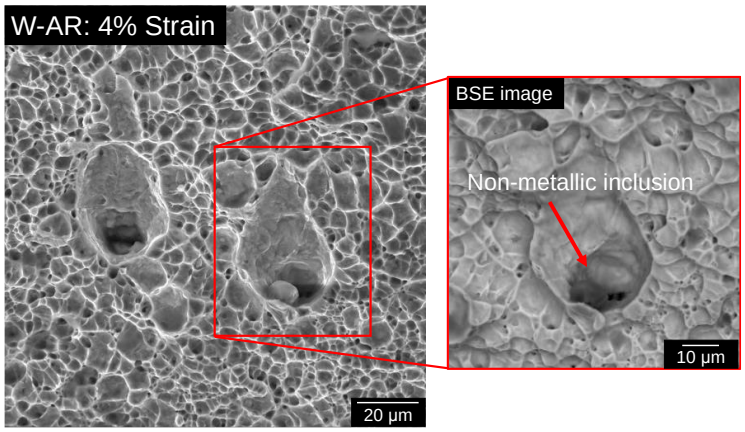

Figure 11: Non-metallic inclusion in W-AR sample. Right: Backscattered electron image of the inclusion.

Although heat treatment was shown to influence the tensile mechanical properties of the AM specimens (yield, strain at fracture, etc.), results indicate a negligible influence on the fatigue performance within the ULCF regime. This result within the ULCF regime is interesting, as it differs from results obtained by Yadollahi et. al. [14] where heat-treated specimens having higher UTS outperformed AM-as-built samples in the LCF regime. The effect of heat treatment (and resulting martensite-phase influence) on AM-HT 17-4 steel performance during high strain-amplitude ULCF loading is likely overshadowed by the internal void defect deformations which precipitate internal micro-cracks. With large (on the order of 100 µm) internal voids from fabrication processes governing the ULCF fracture initiation behavior, improvement in tensile material properties from treatment processes likely do not result in an improvement in ULCF performance for AM metals.

2.4.5 Observations of ULCF Initiation Mechanisms from Fractographic Investigations

Fractographic investigations using scanning electron microscopy revealed material porosity, internal cracks, and un-melted pockets of metal powder in the AM SLM 17-4 PH steel

specimens, while a dimpled fracture surface typical of micro void coalescence during ductile fracture was observed in the wrought 17-4 PH specimens. Figure 12 shows the fractographic images of the specimen fracture surfaces following fatigue cycles at 4% strain amplitude. In Figure 12, the AM-AB material shows elongated pockets containing un-melted metal particles while the AM-HT fracture surfaces contain a more textured surface, showing porosity, internal cracking, and semi-cleavage fracture characteristic of a brittle fracture. Note that fracture surface features are more pronounced in the tensile specimens, as compared to the reversed cycle fatigue specimens. Figure 13 shows the tensile specimen fracture surface features with several pores observable in the AM-AB specimens, and internal cracking or decohesion due to poor melting observable in the AM-HT specimens. Also shown in Figure 13 is the internal cracking within the W-HT specimens.

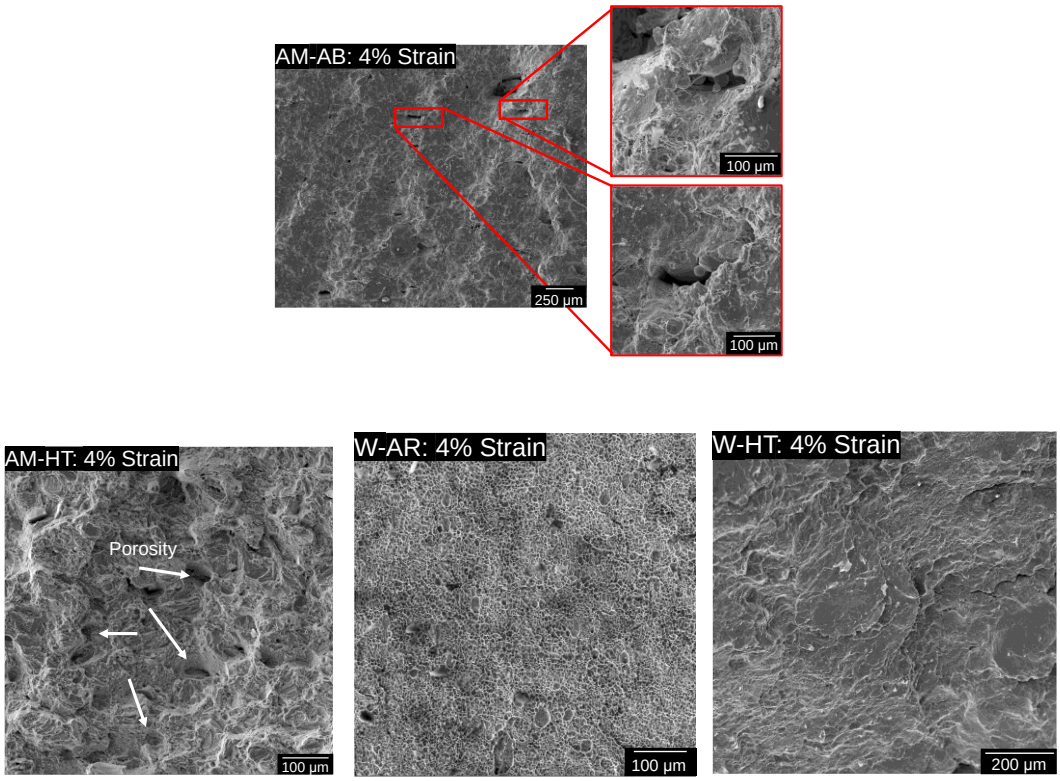

Figure 12: Fracture surface of sample subjected to fatigue testing at 4% strain amplitude. Top: AM-AB sample showing elongated crack having un-melted particles. Bottom Left: AM-HT sample with semi-cleavage surface and porosity. Bottom Center: W-AR sample showing a dimpled fracture surface typical of ductile fracture. Bottom Right: W-HT specimen showing similar fracture surface to AM-AB in appearance but without voids due to unmelted particles

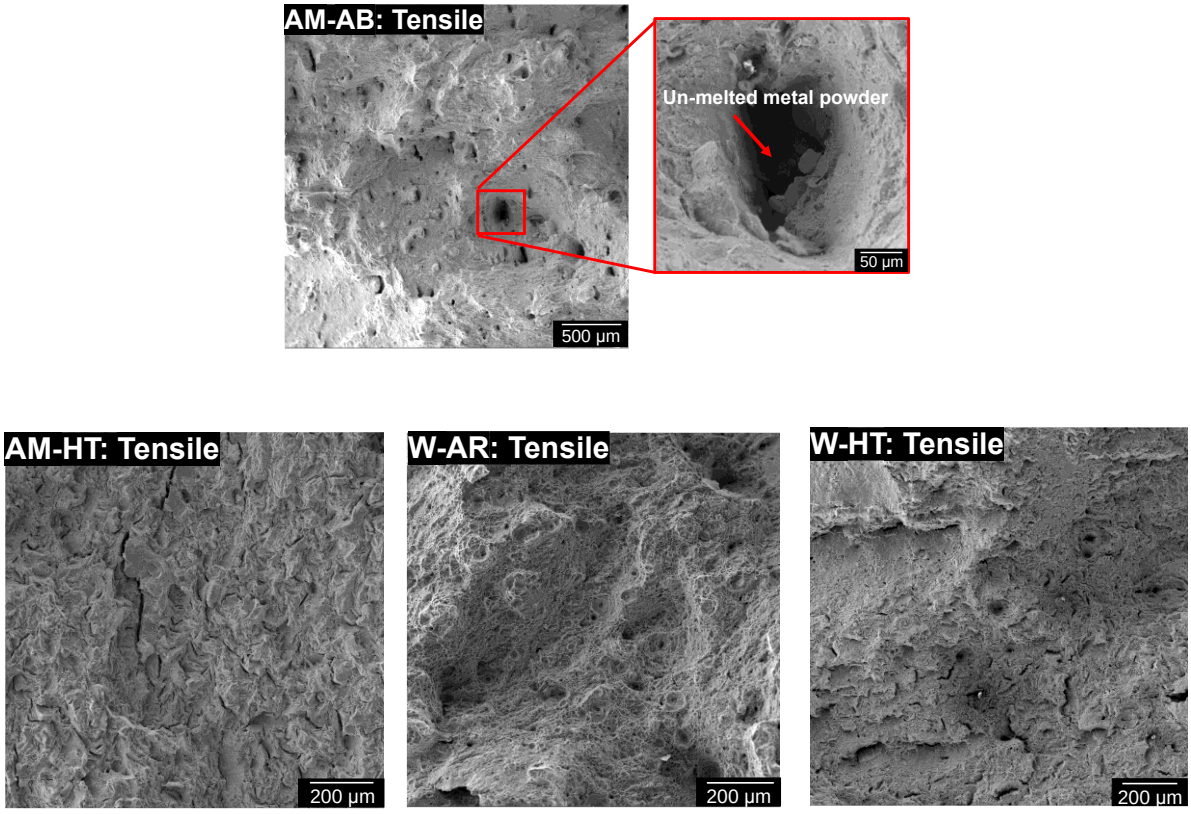

Figure 13: Sample fracture surface resulting from uni-directional tension test. Top: AM-AB sample. Bottom: AM-HT, W-AR and W-HT samples.

2.4.6 AM 17-4 PH Fatigue-Life Comparison with Existing LCF Prediction Models

Existing LCF prediction models often relate monotonic material properties (such as yield strength, fracture strain, elastic modulus, etc.) to cyclic material performance using assumed void growth mechanics and empirically derived strain-cycle relationships [19,25–28]. The Coffin-Manson equation (provided in Equation 1) [29,30]is one widely used LCF prediction model for steel materials that has provided promising predictive results in many studies [31–33]; however, it is unclear if the monotonic properties in Equation 1 apply to ULCF prediction for AM steel

materials having large fabrication void defects. Considering the coefficients in Equation 1 (σ'_f, ε'_f, b, and c) to be those presented in Manson's universal slopes equation [34] ($\sigma'_f = 1.9\sigma_u$, $\varepsilon'_f = 0.76\left[\ln\left(\frac{1}{1-R_A}\right)\right]^{0.6} \approx 0.76\varepsilon_f$, b = -0.12, and c = -0.6) provides a fatigue-life estimation equation based on material ultimate stress (σ_u), fracture strain (ε_f), and elastic modulus (E) as shown in Equation 2.

$$\frac{\Delta\varepsilon_i}{2} = \frac{\sigma'_f}{E}(2N_i)^b + \varepsilon'_f(2N_i)^c \quad (1)$$

$$\Delta\varepsilon_i = 3.5\frac{\sigma_u}{E}(N_i)^{-0.12} + \varepsilon_f{}^{0.6}(N_i)^{-0.6} \quad (2)$$

Figure 14 compares the AM 17-4 PH and wrought steel fatigue performance with that predicted in Equation 2 from the AM 17-4 PH monotonic material properties. From Figure 14, the universal slopes equation over-predicts the AM steel fatigue life by between 119% and 213% on average at an applied strain amplitude of 3% and 4% respectively. In Figure 14, the Coffin-Manson fatigue life prediction more closely matches the fatigue performance of the wrought specimens having fewer internal fabrication voids.

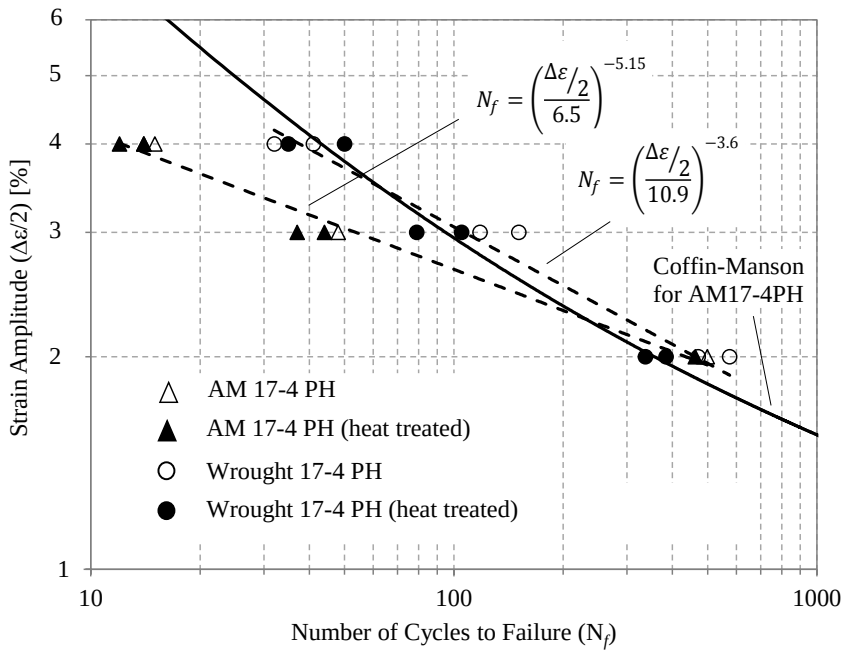

Figure 14: Coffin-Manson universal slopes comparison to measured fatigue data and proposed ULCF regression.

With the inaccuracies demonstrated by Equation 2, and given the scale of the observed AM material voids formed during fabrication (see again Figure 10), an empirical fatigue-life prediction approach is proposed herein. Equation 3, represents a power-law relationship between applied strain amplitude and the number of cycles for specimen failure (defined as complete fracture of the material cross-section) fit to the mean of the measured AM fatigue data gathered in this study. In Equation 3, the strain-based ULCF prediction requires only the input of applied strain-amplitude as is valid within the ULCF and LCF regimes.

$$N_f = \left(\frac{\Delta\varepsilon/2}{6.5}\right)^{-5.15} \quad (3)$$

To verify the predictive capabilities of Equation 3, two additional AM-HT specimens (designated V1 and V2) were fatigue tested at 3.5% strain amplitude under the same material

characterization procedures described earlier. Figure 15 shows the resulting material response to the 3.5% strain amplitude cyclic loading, with specimens V1 and V2 completely fracturing during the 19th cycle and 24th cycle respectively. Note that from the proposed ULCF capacity curve in Equation 3 provides a reasonable estimation of fatigue life, predicting 24 cycles for the AM17-4 specimens subjected to an applied strain amplitude of 3.5%.

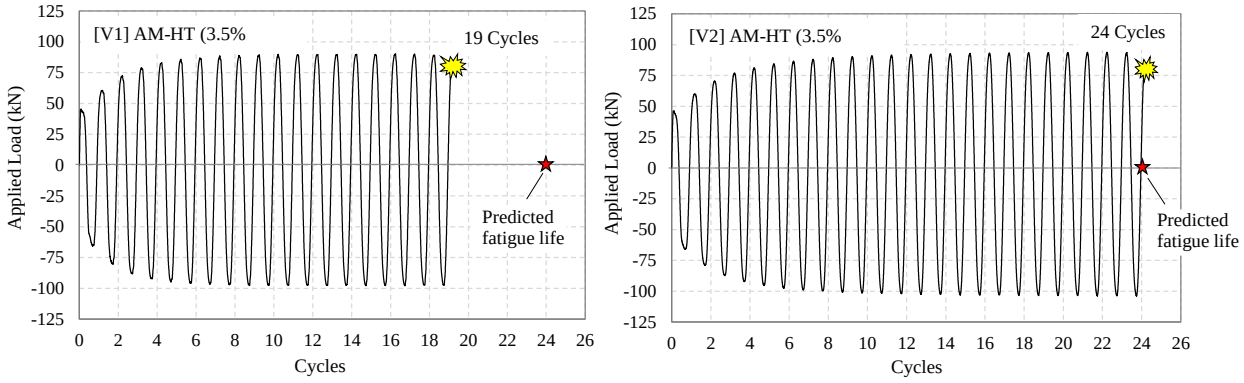

Figure 15: Verification results from the proposed empirical ULCF Equation.

2.5 Conclusions from Work Completed on Objective 1

This study compared the ULCF behavior of 17-4 PH stainless steel produced through SLM AM processes with traditionally material fabrication processes. In this study, AM-HT 17-4 PH, AM-AB 17-4 PH, and wrought 17-4 PH stainless steel specimens were investigated in ULCF under fully-reversed (R= -1) strain-controlled conditions to better understand mechanisms affecting ULFC performance. Additional material tensile characterization tests were conducted to investigate material tensile property relationships and ULCF behavior. To help identify ULCF mechanisms leading to fracture, each sample was investigated using scanning electron microscopy, micro-hardness testing, computer tomography (CT) scanning and XRD. The following conclusions are based on material testing observations and measurements:

1) SLM AM fabrication processes result in un-melted particles and gas entrapment which can create internal material voids on the order of 100 to 200 μm.
2) Large internal void defects result in decreased ULCF performance for AM 17-4 PH steel specimens as compared to the wrought steel counterparts, which have inclusion defects of approximately 20 μm. A decrease in fatigue life of between 62% and 65% was observed at strain amplitudes of 3% and 4% respectively.
3) Within the LCF regime (Nf >100, resulting from strain amplitudes near 2%), fatigue behavior of the AM and wrought steel specimens are similar.
4) Post fabrication heat treatment processes have no observable effect on the ULCF or LCF behavior of AM 17-4 PH stainless steel materials. Although heat treatment processes were found to alter the AM material tensile properties (yield, strain hardening, etc.), the ULCF behavior of heat-treated and non-heat-treated AM 17-4 PH stainless steels were similar (likely due to the fatigue processes being governed by void/defect size).
5) The existing Coffin-Manson universal slopes equation for LCF prediction over estimated the fatigue life of the AM specimens at applied strain amplitudes of 3% and 4%. Fatigue-life predictions at the 3% and 4% strain amplitudes were over-estimated by 119% and 213% respectively.
6) An empirical ULCF capacity equation for AM 17-4 PH stainless steel is proposed herein. Additional testing demonstrated good agreement with the proposed equation predictions (providing fatigue-life estimations within 10% on average between the two additional verification tests). Future ULCF testing would be beneficial in further refining the proposed empirical model.

2.6 References

1. Carlton, H.D.; Haboub, A.; Gallegos, G.F.; Parkinson, D.Y.; MacDowell, A.A. Damage Evolution and Failure Mechanisms in Additively Manufactured Stainless Steel. *Materials Science and Engineering: A* **2016**, *651*, 406–414, doi:https://doi.org/10.1016/j.msea.2015.10.073.

2. Bao, J.; Wu, S.; Withers, P.J.; Wu, Z.; Li, F.; Fu, Y.; Sun, W. Defect Evolution during High Temperature Tension-Tension Fatigue of SLM AISi10Mg Alloy by Synchrotron Tomography. *Materials Science and Engineering A* **2020**, *792*, doi:10.1016/j.msea.2020.139809.

3. Haghdadi, N.; Laleh, M.; Moyle, M.; Primig, S. Additive Manufacturing of Steels: A Review of Achievements and Challenges. *J Mater Sci* 2021, *56*, 64–107.

4. Karthik, G.M.; Kim, H.S. Heterogeneous Aspects of Additive Manufactured Metallic Parts: A Review. *Metals and Materials International* 2021, *27*.

5. Zhao, L.; Santos Macías, J.G.; Douillard, T.; Li, Z.; Simar, A. Unveiling Damage Sites and Fracture Path in Laser Powder Bed Fusion AlSi10Mg: Comparison between Horizontal and Vertical Loading Directions. *Materials Science and Engineering: A* **2021**, *807*, 140845, doi:10.1016/J.MSEA.2021.140845.

6. Ben, D.D.; Ma, Y.R.; Yang, H.J.; Meng, L.X.; Shao, X.H.; Liu, H.Q.; Wang, S.G.; Duan, Q.Q.; Zhang, Z.F. Heterogeneous Microstructure and Voids Dependence of Tensile Deformation in a Selective Laser Melted AlSi10Mg Alloy. *Materials Science and Engineering: A* **2020**, *798*, 140109, doi:10.1016/J.MSEA.2020.140109.

7. Shifeng, W.; Shuai, L.; Qingsong, W.; Yan, C.; Sheng, Z.; Yusheng, S. Effect of Molten Pool Boundaries on the Mechanical Properties of Selective Laser Melting Parts. *J Mater Process Technol* **2014**, *214*, 2660–2667, doi:10.1016/J.JMATPROTEC.2014.06.002.

8. Xiong, Z.H.; Liu, S.L.; Li, S.F.; Shi, Y.; Yang, Y.F.; Misra, R.D.K. Role of Melt Pool Boundary Condition in Determining the Mechanical Properties of Selective Laser Melting AlSi10Mg Alloy. *Materials Science and Engineering: A* **2019**, *740–741*, 148–156, doi:10.1016/J.MSEA.2018.10.083.

9. LeBrun, T.; Nakamoto, T.; Horikawa, K.; Kobayashi, H. Effect of Retained Austenite on Subsequent Thermal Processing and Resultant Mechanical Properties of Selective Laser Melted 17–4 PH Stainless Steel. *Mater Des* **2015**, *81*, doi:10.1016/j.matdes.2015.05.026.

10. Liverani, E.; Toschi, S.; Ceschini, L.; Fortunato, A. Effect of Selective Laser Melting (SLM) Process Parameters on Microstructure and Mechanical Properties of 316L Austenitic Stainless Steel. *J Mater Process Technol* **2017**, *249*, doi:10.1016/j.jmatprotec.2017.05.042.

11. Mahmoudi, M.; Elwany, A.; Yadollahi, A.; Thompson, S.M.; Bian, L.; Shamsaei, N. Mechanical Properties and Microstructural Characterization of Selective Laser Melted 17-4 PH Stainless Steel. *Rapid Prototyp J* **2017**, *23*, doi:10.1108/RPJ-12-2015-0192.

12. Mower, T.M.; Long, M.J. Mechanical Behavior of Additive Manufactured, Powder-Bed Laser-Fused Materials. *Materials Science and Engineering: A* **2016**, *651*, doi:10.1016/j.msea.2015.10.068.

13. Brodie, E.G.; Richter, J.; Wegener, T.; Niendorf, T.; Molotnikov, A. Low-Cycle Fatigue Performance of Remelted Laser Powder Bed Fusion (L-PBF) Biomedical Ti25Ta. *Materials Science and Engineering A* **2020**, *798*, doi:10.1016/j.msea.2020.140228.

14. Yadollahi, A.; Shamsaei, N.; Thompson, S.M.; Elwany, A.; Bian, L. Effects of Building Orientation and Heat Treatment on Fatigue Behavior of Selective Laser Melted 17-4 PH Stainless Steel. *Int J Fatigue* **2017**, *94*, doi:10.1016/j.ijfatigue.2016.03.014.

15. Yadollahi, A.; Shamsaei, N. Additive Manufacturing of Fatigue Resistant Materials: Challenges and Opportunities. *Int J Fatigue* **2017**, *98*, doi:10.1016/j.ijfatigue.2017.01.001.

16. Rafi, H.K.; Pal, D.; Patil, N.; Starr, T.L.; Stucker, B.E. Microstructure and Mechanical Behavior of 17-4 Precipitation Hardenable Steel Processed by Selective Laser Melting. *J Mater Eng Perform* **2014**, *23*, doi:10.1007/s11665-014-1226-y.

17. Huo, C.Y.; Gao, H.L. Strain-Induced Martensitic Transformation in Fatigue Crack Tip Zone for a High Strength Steel. *Mater Charact* **2005**, *55*, doi:10.1016/j.matchar.2005.02.004.

18. Kanvinde, A.M.; Deierlein, G.G. Continuum Based Micro-Models for Ultra Low Cycle Fatigue Crack Initiation in Steel Structures. In Proceedings of the Structures Congress 2005; American Society of Civil Engineers: Reston, VA, April 18 2005.

19. Kanvinde, A.M.; Deierlein, G.G. Cyclic Void Growth Model to Assess Ductile Fracture Initiation in Structural Steels Due to Ultra Low Cycle Fatigue. *J Eng Mech* **2007**, *133*, doi:10.1061/(ASCE)0733-9399(2007)133:6(701).

20. Pereira, J.C.R.; de Jesus, A.M.P.; Xavier, J.; Fernandes, A.A. Ultra Low-Cycle Fatigue Behaviour of a Structural Steel. *Eng Struct* **2014**, *60*, doi:10.1016/j.engstruct.2013.12.039.

21. Komotori, J.; Shimizu, M. Fracture Mechanism of Ferritic Ductile Cast Iron in Extremely Low Cycle Fatigue. *Low Cycle Fatigue and Elasto-Plastic Behaviour of Materials* **1998**, 39–44.

22. Prinz, G.S.; Richards, P.W. Demands on Reduced Beam Section Connections with Out-of-Plane Skew. *Journal of Structural Engineering* **2016**, *142*, 04015095, doi:10.1061/(asce)st.1943-541x.0001360.

23. Desrochers, C.; Prinz, G.S.; Richards, P.W. Column Axial Load Effects on the Performance of Skewed SMF RBS Connections. *J Constr Steel Res* **2018**, *150*, 505–513, doi:10.1016/j.jcsr.2018.09.007.

24. ASTM Standard Practice for Strain-Controlled Fatigue Testing 1., doi:10.1520/E0606_E0606M-21.

25. Kanvinde, A.M.; Deierlein, G.G. Validation of Cyclic Void Growth Model for Fracture Initiation in Blunt Notch and Dogbone Steel Specimens. *Journal of Structural Engineering* **2008**, *134*, doi:10.1061/(ASCE)0733-9445(2008)134:9(1528).

26. Rice, J.R.; Tracey, D.M. On the Ductile Enlargement of Voids in Triaxial Stress Fields∗. *J Mech Phys Solids* **1969**, *17*, doi:10.1016/0022-5096(69)90033-7.

27. Wen, H.; Mahmoud, H. New Model for Ductile Fracture of Metal Alloys. II: Reverse Loading. *J Eng Mech* **2016**, *142*, doi:10.1061/(ASCE)EM.1943-7889.0001010.

28. Kanvinde, A.M.; Deierlein, G.G. Micromechanical Simulation of Earthquake -Induced Fracture in Steel Structures, Stanford University: Ann Arbor, 2004.

29. Coffin Jf., L.F. A Study of the Effects of Cyclic Thermal Stresses in Ductile Metals." . *ASME* **1954**, *76*, 931–950.

30. Manson, S.S. Behavior of Materials under Conditions of Thermal Stress. *National Advisory Committee for Aeronautics* **1953**, *2933*.

31. Prinz, G.S.; Coy, B.; Richards, P.W. Experimental and Numerical Investigation of Ductile Top-Flange Beam Splices for Improved Buckling-Restrained Braced Frame Behavior. *Journal of Structural Engineering* **2014**, *140*, doi:10.1061/(ASCE)ST.1943-541X.0000930.

32. de Castro Sousa, A.; Nussbaumer, A. *Ultra Low Cycle Fatigue of Welded Steel Joints under Multiaxial Loading*; 2016;

33. de Castro e Sousa, A.; Nussbaumer, A. Multiaxial Ultra Low Cycle Fatigue in Welded High Strength Steel Structural Components. *J Constr Steel Res* **2019**, *153*, 473–482, doi:10.1016/J.JCSR.2018.10.028.

34. Manson, S.S. Fatigue: A Complex Subject—Some Simple Approximations. *Exp Mech* **1965**, *5*, doi:10.1007/BF02321056.

Chapter 3: Micromechanical Tension Testing of Additively Manufactured 17-4 PH Stainless Steel Specimens - Methodology

3.1 Research Objective Summary and Findings from Completed Work

This research objective aims to quantify the micromechanical material behavior leading to ductile fracture in AM steels through micro-scale material testing. As part of this research objective, a detailed methodology is developed for high-throughput micro-mechanical testing. This section presents the detailed methodology already developed for the rapid fabrication and micro-tensile testing of AM 17-4 PH stainless steels and discusses the detailed research plan for characterizing micromechanical fracture mechanisms for later upscaling research tasks. The developed methodology combines photolithography, wet-etching, FIB milling, and modified nanoindentation. Detailed procedures for proper sample surface preparation, photo-resist placement, etchant preparation, and FIB sequencing are described herein to allow for high throughput (rapid) specimen fabrication from bulk AM 17-4 PH stainless steel volumes. Additionally, procedures for the nano-indenter tip modification to allow tensile testing are presented and a representative micro specimen is fabricated and tested to failure in tension. Tensile-grip-to-specimen alignment and sample engagement were the main challenges of the micro-tensile testing; however, by reducing the indenter tip dimensions, alignment and engagement between the tensile grip and specimen was improved. Results from the representative micro-scale in-situ SEM tensile test indicate a single slip plane specimen fracture (typical of a ductile single crystal failure), differing from macro-scale AM 17-4 PH post-yield tensile behavior.

3.2 Introduction

Mechanical material testing at the micro- and nano-scales can provide important information on fundamental material behavior through identifying length-scale dependencies caused by void or inclusion effects in bulk material volumes. Nanoindentation and micro compression are currently the most common micro- and nano-mechanical material testing approaches; however, the resulting compression and modulus measurements are often insufficient to characterize material failure mechanisms present in larger bulk material volumes. To identify differences between bulk and micro-mechanical material behavior, particularly for materials having many inclusions and void defects such as those created during AM processes, efficient methods for micro-tension testing are needed.

Although several micromechanical tension testing studies exist for electronic and single-crystalline materials [1–3], specimen fabrication and tension testing procedures for AM steel materials are lacking. Material length-scale dependencies documented in [1,3–6] suggest material hardening effects in single-crystalline materials at sub-micron length-scales. As an example, observations from micro-mechanical tension testing of single-crystal copper highlight material hardening due to dislocation starvation and truncation of spiral dislocation sources [5–7]. Reichardt et al. [8] identifies irradiation hardening effects at the micro scale, observable through micro-mechanical tension testing.

Micro-tensile material measurements requiring attachment of the indenter probe to the specimen are more complex than corresponding micro-compression tests but provide material fracture behavior applicable for bulk material volume predictions under more complex loading (axial tension, bending, etc.). Fabrication of micro-tensile specimens often relies heavily on FIB milling from the bulk material volumes. Because FIB milling processes involve highly localized

material removal (at the micro and nano-scales), large area removal through FIB milling often results in lengthy micro-specimen fabrication times. The work presented herein explores a methodology to improve efficiency in micro-tensile specimen fabrication for AM 17-4 PH stainless steels by combining photolithographic processes, chemical etching, and FIB milling. Additionally, procedures for the micro-mechanical tension testing of fabricated AM steel specimens are presented and testing results are discussed.

3.3 Developed Micromechanical Testing Protocol

3.3.1 Sample preparation for photolithography process and wet etching.

- Cut a sample from the area of interest and polish it using a semi-automatic polishing machine.
    - Using a slow dicing saw or a band saw, cut a section of ~ 6 mm from the area of interest to be studied. For this study, the material was cut from the gage section of an AM 17-4 PH fatigue specimen, as shown in Figure 16.
    - Prepare the cut sample in a metallographic mount for polishing.
    - Starting from 400 grit abrasive paper and moving to 1 μm diamond particles, polish the sample to mirror-like surface (having a surface roughness on the order of 1 μm), using a semi-automatic polisher. To ensure sufficient polish at each abrasion level, alternate the polishing direction by 90 ° following each grit level to ensure uniform surface abrasions. It is important to maintain a flat surface during polishing to avoid issues during a later spin coating process.
- Section the material into a thin disk.

- Protect the polished surface using an adhesive tape.
- Using a slow speed saw, align and cut a thin section (0.5 mm – 1 mm). An even section will be important for the spin coating process.

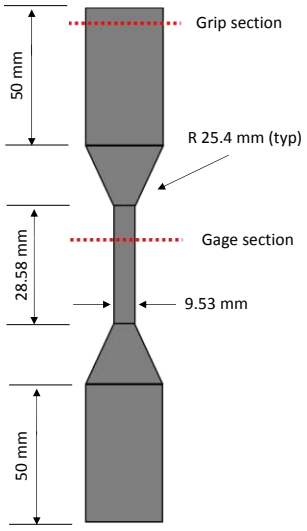

Figure 16: Bulk material where the sample were taken from.

3.3.2 Photolithography.

- <u>Clean the sample.</u>
  - Remove the protective adhesive tape from the polished surface and place the sample, polished surface facing up, in a beaker with acetone and clean the sample, using an ultrasonic cleaner, for 5 min. Use enough acetone to cover the sample.
  - Remove the sample from the acetone and dry it using compressed air.
  - Submerge the sample in isopropanol, and clean the sample for 5 min in an ultrasonic cleaner. Use enough isopropanol to cover the sample.

- Remove the sample from the container with isopropanol and dry the sample with compressed air.
- Place the sample in a holding container and perform an oxygen plasma cleaning for 1 minute.

- Prepare photoresist solution. This can be performed beforehand.
  - Using a mixer, mix 27.2 g (50 wt%) of liquid PGMEA and 25.1 g (50 wt%) of SU-8 3025 for 2 min.
  - De-foam the mixture for 1 min.
- Perform the photo-resist patterning.
  - Place the sample (polished side up) on the spin-coater.
  - Use compressed air to remove any dust or particle on the surface of the sample.
  - Apply photoresist on the sample and run the spin-coater using the parameters shown in Table 4. Note that the thickness of the resulting SU-8 photoresist used in this study was measured to be near 1.5 microns on average.

Table 4: Parameters used for the spin-coating.

Process	Details	Time (s)
Acceleration	From 0 to 500 rpm at 100 rpm/s	5
Spin	500 rpms	5
Acceleration	From 500 rpm to 3,000 rpm at 500 rpm/s	5
Spin	3,000 rpm	25

- Place the sample on a hot plate and heat at 65 ℃ for 5 min.
- Heat the sample at 95 ℃ for 10 min.
- Remove the sample from the hot plate and allow the sample to cool to room temperature.
- Using a photomask with an array of squares measuring 70 μm on each side, expose the sample for 10 - 15 seconds at a power density of ~75 mJ/cm^2.
- Heat the sample to 65 ℃ for 5 min on a hotplate.
- Heat the sample to 95 ℃ for 10 min on a hotplate and then let the sample to cool to room temperature before continuing to the next step.
- Submerge the sample (with the pattern facing up) in a clean container with propylene glycol monomethyl ether acetate (PGMEA) and agitate it for 10 min. Use enough PGMEA to cover the sample.
- Remove the sample and splash with isopropanol before carefully drying with compressed air. Figure 17 shows the final result of a patterned SU-8 on the sample. In Figure 17, there are locations on the steel surface having no photoresist (note the bottom left specimen surface) likely due to uneven surface affecting the spin coat. For the purpose of this study (creating local micro-tensile specimens), it is considered a satisfactory pattern.

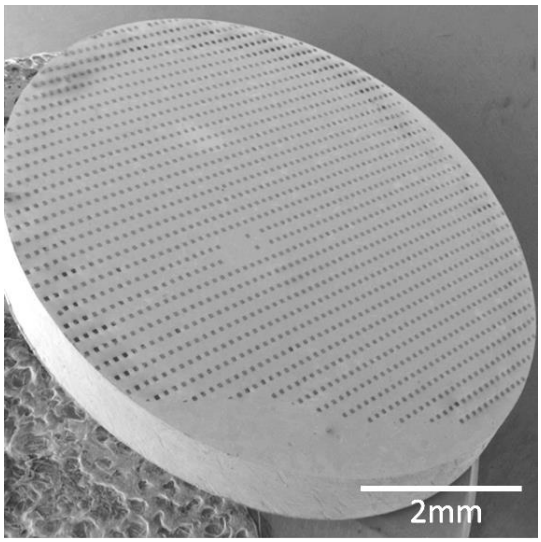

Figure 17: Material section having an array of squares (70 μm X 70 μm) patterned using photolithography.

3.3.3 Wet etching.

- Prepare the AM 17-4 PH stainless steel aqueous etchant [9] shown in Table 5.

Table 5: Chemical composition of the etchant used for AM 17-4 PH Stainless Steel.

$FeCl_3$ (wt%)	HCl (wt%)	HNO_3 (wt%)
10	10	5

- Inside of a fume hood, place the sample in a beaker and place it on top of a hotplate at ~ 65 – 70 °C.
- Leave the sample on the hot plate for 5 minutes.

- With the sample on the hot plate, place a few drops of the prepared etchant so that the patterned surface is completely covered. Leave the etchant for 5 min.
- Remove the sample from the beaker and neutralize the etchant with water. Figure 18 shows the resulting sample after etching. Note in Figure 18 that the remaining photoresist prevents the etchant from reacting the steel surface, creating localized platform areas of unremoved material.

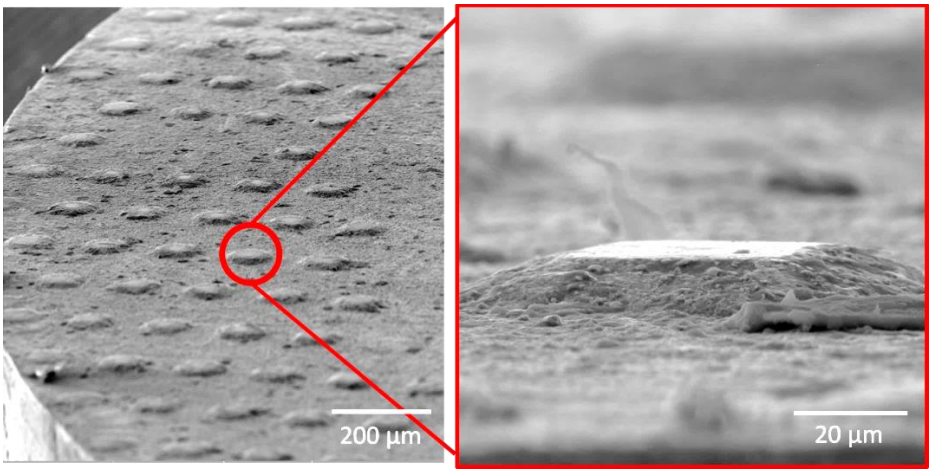

Figure 18: SEM images of the AM 17-4 PH steel surface following etching.

3.3.4 Focused Ion Beam Milling of Specimen Geometry

- Prepare the sample for the FIB-milling process.
  - Place the sample in a container with isopropanol and, using an ultrasonic cleaner, clean the sample for 5 min. Use enough isopropanol to cover the sample.
  - Remove and dry the sample with compressed air.

- Using a conductive adhesive, mount the sample on a stub compatible with the nanoindentation device to be used during later testing.
- Drill a hole in a 45 ° SEM mounting stub and use a carbon tape to place the indenter stub and specimen on a 45 ° SEM stub, as shown in Figure 19. This step is intended to reduce direct contact with the sample once the micro tensile specimen is fabricated, decreasing the chance of damaging the sample.
- Place the sample in an SEM and identify an etched square to perform the FIB milling. For this study, remaining material squares ~ 9 µm in height or larger were desired due to the chosen specimen geometry.
- Orient the chosen FIB location at the top of the SEM stub to avoid contact issues during alignment in the SEM.

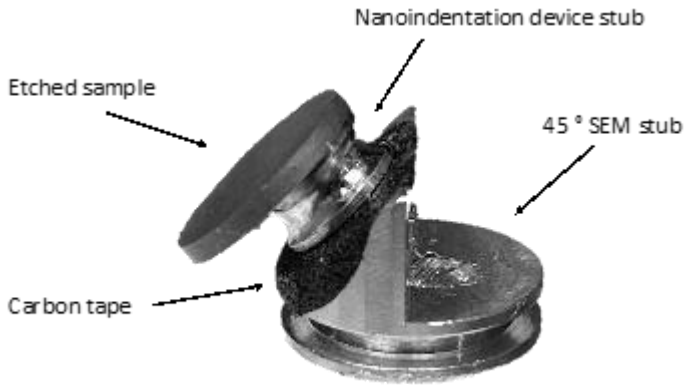

Figure 19: Sample holder set-up which helps the direct contact of the sample once the micro-tensile specimen is fabricated.

- Perform FIB milling. A SEM operated at 30 kV was used in this study. Although a specific procedure cannot be specified, as it requires adjustment based on specific

equipment, milling from outside to inside is a good practice to avoid material re-deposition within the specimen location. Additionally, it is good practice to use maximum energy to remove bulk material but reduce the FIB energy while approaching the final specimen dimensions.

- Using the maximum power (20 mA, 30 kV) to remove any undesired bulk material from the remaining etched platform as shown in Figure 20
- Using lower power, (7 mA, 30 kV) or (5 mA, 30 kV) make a rectangle with slightly larger dimensions than needed for the final specimen geometry (see Figure 21).
- With even lower power (1 mA, 30 kV) or (0.5 mA, 30 kV), perform cross section cuts near to the final micro-tensile specimen dimensions. Following this FIB step (shown in Figure 22), the sample should have the required outer dimensions but be missing the "dog-bone" shape profile.
- Rotate the sample 180 °.
- Using low power (0.5 mA, 30 kV) or (0.3 mA, 30 kV), perform the final FIB milling step to create the specimen geometry desired. The creation and use of a bitmap is recommended to control the FIB intensity and location for the repeatability in the creation of final geometry for multiple specimens. Figure 23 shows an SEM image of the resulting micro-tensile specimen fabricated from the steps described in Sections 4.2.1 through 4.2.5. Dimensions of the tensile specimen are shown in Figure 24.

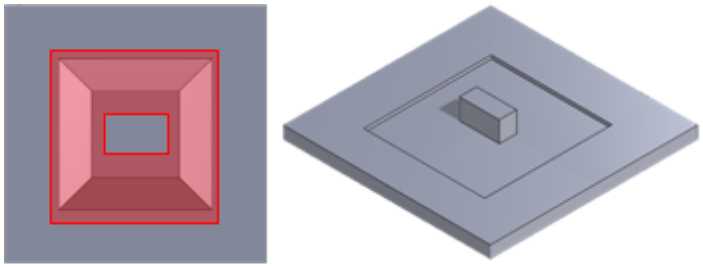

Figure 20: Illustration of first FIB milling step with area to be removed by FIB (left), and remaining material (right).

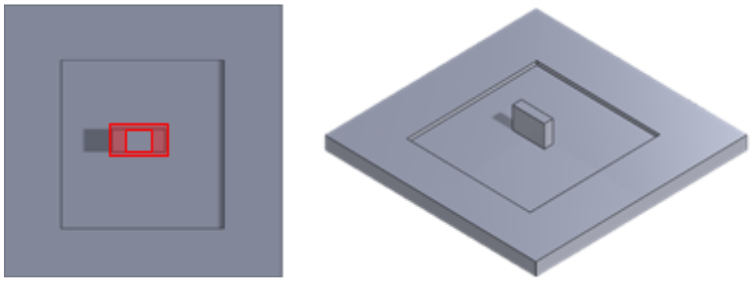

Figure 21: Illustration of second FIB milling step.

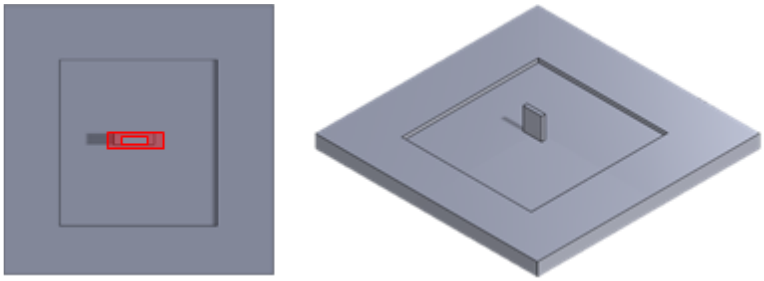

Figure 22: Illustration of third FIB milling step.

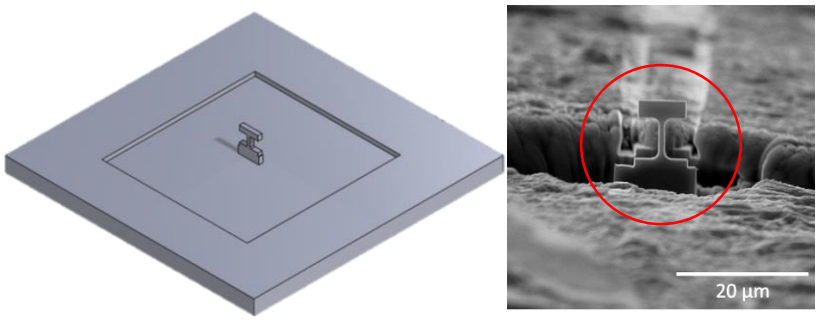

Figure 23: SEM image of a micro-tensile sample.

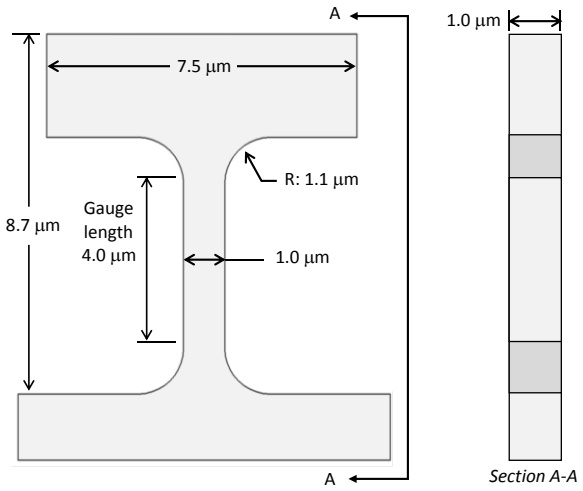

Figure 24: Micro-tensile specimen dimensions.

3.3.5 Grip fabrication

- Following manufacture's recommendation, make alignment marks on the nanoindentation device's tip.
  - Mount the tip on the desired nanoindentation transducer.
  - Using a laser scribe, make two alignment marks near the tip, as shown in Figure 25, to allow for proper tip orientation prior to fabrication of the tensile grip through FIB milling. A circular notch and line-scribe are used

as two alignment sources since the tip will be rotated during fabrication of tensile grip geometry.

- FIB-mill the nanoindentation device's tip to make the tension grip.

  - Place the marked tip on a SEM stub and align the markings as shown in Figure 25.

  - Using the FIB, reduce the width of the indenter tip as shown in Figure 26 (A). Reducing the indenter tip width is helpful in the maneuverability and clearance of the final tensile grip during tension testing.

  - Remove the indenter tip from the SEM, rotate the tip 90 ° using the alignment marks, and reduce the thickness of the indenter tip using the FIB as shown in Figure 26 (B).

  - Remove the indenter tip from the SEM and rotate back to 0 ° (front view) using the alignment marks and create the final tensile grip geometry with the FIB as shown in Figure 26 (C). To reduce re-deposition of the removed material during the FIB process, remove the narrow tensile grip area before removing the wider grip area.

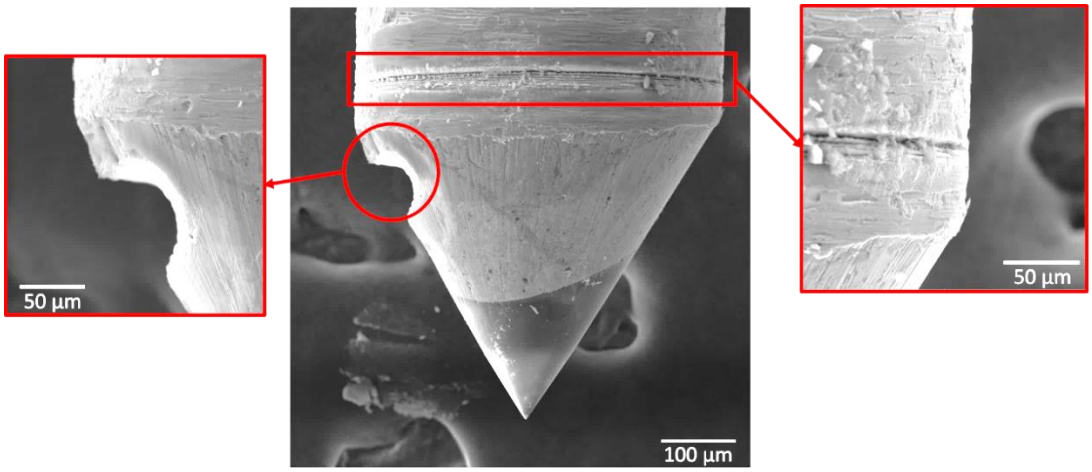

Figure 25: Alignment marks performed in the tip for reference.

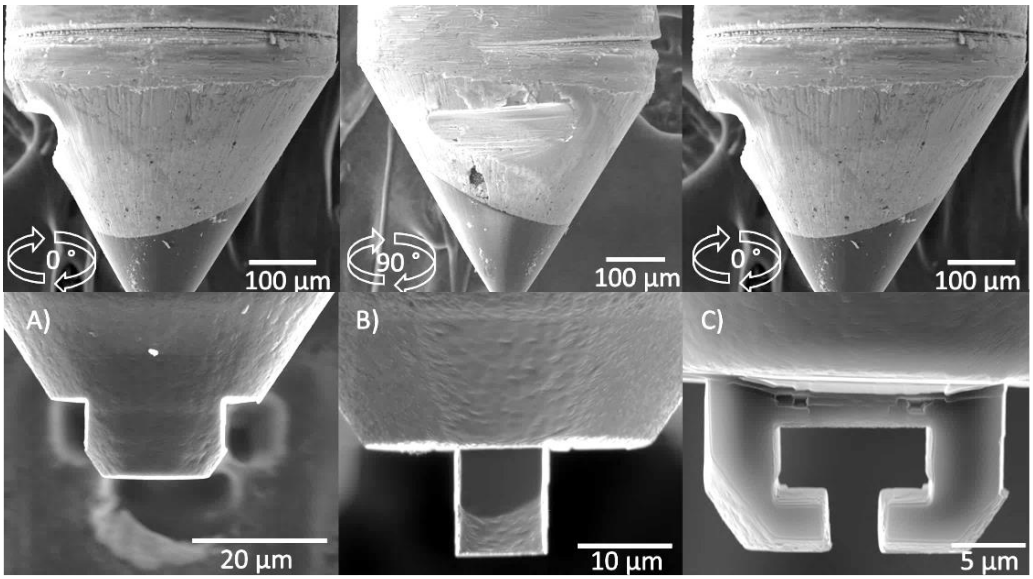

Figure 26: Sequential tensile grip fabrication steps.

3.3.6 Micro-tensile test

- Mount the specimen and indenter tip on the nanoindenter device.
- Install the nanoindentation machine in the SEM following the manufacturer recommendations. To ensure adequate imaging during in-situ testing, it is

recommended to avoid significant machine tilt. For this test, a tilt of 5 ° was used. Excessive tilting will result in a perspective view and make it difficult to align the tensile grip with the test sample.

- To prevent an unexpected event during the tensile testing, it is suggested to perform the desired displacement-based tensile loading protocol in air, away from the sample. This air displacement test will preserve the fabricated tensile grip in the event of unexpected displacements during the protocol.
- With caution, slowly approach the tip to the sample's surface.
- Move and align the tensile grip with the test sample, as shown in Figure 27.
- Perform the tensile test. The test performed in this study considered a displacement-controlled protocol at a rate of 0.004 μm/sec (resulting in an applied strain rate of 0.001 μm/μm/sec for the 4 μm tall specimen), a maximum displacement of 2.5 μm and a returning rate of 0.050 μm/sec. To perform the tensile test in the transducer used for this test, a negative displacement indentation (- 2.5 μm) and negative rate (-0.004 μm/sec) was used.

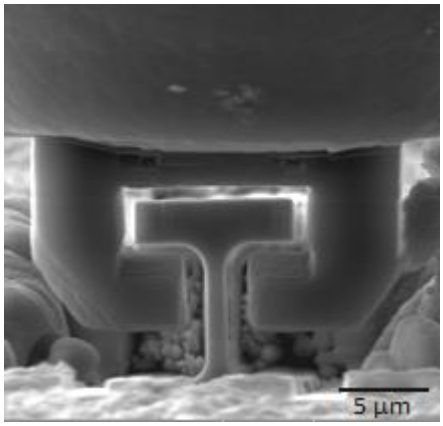

Figure 27: Grip and sample aligned to perform the tensile test.

3.4 Representative Result

A material sample from an AM 17-4 PH stainless steel specimen (previously tested in low-cycle fatigue) was prepared and tested using the protocol described, to understand the fundamental material behavior of AM metals (independent of structural defect influence). Typical sample volumes used for material characterization can contain distributed fabrication/structural defects that make discerning between actual material behavior and structural fabrication effects difficult. Following the protocol described in Sections 2 through 7, a micro specimen was fabricated and tested to failure in tension, successfully demonstrating the described techniques and producing material test data at scales free from volumetric defect influences. Prior to micro-mechanical testing, XRD spectra from the prepared steel surface (see Figure 28), show a mostly martensitic grain structure as would be expected from a previously strained material [10].

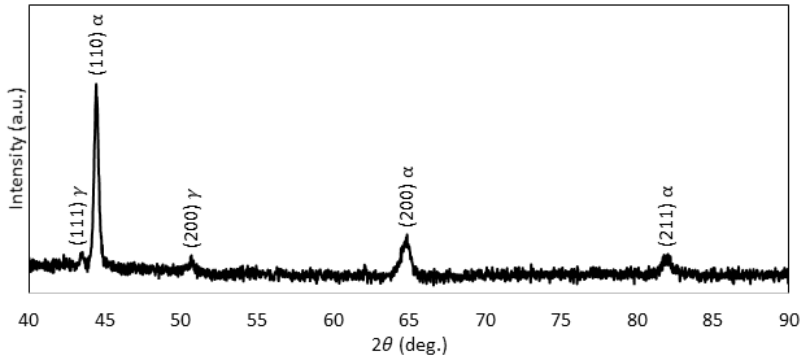

Figure 28: XRD spectra of tested sample.

Figure 29 shows the resulting load-displacement behavior of the micro-tensile AM 17-4 PH steel sample, having a maximum tensile load of 3145 μN at a displacement of 418 nm. From in-situ SEM observations during loading, fracture of the micro-specimen occurred along a single slip plane (typical of a ductile single crystal failure) and different from typical post-yield strain hardening behavior observed during macro-scale material tension testing of AM 17-4 PH stainless

steels. Frames 4-6 of Figure 29 show the single failure slip plane during tension testing of the fabricated micro specimen.

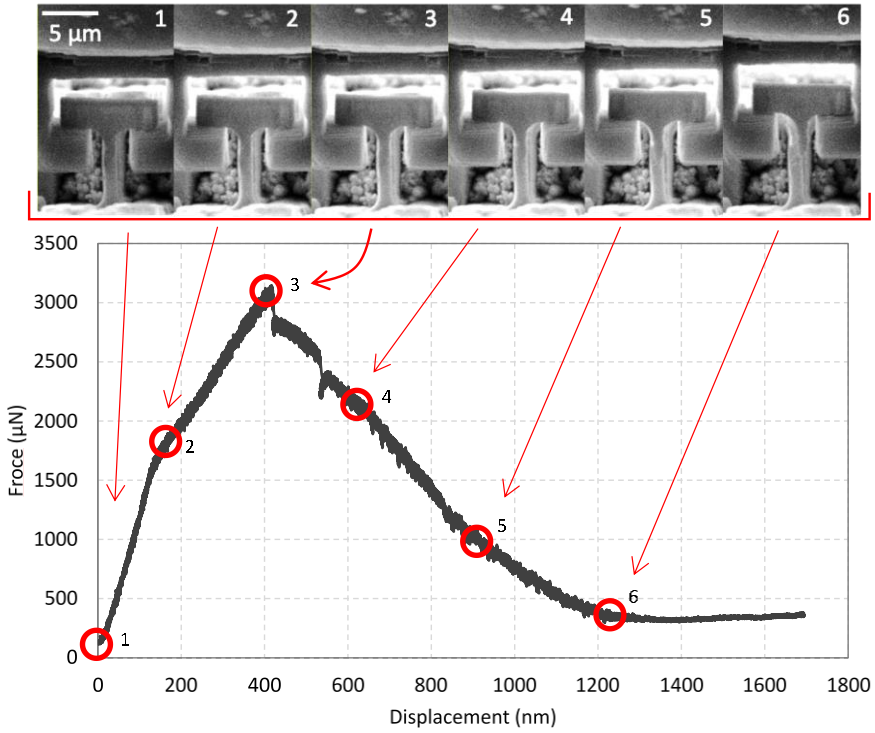

Figure 29: Tensile load-displacement curve of AM 17-4 PH Steel. Top) Frames at different point of the testing.

3.5 Discussion

A verified methodology for AM 17-4 PH stainless steel micro-specimen fabrication and tension testing was presented, including a detailed protocol for fabrication of a micro-tensile grip. Specimen fabrication protocols described result in improved fabrication efficiency by combining photolithography, wet-etching, and FIB milling procedures. Material etching prior to FIB milling helped to remove bulk material and reduce material re-deposition that often occurs during FIB use. The described photolithography and etching procedures allowed for fabrication of the micro-tensile specimens above the surrounding material surface, providing clear access for the tensile

grip prior to testing. While this protocol was described and performed for micro-tensile testing, the same procedures would be helpful for micro-compression testing.

3.5.1 Photolithography process and wet etching.

During the development of this process, variation within the photo-resist mask patterning was noticed, as shown in Figure 17. This is likely caused by surface inconsistencies created during dicing or poor adhesion of the photoresist to the sample surface. It was noticed that when wet etching was performed at room temperature, much of the photoresist was removed, due to under etching or poor adhesion; therefore, it is recommended to warm the sample before and during the etching process, as mentioned in the protocol. If significant under-etching (etching below the photoresist) is noticed, increasing the sample temperature may help. The provided protocol uses an SU-8 photoresist due to availability; however, other photoresist and etchant combinations may also be effective.

3.5.2 Micro-tensile test.

Tensile-grip-to-specimen alignment and sample engagement were the main challenges of the micro-tensile testing. By reducing the indenter tip dimensions as described in the protocol, alignment and engagement between the tensile grip and specimen was improved. Due to SEM view perspective limitations, it was often difficult to tell if the sample was within the tensile grip. Reducing the grip thickness will likely provide better perspective control.

Micro-specimen preparation and micro-tensile material testing is often a lengthy process, requiring several hours of FIB fabrication time and indenter alignment. The methods and protocols prepared herein serves as a verified guide for efficient micro-tensile fabrication and testing. Note that the micro specimen protocol allows for high throughput (rapid) specimen fabrication from

bulk AM 17-4 PH stainless steel volumes by combining photolithography, chemical etching, and FIB milling.

3.6 References

1. Greer, J.R.; Kim, J.-Y.; Burek, M.J. The In-Situ Mechanical Testing of Nanoscale Single-Crystalline Nanopillars. *The Journal of The Minerals, Metals & Materials Society* **2009**, *61*, 19–25, doi:https://doi.org/10.1007/s11837-009-0174-8.

2. Kim, J.Y.; Jang, D.; Greer, J.R. Tensile and Compressive Behavior of Tungsten, Molybdenum, Tantalum and Niobium at the Nanoscale. *Acta Mater* **2010**, *58*, 2355–2363, doi:10.1016/j.actamat.2009.12.022.

3. Kim, J.Y.; Greer, J.R. Tensile and Compressive Behavior of Gold and Molybdenum Single Crystals at the Nano-Scale. *Acta Mater* **2009**, *57*, 5245–5253, doi:10.1016/J.ACTAMAT.2009.07.027.

4. Kihara, Y.; Nagoshi, T.; Chang, T.F.M.; Hosoda, H.; Tatsuo, S.; Sone, M. Tensile Behavior of Micro-Sized Specimen Made of Single Crystalline Nickel. *Mater Lett* **2015**, *153*, 36–39, doi:10.1016/J.MATLET.2015.03.119.

5. Kiener, D.; Grosinger, W.; Dehm, G.; Pippan, R. A Further Step towards an Understanding of Size-Dependent Crystal Plasticity: In Situ Tension Experiments of Miniaturized Single-Crystal Copper Samples. *Acta Mater* **2008**, *56*, 580–592, doi:10.1016/J.ACTAMAT.2007.10.015.

6. Sumigawa, T.; Byungwoon, K.; Mizuno, Y.; Morimura, T.; Kitamura, T. In Situ Observation on Formation Process of Nanoscale Cracking during Tension-Compression Fatigue of Single Crystal Copper Micron-Scale Specimen. *Acta Mater* **2018**, *153*, 270–278, doi:10.1016/J.ACTAMAT.2018.04.061.

7. Kiener, D.; Minor, A.M. Source Truncation and Exhaustion: Insights from Quantitative in Situ TEM Tensile Testing. *Nano Lett* **2011**, *11*, 3816–3820, doi:10.1021/nl201890s.

8. Reichardt, A.; Ionescu, M.; Davis, J.; Edwards, L.; Harrison, R.P.; Hosemann, P.; Bhattacharyya, D. In Situ Micro Tensile Testing of He+2 Ion Irradiated and Implanted Single Crystal Nickel Film. *Acta Mater* **2015**, *100*, 147–154, doi:10.1016/j.actamat.2015.08.028.

9. Nageswara Rao, P.; Kunzru, D. Fabrication of Microchannels on Stainless Steel by Wet Chemical Etching. *Journal of Micromechanics and Microengineering* **2007**, *17*, doi:10.1088/0960-1317/17/12/N01.

10. Okayasu, M.; Fukui, H.; Ohfuji, H.; Shiraishi, T. Strain-Induced Martensite Formation in Austenitic Stainless Steel. *J Mater Sci* **2013**, *48*, 6157–6166, doi:10.1007/s10853-013-7412-8.

Chapter 4: Micro-Mechanical Characterization of Selective Laser Melting 17-4 PH (AISI 630) Stainless Steels through In-Situ SEM Experimentation

4.1 Research Objective and Finding

Metal additive manufacturing (AM) technologies, such as selective laser melting (SLM), allow for rapid fabrication of geometrically complex parts that would be difficult to create using traditional casting or subtractive fabrication processes. Research into AM metals has shown that fabrication defects resulting from SLM processes (i.e. voids, un-melted particles, etc.) can have deleterious effects on mechanical behavior. Material testing using traditional macro (coupon-scale) volumes may not accurately capture actual material behavior, as the distribution of fabrication defects is volume dependent. To understand fundamental material behavior at scales independent of geometrical fabrication defects, this project conducts in-situ micro-tensile testing of AM SLM 17-4 PH stainless steel materials. Comparison between micro-tensile testing and bulk (macro) tensile testing indicate that micro-tensile specimens have a greater ultimate tensile strength (1359 MPa ± 99.9 MPa) and strain before failure (0.31 ± 0.063) than the macro-tensile specimens (1025 MPa tensile strength and 0.190 strain at fracture respectively).

4.2 Introduction

Small-scale mechanical testing (SSMT) has been of particular interest in the study of micro-material behavior by applying macro-scale concepts to micro-level research. For instance, micro-tensile testing has been widely used to understand the performance of materials at the micro- and nanoscale, because inferring nano-mechanical behavior from bulk properties is not accurate due to size-dependent properties [1]. Mechanical testing at this scale provides an understanding of a single crystal's performance [1–7] or specific microstructure [8] via isolation, along with other

types of material research. Kim et al. [3] performed tensile and compression tests at the nanoscale on four body centered cubic metals – tungsten, molybdenum, tantalum, and niobium- and found that yield strength is a strong function of size, but strain hardening is not. In a different field, Casari et al. [9,10] used micro-tensile tests to study properties and failure mechanism of bones, finding a size effect on properties - strength decreased with increasing specimen size.

Moreover, micro-tensile testing could be beneficial for the additive manufacturing (AM) industry by enabling the examination of parts at a scale level where macro fabrication defects are non-existent. A popular AM technique is selective laser melting (SLM), which relies on a high-power laser to melt layers of metal powder to produce a near fully dense part. During this melting process, a fine microstructure is created by a high cooling rate [11,12], influencing its mechanical behavior. Additionally, voids and un-melted regions, referred to as crack initiators, are formed during this process which are of great concern due to their detrimental effect on SLM parts [13,14], especially during cyclic loading [13,15–18]. The randomness of these manufacturing defects' dispersion poses further complexities for material behavior prediction. Particularly, defects are volume-dependent, possibly indicating scale-dependent performance [19]. Thus, sample volume could temper mechanical behavior on SLM parts, questioning the accuracy of laboratory specimen testing to predict the performance of actual parts with complex geometries [15].

The 17-4 PH stainless steel is a popular material among AM studies. It is characterized by great strength and corrosion resistance, making it suitable for numerous industries. Its microstructure is constituted by austenite and martensite which its ratio (austenite|martensite) impacts material properties [20]. LeBrun et al. [20] analyzed the performance of SLM 17-4 PH steel with different post-processing heat treatments and found that samples with a higher austenite content displayed lower yield strength as well as greater work-hardening and ductility when

compared to those with a higher martensite structure. Upon tensile testing, SLM 17-4 PH steel performs similarly to its wrought counterpart [17,21]. Nevertheless, when subjected to cyclic loading, SLM 17-4 PH steel underperforms. Voids and un-melted regions are responsible for material reduced fatigue life by operating as crack initiation sites [16,17]. During high- and low-cycle fatigue, heat treatment could improve the performance of the material [16]; yet, in ultra-low cycle fatigue, it may not be effective [17]. Thus, a proper understanding of this material is crucial for the development of predictive models and, therefore, the integration of SLM 17-4 PH in structural applications.

In this study, in-situ micro-tensile experimentation was used to characterize SLM 17-4 PH steel. The tests were performed as displacement controlled using a pico-indenter with a customized diamond tip as the sample grip. For comparison, micro-tensile specimens were fabricated by focused ion beam (FIB) from the un-strained and pre-strained area of an as-built SLM 17-4 PH sample used in a previous study. This work seeks to highlight research gaps regarding SLM 17-4 PH performance at the micro-scale. Previous work done by AlMangour et al. [22] assessed micro-compression on this material, however, no evidence of micro-tensile testing has been published.

4.3 Materials and experimental procedure

4.3.1 Hardness and Elastic Modulus

A nano-indenter (TriboIndenter, Hysitron) was used to perform load-controlled indentations to various maximum normal loads using an indentation probe with a diamond Berkovich tip that has a 150 nm tip-radius. The elastic modulus and hardness of the material were calculated according to the methods developed by Oliver and Pharr [23,24]. Three indentations

were performed to each maximum normal load of 1000, 2000, 3000, 4000, 5000, 6000, 7000, and 8000 µN with loading and unloading rates of 100 µN/s and a holding time of 5 s.

4.3.2 Micro-tensile material behavior

Table 6: Chemical composition of the etchant used.

$FeCl_3$ (wt%)	HCl (wt%)	HNO_3 (wt%)	Ref.
10	10	5	[25]

Micro-tensile specimens were fabricated from an as-built SLM 17-4 PH sample. A section of the gauge and a section from the grip area, from the bulk sample that was tested in [17], were used to fabricate and test the micro tensile sample, as shown in Figure 30. Photolithography and wet etching were used to fabricate micro-columns where micro-tensile dog bones were milled via Focused Ion Beam (FIB). For the photolithography process, SU-8 was used as the photoresist, while the aqueous etchant shown in Table 6 was used to perform the etching. A FEI Nova Nanolab 200 Dual-Beam FIB-SEM operated at 30 kV and 20 nA was used to remove the bulk material of the micro column. FIB power was reduced on every milling step. For the final dog-bone mill-process, a power of 0.3 nA and 30 kV was used. The micro dog bone has dimensions of 1µm wide by 4 µm tall in the gauge area, as shown in Figure 31, while thickness ranges from 1µm up to 2 µm. A more detailed sample fabrication procedure is described in [26].

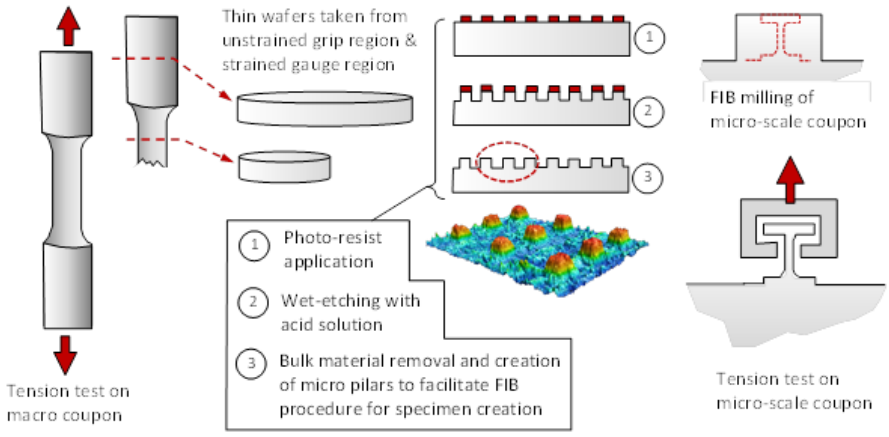

Figure 30: Sample preparation and test methodology flow chart.

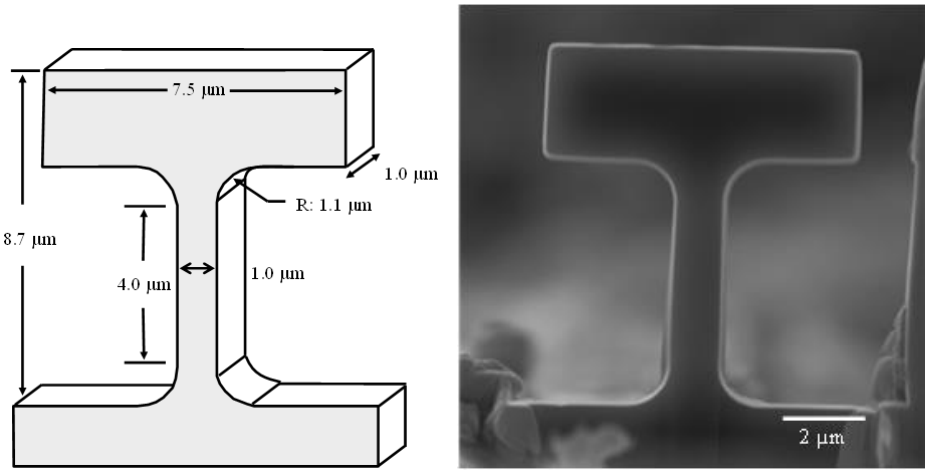

Figure 31: Micro-tensile specimen dimensions.

A picoindenter Hysitron PI-88 was used to perform in-situ micro tensile experiments in a SEM Tescan Vegas 3. To form the sample grip, a T-shaped slit was FIB milled from a diamond tip with a 60˚cone shape. For a better orientation during the grip fabrication, a laser scriber was used to perform alignment marks on the tip. Figure 32 shows a visual procedure of the sample grip fabrication. First, three cuts were made to the tip to remove the cone-shape and make a 20 µm wide square. Then, the tip was rotated 90° to reduce the square depth to 10 µm. Finally, the tip

was rotated 90°, and the final T- shaped slit was milled. Tensile tests were performed as displacement controlled at 4 nm/s (10^{-3} s^{-1} strain rate). A more detailed experimental procedure can be found in [26]. An in-house Matlab code was used to measure the displacement of the sample from the in-situ SEM video. Micro-tensile test results were compared to macro-scale tensile test.

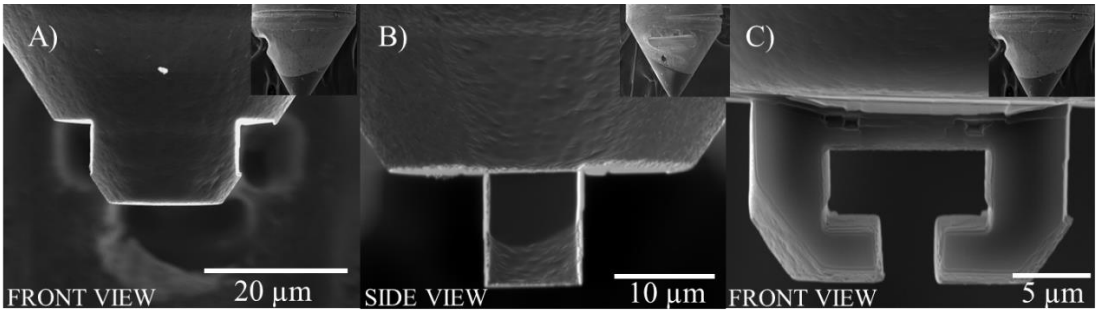

Figure 32: Visuals of sample grip fabrication procedure.

4.3.3 In-Situ Strain Measurement Correction using Matlab Script

A Matlab code was developed to perform a strain correction using videos taken during the in-situ test. In summary, the code reads the video taken from the test as show in Figure 33A. Then, the video is crops the video in a rectangular shape; the width should be as close to the gage dimension, and the height should cover part of the head the specimen and should be slightly higher than the yellow line that appears in the video, as shown in the Figure 33B. Then, some filtering process and thresholding definition is applied to convert the video to black and white, displaying our object of interest as white, as shown in the image Figure 33C. All white objects detected by the code are boxed using boundingbox function. The box 1 is the square that is above the yellow line and box 2 is the head of the specimen, as shown in Figure 33D. The displacement of the tensile specimen is calculated using *extrema* function, by tracking the pixel location of both top corners of the box 2 (specimen) along the video. The Matlab code can be found in Appendix A.

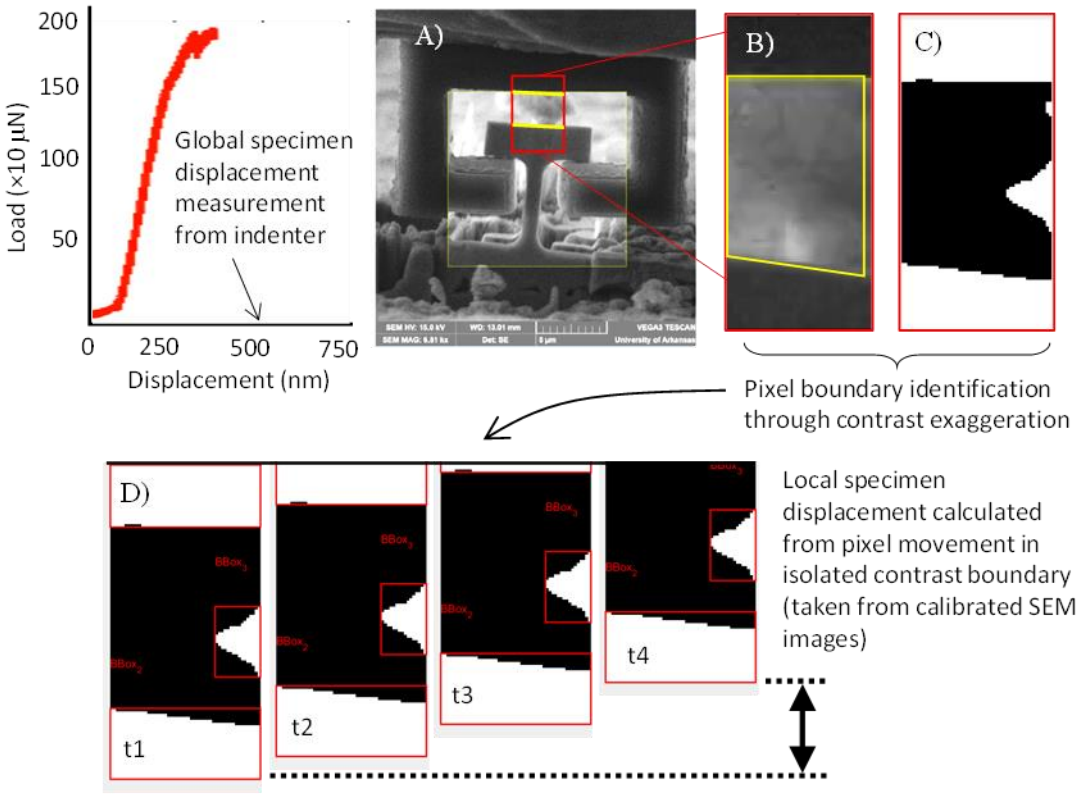

Figure 33: Illustration of specimen strain correction procedure.

4.3.4 Micro-compression behavior

Micro-pillars of ~4 μm of diameter and ~12-14 μm tall were fabricated via FIB. A maximum power of 30 kV and 20 nA was used to remove the outer material, and current was decreased while reaching to the desired diameter. The final diameter was milled at 30 kV and 0.3 nA. Figure 34 shows a micro-compression specimen. A flat punch with a diameter of 10 μm was used to performed micro-compression test. Three micro-compression tests were done as displacement controlled at 4 nm/s (strain rate ~0.0003 /s) and one was done at 10 nm/s (strain rate ~0.00083 /s) using a pico-indenter Hysitron PI-88.

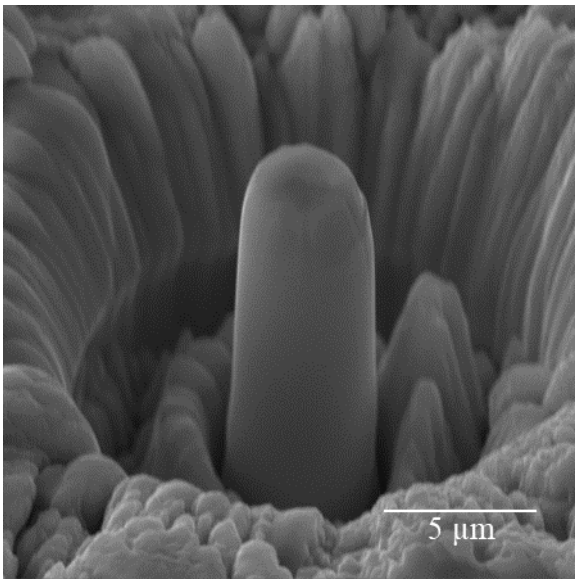

Figure 34: Micro-compression sample geometry.

4.4 Results/Discussion

4.4.1 Elastic Modulus and hardness

Figure 35 shows the load-displacement plots from one indentation performed to each maximum normal load of 1000, 2000, 3000, 4000, 5000, 6000, 7000, and 8000 μN. The modulus of Elasticity (E) and hardness (H) of the material were determined through analysis of the load-displacement behavior [23,24] and these measurements are shown in Figure 36 and Figure 37, respectively. Across all indentations, the average E is 187.6 ± 18.2 GPa, and the average H is 6.52 ± 0.81 GPa. E and H were greater at the lower indentation loads than at the higher loads, which is commonly observed due to the nanoscale indentation size effect [27,28]. It should be noted that the boundary conditions present during indentation differ from those of the micro-compression testing. During indentation, surrounding material provides confinement and a modified stress state within the material as compared to that of the micro-compression testing. For this reason both micro-compression and nano-indentation are performed and compared herein.

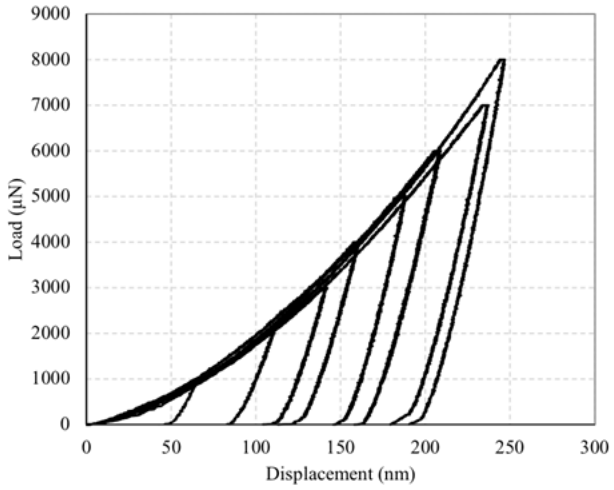

Figure 35: Load-Displacement curves for 1000-8000 µN indents on SLM 17-4 PH Steel using Berkovich indenter.

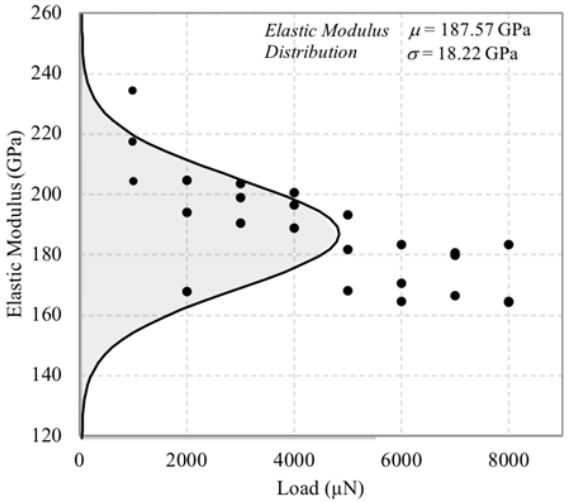

Figure 36: Elastic modulus of SLM 17-4 PH steel measured by nanoindentation.

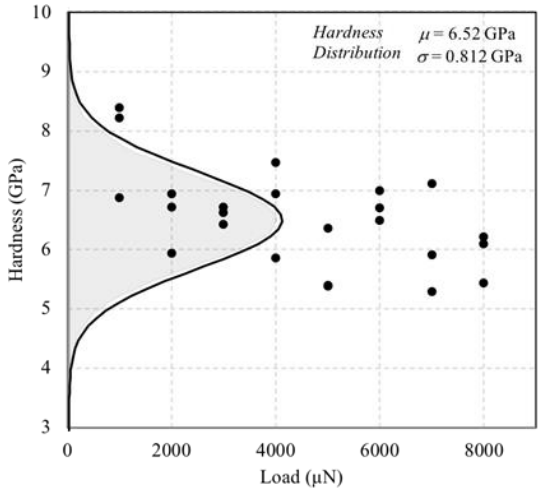

Figure 37: Hardness of SLM 17-4 PH steel measured by nanoindendation.

4.4.2 Micro-specimens versus Macro-specimens

Micro-compression behavior from the grip section from a SLM 17-4 PH steel is shown in Figure 38, where an average compressive yield strength of 759 MPa ± 207 MPa was seen. A strain-hardening can be observed, possibly due to the presence of retained-austenite as observed by AlMangour et al. in [22]. Also, in Figure 38, tensile test from the grip section is shown, where a maximum UTS of 1413 MPa and an average of 1359 MPa ± 99.9 MPa, while a maximum strain at failure of 0.425 with an average of 0.31 ± 0.063 was measured. A reduction of 19% in average strain is observed when samples from the grip are compared to the gage section, while average UTS in each section was similar. A maximum UTS of 1526 MPa with an average of 1329 MPa ± 183 MPa was observed for the gage section, shown in Figure 39, and a maximum strain at failure of 0.313 with an average of 0.25 ± 0.039 was measured. A difference in mechanical behavior can be seen when comparison is made between micro- and macro- scale tensile test.

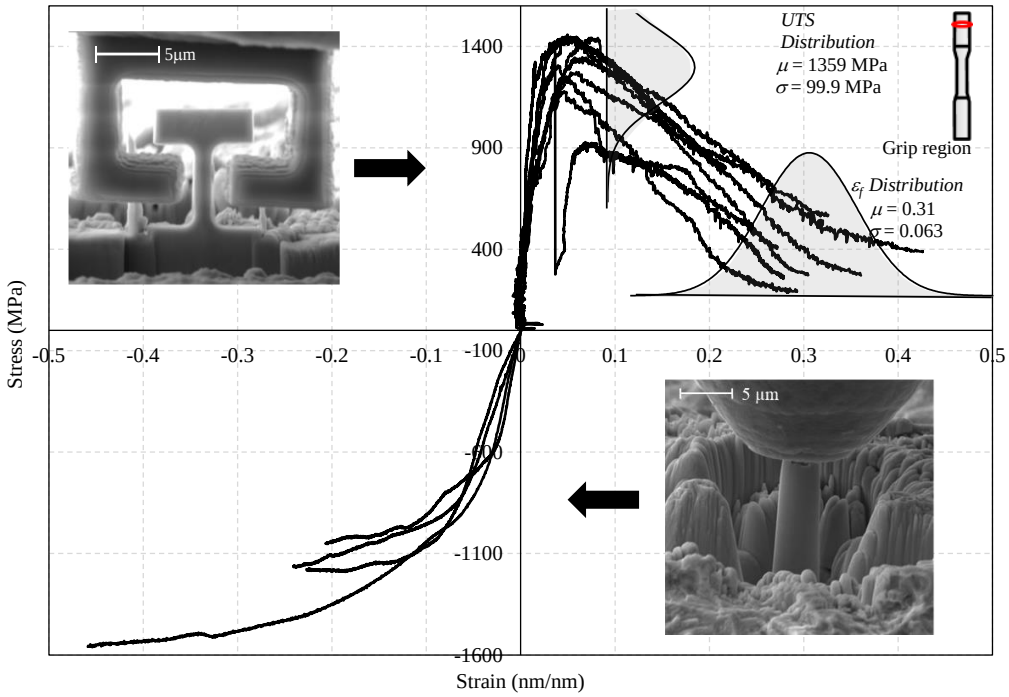

Figure 38: Stress-strain micro-tensile and micro-compression behavior of SLM 17-4 PH steel from the grip area.

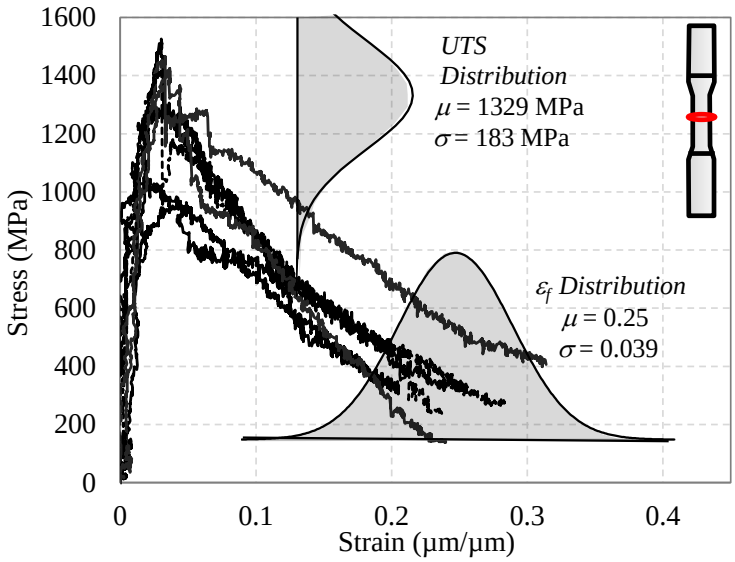

Figure 39: Stress-strain micro-tensile behavior of SLM 17-4PH Steel from the pre-strained (gage) area.

Table 7: Macro- and micro- tensile properties of SLM 17-4 PH steel.

Material	Yield (0.2%) (MPa)	UTS (MPa)	Fracture Strain
Bulk SLM 17-4 PH as-built	720.5	1115	0.22
Micro SLM 17-4 PH as-built (grip)	1266	1359 ± 99.9	0.31 ± 0.063

Micro-tensile specimens, when compared to macro-specimen, exhibit an improved yield strength (0.2%), UTS and strain at failure by 75%, 21%, and 41%, respectively, shown in Table 7. However, a significant difference in strain-hardening in macro-scale can be appreciated in Figure 40. For micro-specimens, the UTS is reached at ~5% strain while for macro-scale, UTS is reached at ~18% strain. This strain-hardening behavior is very common on SLM 17-4 PH as-built samples due to the presence of retained-austenite [16,20].

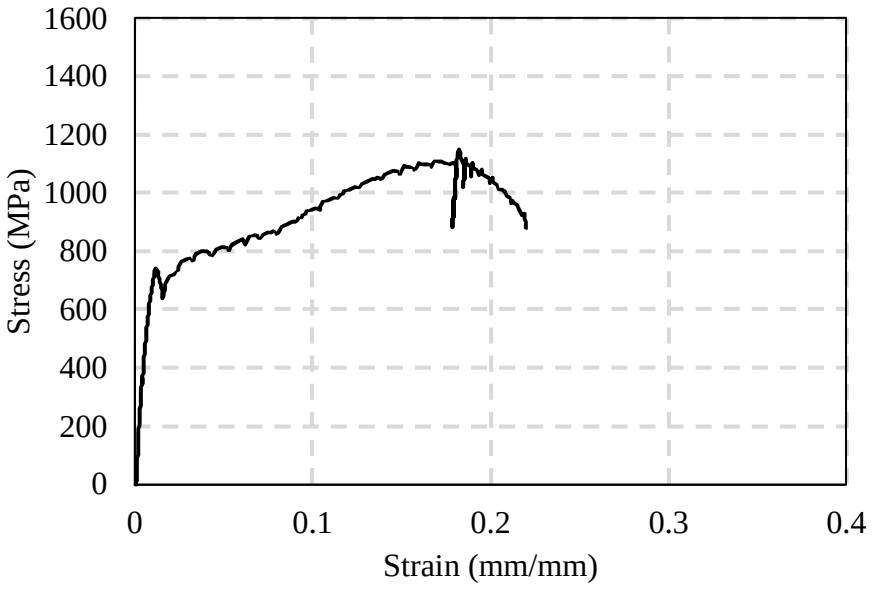

Figure 40: Stress-strain tensile curve of macro-scale SLM 17-4 PH steel.

The absence of macro SLM fabrication induced defects, such as voids, un-melted particles, and partially melted regions, can play a role in the difference in mechanical behavior between micro and macro scales. A significant number of studies have shown the detrimental role that these defects play in the performance of SLM parts [13,15–17,20]. Also, scale dependency of properties has been reported for micro- and nano- scale specimens [3,6,29–31]. Two mechanisms, truncation of spiral dislocation source and exhaustion of defects, have been discussed to explain high strength in small specimens [31].

Another difference between micro- and macro- tensile specimen can be appreciated in the fracture surface, where some micro-specimens exhibit shear failure, shown in Figure 41, compared to the ductile cone and cup fracture from the macro-scale specimen, shown in Figure 42. Figure 41 shows post-tensile fracture surface (A & B from grip section and C & D from gage section) of some specimen. Fracture surface shown in A and C resemble a 45˚shear failure, which is typical of ductile single crystal failure. On the other hand, Figure 41 B) and D) show a fracture surface which could indicate a different failure mechanism in these two samples. Although different fracture surfaces were seen in micro-tensile specimens, no correlation between fracture surface and mechanical behavior was seen.

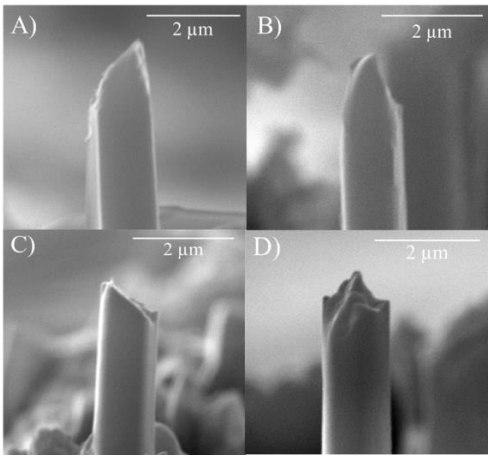

Figure 41: Fracture surface post-micro-tensile test. A & B show fracture surface from grip section and C & D show fracture surface from gage section.

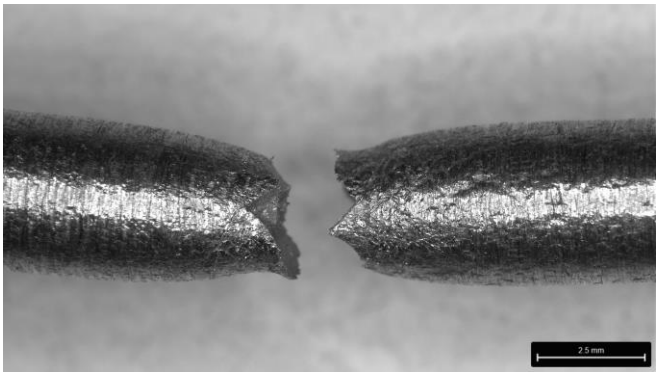

Figure 42: Ductile fracture from macro-tensile specimen.

The ability to perform mechanical testing at micro- and nano- scale, could open the possibility of further understanding on the influence of microstructure to mechanical performances of SLM parts. The combination of SSMT with other characterization techniques such as EBSD, can be used to isolate a microstructure feature as a phase or melting pool, and use the information for a microstructure based predictive model.

4.5 Conclusion

A series of SSMT (micro-compression, micro-tensile, and nano-indentation) were used to characterize *as-built* SLM 17-4 PH steel. Results from micro- and macro- tensile specimens were compared. In general, an elastic modulus of 187.6 GPa was measured via nano-indentation. A difference in tensile behavior in macro- and micro- specimen was seen. A significant strain hardening was observed for the macro-specimen, reaching the UTS at 18% strain, while for micro-specimen UTS was reached at ~ 5%. On the other hand, an UTS of 1359 MPa and 1329 MPa were measured during micro-tensile test, from the grip and gage section, which is ~21% higher than the bulk SLM 17-4 PH. Difference in mechanical performance can be attributed to the lack of macro fabrication induced defects in micro- specimens, or to other hardening mechanism in micro-scale testing such as truncation of spiral dislocation source and exhaustion of defects.

4.6 References

1. Greer, J.R.; Kim, J.-Y.; Burek, M.J. The In-Situ Mechanical Testing of Nanoscale Single-Crystalline Nanopillars. *JOM* **2009**, *61*, 19–25, doi:10.1007/s11837-009-0174-8.
2. Sumigawa, T.; Byungwoon, K.; Mizuno, Y.; Morimura, T.; Kitamura, T. In Situ Observation on Formation Process of Nanoscale Cracking during Tension-Compression Fatigue of Single Crystal Copper Micron-Scale Specimen. *Acta Mater* **2018**, *153*, 270–278, doi:10.1016/J.ACTAMAT.2018.04.061.
3. Kim, J.Y.; Greer, J.R. Tensile and Compressive Behavior of Gold and Molybdenum Single Crystals at the Nano-Scale. *Acta Mater* **2009**, *57*, 5245–5253, doi:10.1016/J.ACTAMAT.2009.07.027.
4. Xu, A.; Susanto, I.; Wei, T.; Ionescu, M.; Daniels, J.; Bhattacharyya, D. Investigation of Mechanical Property Changes in He2+ Ion Irradiated MA957 through Nanoindentation and in Situ Micro-Tensile Testing. *Journal of Nuclear Materials* **2021**, *547*, doi:10.1016/j.jnucmat.2021.152819.
5. Li, X.; Minor, A.M. Precise Measurement of Activation Parameters for Individual Dislocation Nucleation during in Situ TEM Tensile Testing of Single Crystal Nickel. *Scr Mater* **2021**, *197*, doi:10.1016/j.scriptamat.2021.113764.
6. Kiener, D.; Grosinger, W.; Dehm, G.; Pippan, R. A Further Step towards an Understanding of Size-Dependent Crystal Plasticity: In Situ Tension Experiments of Miniaturized Single-

Crystal Copper Samples. *Acta Mater* **2008**, *56*, 580–592, doi:10.1016/J.ACTAMAT.2007.10.015.

7. Kihara, Y.; Nagoshi, T.; Chang, T.F.M.; Hosoda, H.; Tatsuo, S.; Sone, M. Tensile Behavior of Micro-Sized Specimen Made of Single Crystalline Nickel. *Mater Lett* **2015**, *153*, 36–39, doi:10.1016/J.MATLET.2015.03.119.

8. Du, C.; Hoefnagels, J.P.M.; Bergers, L.I.J.C.; Geers, M.G.D. A Uni-Axial Nano-Displacement Micro-Tensile Test of Individual Constituents from Bulk Material. *Exp Mech* **2017**, *57*, 1249–1263, doi:10.1007/s11340-017-0299-6.

9. Casari, D.; Michler, J.; Zysset, P.; Schwiedrzik, J. Microtensile Properties and Failure Mechanisms of Cortical Bone at the Lamellar Level. *Acta Biomater* **2021**, *120*, 135–145, doi:10.1016/j.actbio.2020.04.030.

10. Casari, D.; Kochetkova, T.; Michler, J.; Zysset, P.; Schwiedrzik, J. Microtensile Failure Mechanisms in Lamellar Bone: Influence of Fibrillar Orientation, Specimen Size and Hydration. *Acta Biomater* **2021**, *131*, 391–402, doi:10.1016/j.actbio.2021.06.032.

11. Xiong, Z.H.; Liu, S.L.; Li, S.F.; Shi, Y.; Yang, Y.F.; Misra, R.D.K. Role of Melt Pool Boundary Condition in Determining the Mechanical Properties of Selective Laser Melting AlSi10Mg Alloy. *Materials Science and Engineering: A* **2019**, *740–741*, 148–156, doi:10.1016/J.MSEA.2018.10.083.

12. Ben, D.D.; Ma, Y.R.; Yang, H.J.; Meng, L.X.; Shao, X.H.; Liu, H.Q.; Wang, S.G.; Duan, Q.Q.; Zhang, Z.F. Heterogeneous Microstructure and Voids Dependence of Tensile Deformation in a Selective Laser Melted AlSi10Mg Alloy. *Materials Science and Engineering: A* **2020**, *798*, 140109, doi:10.1016/J.MSEA.2020.140109.

13. Carlton, H.D.; Haboub, A.; Gallegos, G.F.; Parkinson, D.Y.; MacDowell, A.A. Damage Evolution and Failure Mechanisms in Additively Manufactured Stainless Steel. *Materials Science and Engineering: A* **2016**, *651*, 406–414, doi:https://doi.org/10.1016/j.msea.2015.10.073.

14. Suryawanshi, J.; Prashanth, K.G.; Ramamurty, U. Mechanical Behavior of Selective Laser Melted 316L Stainless Steel. *Materials Science and Engineering A* **2017**, *696*, 113–121, doi:10.1016/j.msea.2017.04.058.

15. Yadollahi, A.; Shamsaei, N. Additive Manufacturing of Fatigue Resistant Materials: Challenges and Opportunities. *Int J Fatigue* **2017**, *98*, doi:10.1016/j.ijfatigue.2017.01.001.

16. Yadollahi, A.; Shamsaei, N.; Thompson, S.M.; Elwany, A.; Bian, L. Effects of Building Orientation and Heat Treatment on Fatigue Behavior of Selective Laser Melted 17-4 PH Stainless Steel. *Int J Fatigue* **2017**, *94*, doi:10.1016/j.ijfatigue.2016.03.014.

17. Gonzalez-Nino, D.; Strasser, T.; Prinz, G.S. Ultra Low-Cycle Fatigue Behavior Comparison between Additively Manufactured and Rolled 17-4 Ph (Aisi 630) Stainless Steels. *Metals (Basel)* **2021**, *11*, doi:10.3390/met11111726.

18. Mower, T.M.; Long, M.J. Mechanical Behavior of Additive Manufactured, Powder-Bed Laser-Fused Materials. *Materials Science and Engineering: A* **2016**, *651*, doi:10.1016/j.msea.2015.10.068.

19. Dzugan, J.; Seifi, M.; Prochazka, R.; Rund, M.; Podany, P.; Konopik, P.; Lewandowski, J.J. Effects of Thickness and Orientation on the Small Scale Fracture Behaviour of Additively Manufactured Ti-6Al-4V. *Mater Charact* **2018**, *143*, 94–109, doi:10.1016/j.matchar.2018.04.003.

20. LeBrun, T.; Nakamoto, T.; Horikawa, K.; Kobayashi, H. Effect of Retained Austenite on Subsequent Thermal Processing and Resultant Mechanical Properties of Selective Laser Melted 17–4 PH Stainless Steel. *Mater Des* **2015**, *81*, doi:10.1016/j.matdes.2015.05.026.

21. Mahmoudi, M.; Elwany, A.; Yadollahi, A.; Thompson, S.M.; Bian, L.; Shamsaei, N. Mechanical Properties and Microstructural Characterization of Selective Laser Melted 17-4 PH Stainless Steel. *Rapid Prototyp J* **2017**, *23*, doi:10.1108/RPJ-12-2015-0192.

22. AlMangour, B.; Yang, J.M. Understanding the Deformation Behavior of 17-4 Precipitate Hardenable Stainless Steel Produced by Direct Metal Laser Sintering Using Micropillar Compression and TEM. *International Journal of Advanced Manufacturing Technology* **2017**, *90*, 119–126, doi:10.1007/s00170-016-9367-9.

23. Oliver, W.C.; Pharr, G.M. An Improved Technique for Determining Hardness and Elastic Modulus Using Load and Displacement Sensing Indentation Experiments. *J Mater Res* **1992**, *7*, 1564–1583, doi:10.1557/JMR.1992.1564.

24. Namburi, H.; Oliver, W.C.; Pharr, G.M. *Measurement of Hardness and Elastic Modulus by Instrumented Indentation: Advances in Understanding and Refinemen... Measurement of Hardness and Elastic Modulus by Instrumented Indentation: Advances in Understanding and Refinements to Methodology*; 2004;

25. Nageswara Rao, P.; Kunzru, D. Fabrication of Microchannels on Stainless Steel by Wet Chemical Etching. *Journal of Micromechanics and Microengineering* **2007**, *17*, doi:10.1088/0960-1317/17/12/N01.

26. Gonzalez-Nino, D.; Sonntag, S.; Afshar-Mohajer, M.; Goss, J.; Zou, M.; Prinz, G.S. Micromechanical Tension Testing of Additively Manufactured 17-4 Ph Stainless Steel Specimens. *Journal of Visualized Experiments* **2021**, *2021*, doi:10.3791/62433.

27. Broitman, E. Indentation Hardness Measurements at Macro-, Micro-, and Nanoscale: A Critical Overview. *Tribol Lett 65*, doi:10.1007/s11249-016-0805-5.

28. Pharr, G.M.; Herbert, E.G.; Gao, Y. The Indentation Size Effect: A Critical Examination of Experimental Observations and Mechanistic Interpretations. **2010**, doi:10.1146/annurev-matsci-070909-104456.

29. Kim, J.Y.; Jang, D.; Greer, J.R. Tensile and Compressive Behavior of Tungsten, Molybdenum, Tantalum and Niobium at the Nanoscale. *Acta Mater* **2010**, *58*, 2355–2363, doi:10.1016/j.actamat.2009.12.022.

30. Greer, J.R.; Kim, J.-Y.; Burek, M.J. The In-Situ Mechanical Testing of Nanoscale Single-Crystalline Nanopillars. *The Journal of The Minerals, Metals & Materials Society* **2009**, *61*, 19–25, doi:https://doi.org/10.1007/s11837-009-0174-8.

31. Kiener, D.; Minor, A.M. Source Truncation and Exhaustion: Insights from Quantitative in Situ TEM Tensile Testing. *Nano Lett* **2011**, *11*, 3816–3820, doi:10.1021/nl201890s.

Chapter 5: Framework for Micromechanical Based Modeling of Selective Laser Melting 17-4 PH Steel Using Statistical and Representative Volume Element

5.1 Research Objectives and Findings

This study explores a framework to develop a predictive model calibrated with micromechanical testing for SLM 17-4 PH stainless steel using statistical and representative volume element. Results from the previous chapter were used in an upscaling procedure to predict the macro-mechanical behavior. Also, the effects of voids in SLM 17-4 PH stainless steel were studied using statistical volume element. Python|Abaqus Scripts were developed to perform mechanical properties upscaling and void study.

When compared to experimental data, the proposed methodology predicts with low accuracy the mechanical behavior of SLM 17-4 PH steel. To improve accuracy, it is suggested to perform mechanical testing at the meso-scale and to combine other material characterization techniques, such as EBSD, with small scale mechanical testing.

5.2 Introduction

Selective Laser Melting (SLM) is an additive manufacturing (AM) process where parts are fabricated by melting layers of metal powder by a high-powered laser. The resulting parts hold a complex refined microstructure due to the thermal history and rapid solidification subjected during the fabrication [1–6] which results in a heterogeneous and anisotropic specimen. Along with this, voids and un-melted particles contribute to the performance unpredictability of AM parts, especially during low cycle fatigue [1,2,7]. This creates a challenge for the full adoption of AM technologies in commercial applications. Great effort has been placed on characterizing mechanical properties of AM metals; however, there are concerns that the mechanical behavior of

laboratory specimens may not be applicable for parts of different size or geometries due to difference in thermal history [1], and possibly a volume dependency of defects. Therefore, predicting the mechanical performance of AM parts is of great importance for future implementation of AM technologies in commercial applications.

Building a homogenous defect-free AM part is challenging, considering that any slight change in printing parameter, building orientation, or part size will influence the thermal history and hence, the microstructure, possibly resulting in a change of mechanical behavior [1,2,8]. Thus, microstructural based predictive models, where microstructure and defect characteristics can be integrated, are suggested as an approach to model AM parts [1]. A model based on internal state variable plasticity-damage was used in [9], where a prediction was made by creating a lower and upper bound estimation. To calibrate this model, the authors examined samples and performed a quantification of the defects. Other microstructural based models have successfully approximated the mechanical behavior of AM parts using microstructural features such as precipitate particles and porosity [10,11]. Although these models have been able to perform predictions on the performance of AM parts, none are based on mechanical tests at the microstructural scale. The scope of this article is to present a framework to develop models calibrated by micro-mechanical testing.

Micro-mechanical testing has opened the possibility to characterize material at small scale, where properties are typically inferred from the bulk [12]. However, small-scale mechanical testing has been used to predict macro-scale behavior on heterogeneous materials, such as cementitious composites in [13] where nanoindentation was used to predict the elastic properties of high-performance cementitious concrete. Some attempts to predict bulk properties based on microstructure involve the use of a homogenization method.

Representative Volume Element (RVE) is a homogenization technique frequently used in multiscale modeling and heterogeneous material simulation, such as for composite and cementitious materials. It is defined as the smallest volume that shows largescale behavior [14]. This technique is typically used to understand the effect that microstructure or small components of the bulk material have on mechanical behavior of the macroscale. In [15], RVEs with randomly distributed fibers were used to predict the mechanical performance of a fiber reinforced composite with a high fiber volume fraction. Results were compared to experimental values, and it achieved comparable results. Shahzamanian et al. [14,16] has performed extensive studies on using RVEs to model cementitious materials. Yin, et al. [17] used a smaller version of RVE, called statistical volume elements (SVE) to study the effect of voids in metals.

The present work shows a basic framework on the development of a multi-scale model to perform predictions of bulk properties based on micro-mechanical testing. Different RVE sizes were explored to perform the upscaling methodology. The RVEs were based on previously conducted micro-tensile tests. Then, the effect of voids in AM steel was studied by performing SVE modeling. The prediction performed was compared with the experimental data. Lastly, suggestions on how to improve the accuracy of this framework are given.

5.3 Representative Volume Element and Statistical Volume Element

Performing simulations of a full-scale heterogeneous material can be complex and computationally expensive. Consequently, RVE are typically used to perform these types of simulations. The concept is to simulate a section of the original part, small enough to reduce computational requirement, but big enough to be representative of the bulk material [14,18–20]. This homogenization technique can provide satisfying results if the following conditions is met:

$$d << l << L, \quad (4)$$

where d is the characteristic length of the microstructural feature, l is the characteristic length of the RVE and L is the characteristic length of the macroscale[17,19]. Typically, the size of the RVE is described by the unitless parameter

$$\delta = l/d. \quad (5)$$

Depending on the problem to be studied, RVEs of δ = 10-100 would reach homogenization[19]. RVEs with small δ values or that have not reached homogenization are called statistical volume elements. SVEs are smaller versions of RVEs, which can capture the spatial correlation information of the material property within a size of δ [17]. As the δ is increased, the SVE will become an RVE, and homogenization will be achieved. As it can be seen in Figure 43, a small δ SVE will capture a fraction of the information of the heterogeneous material; however, when the size is increased, it become more representative of the bulk material, becoming a RVE.

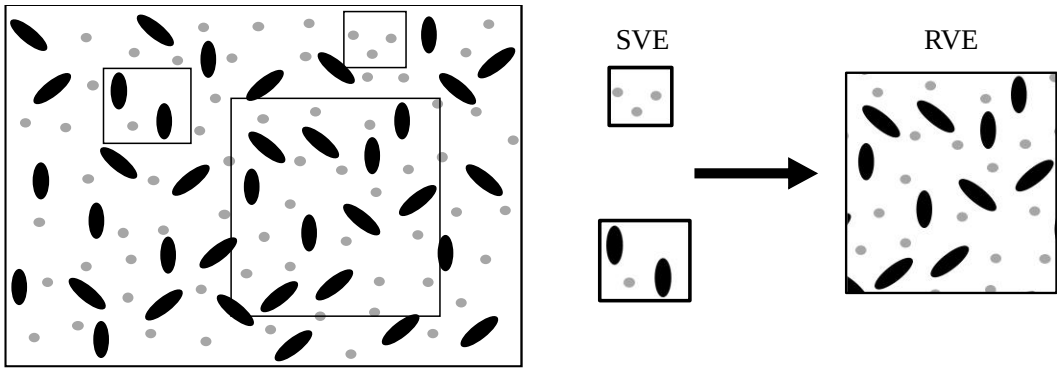

Figure 43: Illustration of a heterogeneous material. SVE and RVE examples are shown.

5.4 Periodic Boundary Condition

Periodic Boundary Condition (PBC) specifies that opposite edge should have same deformation profile after loading [18,20], as illustrated in Figure 44 and equation (6). Periodic

meshing, having the same number of nodes on opposite edges, is utilized to facilitate the PBC implementation. To analyze the mechanical response of the RVE, the corner nodal reaction force ($\mathbf{f_i}$) and displacement ($\mathbf{x_i}$) are examined [20], as shown in equation (7).

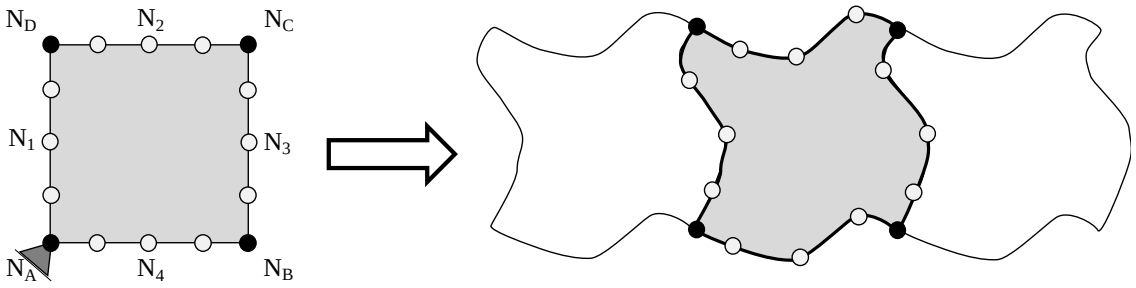

Figure 44: Illustration of a deformation profile in a 2D RVE when PBC is applied.

$$U_{(x,y)}^{N_3} = U_{(x,y)}^{N_1}; \mathrm{U}_{(x,y)}^{N_2} = \mathrm{U}_{(x,y)}^{4}; \mathrm{U}_{(x,y)}^{N_D} = \mathrm{U}_{(x,y)}^{N_C}; \mathrm{U}_{(x,y)}^{N_B} = \mathrm{U}_{(x,y)}^{N_A} \quad (6)$$

$$\sigma = \frac{1}{\mathrm{Vol}}(\mathrm{x}_A f_A + \mathrm{x}_B f_B + \mathrm{x}_C f_C + \mathrm{x}_D f_D) \quad (7)$$

5.5 Methodology

5.5.1 Micro-tensile testing

Micro-tensile samples were made from SLM 17-4 Ph steel using Focused Ion Beam milling. Since FIB-milling is a time-consuming process, photolithography and wet-etching processes were performed to pre-make ~12µm columns, shown in Figure 45, where specimens would be milled from as shown in Figure 46. To perform *in-situ* SEM micro-mechanical testing, a pico-indenter Hysitron PI-88, with a modified stock tip, was used. Tensile tests were performed as strain-controlled at ~ 4 nm/s (10^{-3} strain rate). For more details on FIB and etching parameters as well as experimental procedures, please refers to [21].

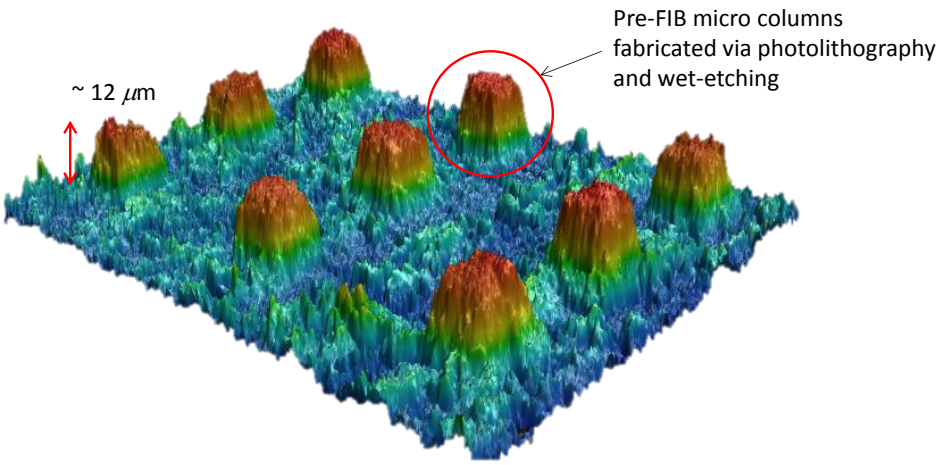

Figure 45: Micro-column array to reduce specimen fabrication FIB time.

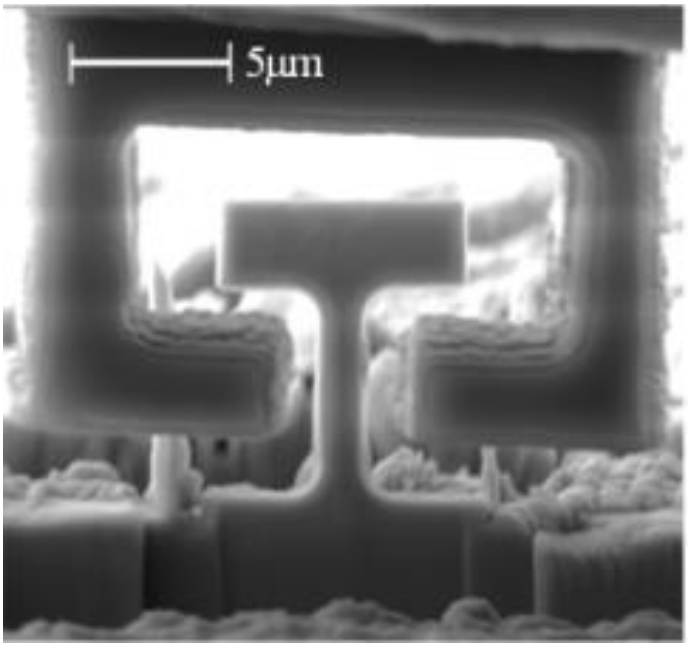

Figure 46: Micro-tensile specimen fabricated via Focused Ion Beam.

5.5.2 Python|Abaqus scripts

Two Youtube channels (Engineering Software and Dr. Michael Okereke - CM Videos) were used as references to develop the Python|Abaqus scripts used in this study. These scripts automatize the creation of square RVEs and voids, the randomization of void size and location, the randomization of properties assignation, and the application of PBC. Both scripts can be found in Appendix B and Appendix C. A post-processing Matlab script, found in Appendix D, was used to extract yield stress, UTS, and plasticity data.

5.5.3 Mechanical Properties up-scaling script

A user defined squared RVE was first created. Then, the RVE was partitioned into 100 squares. The properties of each partition were randomly assigned based on micro-mechanical testing or previous RVE scale. A periodic boundary condition was applied to the RVE by enforcing same deformation on opposite faces. Then, tensile simulation was performed. Figure 47 shows an illustration of the RVE generation and tensile simulation.

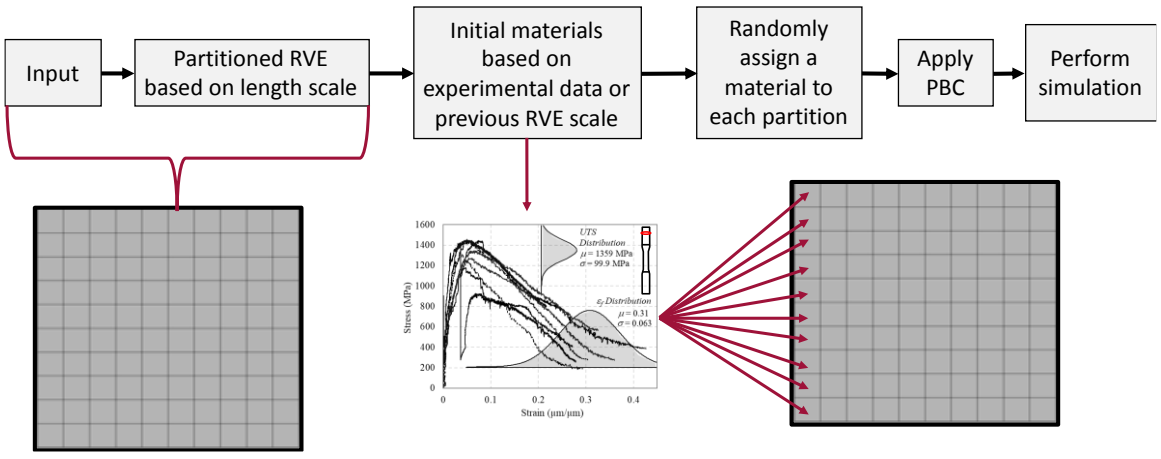

Figure 47: Illustration of the process to create partitioned RVE with random material assignation.

5.5.4 Properties up-scaling procedure

To scale-up properties, RVEs of different sizes were used. For the first scale, a 10 µm x 10 µm RVE was used with 1 µm x 1 µm partitions, the size of the cross-sectional area of the micro-tensile specimen tested previously. In the same manner, RVEs of 100 µm x 100 µm and 1 mm x 1 mm were created. The mechanical properties of each RVE were based on the previous RVE scale as shown in Figure 48.

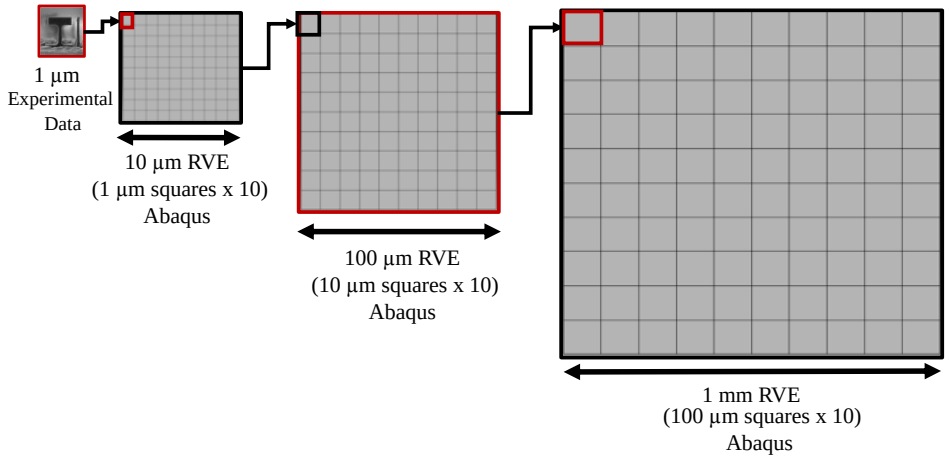

Figure 48: Illustration of mechanical property scale-up methodology.

5.5.5 Voided RVE script

After homogenization was achieved during the upscaling of mechanical properties, the predicted behavior was used to perform voided RVE simulations. To do so, a RVE was created. Then, void parameters such as diameter range and volume fraction were defined. Subsequently, the algorithm shown in Figure 49 is followed. To perform voids simulations, 1 mm x 1 mm RVEs were used along with voids of an average diameter of 50 µm, so that $\delta = 20$. A similar δ parameter was used in [17] to study the effect of voids in a porous 4330 Steel.

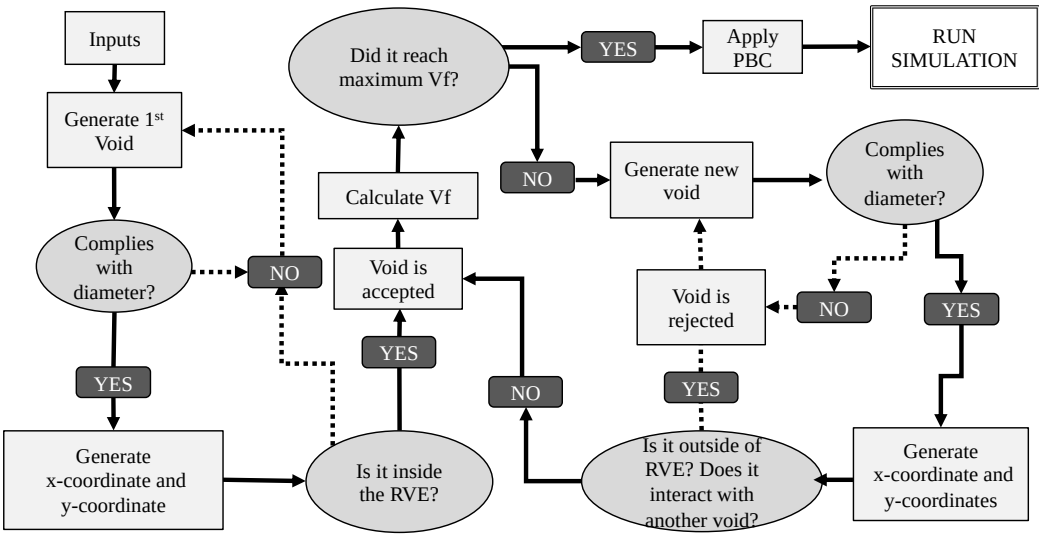

Figure 49: Python|Abaqus algorithm for voided RVE simulation.

To simplify RVE simulations and analysis, some considerations were taken. 2D RVEs were used to study the effect of voids in AM parts, as shown in Figure 50. Using a 2D RVE simplifies the periodic meshing and the application of the PBC. Voids are modeled as circles instead of a random shape to simplify the script and volume fraction calculation. Also, voids cannot touch the edges of the RVE.

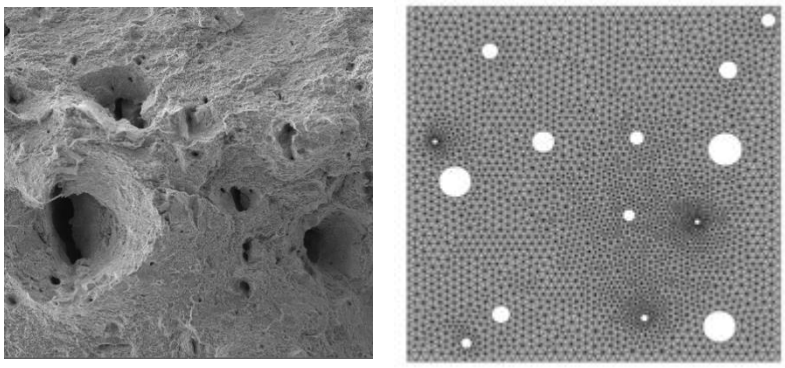

Figure 50: Left) Post fracture SEM micrograph showing voids in SLM 17-4 PH; Right) illustration of a RVE containing voids.

5.5.6 Mesh

To perform the upscaling methodology, 2500 square elements were used, representing 25 elements per partition as shown in Figure 51. For the void simulations, triangular elements were chosen with a size determined as ~1/3 of the average void size, as shown in Figure 51.

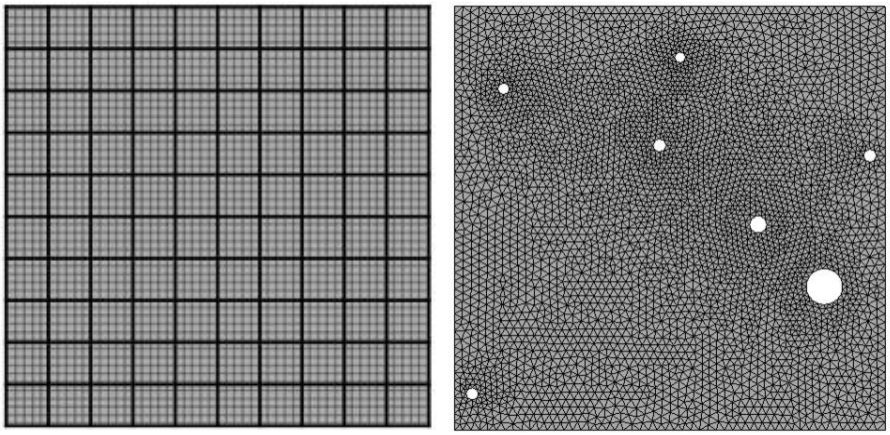

Figure 51: Left) structured mesh for material property upscaling simulations and Right) adaptive mesh for void simulations.

5.6 Results and Discussion

5.6.1 Up-scaling methodology

To study the effect of RVE size on the property prediction, 3 RVE length-scale were used. Since the cross-sectional area of the experimental data was 1 µm x 1 µm, the first RVE size was $\delta = 10$ (10 µm x 10 µm). The second size was $\delta = 100$ (100 µm x 100 µm) and the last one was $\delta = 1000$ (1000 µm x 1000 µm). Figure 52 shows a screenshot from a property up-scaling simulation. Due to the periodic boundary condition, the same image can be side by side in any direction to form a composite image as seen in Figure 52.

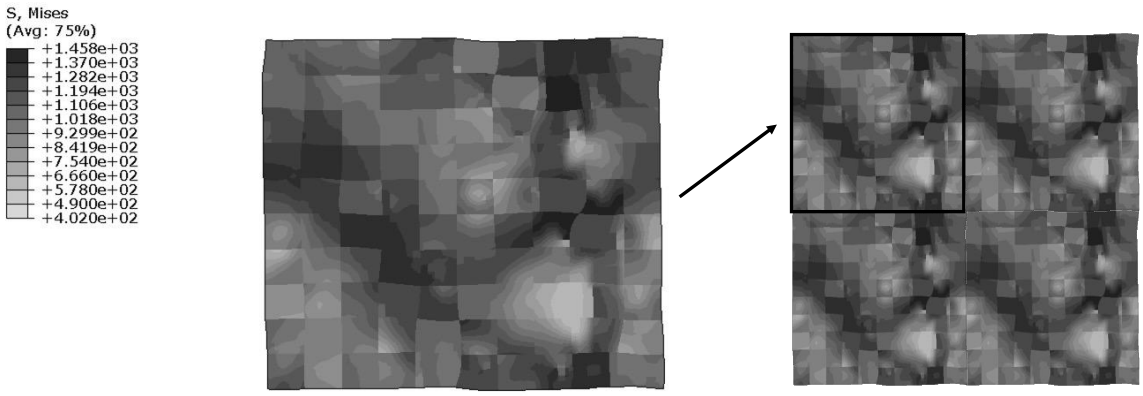

Figure 52: Illustration of a run performed to up-scale mechanical properties. Composite image conformed by 4 screenshots of the same result.

For the first scale, δ =10 RVE (10 μm x 10 μm) shown in Figure 53, scatter in the results can be seen. The scatter indicates that homogenization has not been reached at this scale, as in accordance with [19]. RVEs should be about δ =10-100, depending on the type of study. Therefore, for the SLM 17-4 PH steel, an RVE of δ = 10 can be still considered an SVE. Hence, variation will be seen as the experimental results are dispersed and the material assignation is randomized as is shown in Figure 47.

Figure 54 shows the results for δ=100 RVEs. The assigned properties in these simulations were chosen from the previous scale, δ =10 RVE. A lower dispersion of the mechanical behavior can be seen for the 100 μm RVE, compared to δ = 10 RVE. It can be said that the SVE – RVE transition for this experiment occurs between δ =10-100, in agreement with [19].

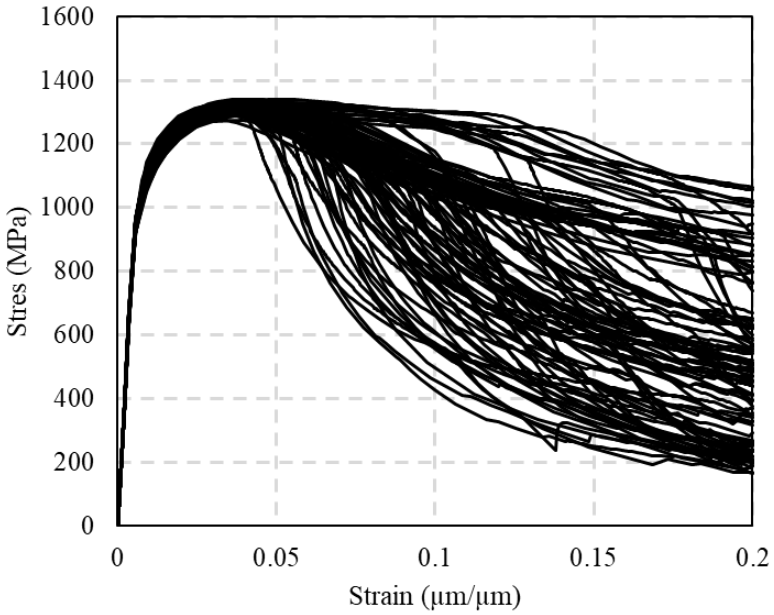

Figure 53: Results obtained from a δ = 10 RVE.

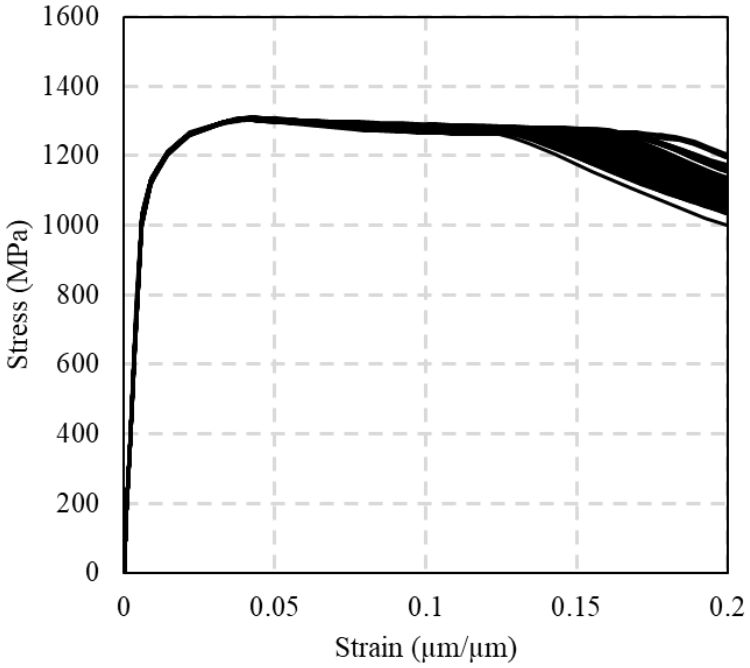

Figure 54: Results obtained from a δ = 100 RVE.

An additional scale was tested to see if there is further improvement on the homogenization of the mechanical behavior. Figure 55 shows the result from simulations using RVEs with δ = 1000, whose properties were assigned from the previous RVE scale δ=100. As seen, there is no further improvement on the homogenization. Further scales, e.g. δ=10000, likely will not represent any homogenization enhancement. On the contrary, increasing the scale will increase the computation cost for little to no improvement.

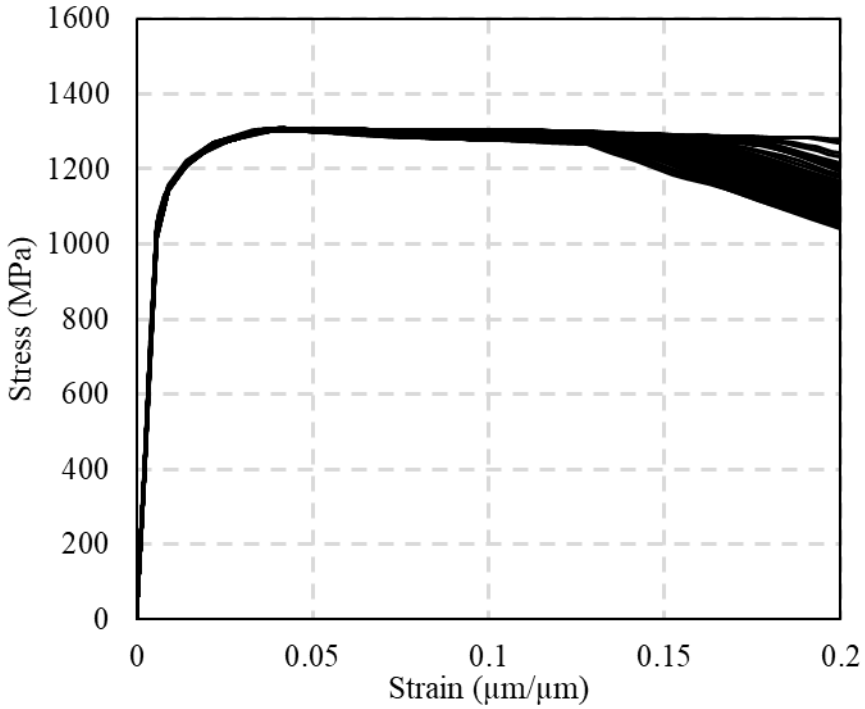

Figure 55: Results from simulation using δ = 1000 RVE.

A macro mechanical behavior was predicted based on RVE simulations of δ=100 and 1000. Figure 56 shows a comparison between the RVE prediction and experimental data, where the model overpredicts the UTS by 17% compared to the experimental data (1305 MPa and 1115 MPa respectively). However, the biggest differences between the RVE prediction and the experimental data is the lack of strain hardening, where the UTS is reached at a strain of 3% for the model, while

at 18% for the experimental data. Also, an over-prediction 55% between the prediction and the actual data is seen in the yield strength, 1115 MPa and 720 MPa, respectively. It is worth noting that this estimate is based solely on the micro-mechanical tensile test, without considering the effect of any other microstructural factors, such as phase, melting pool, or voids.

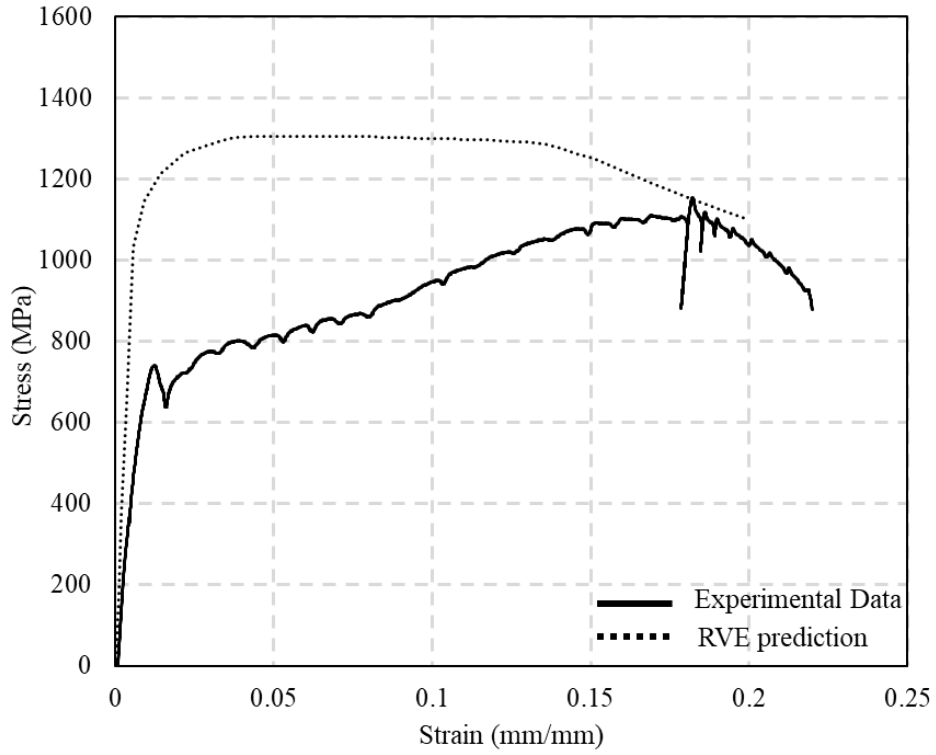

Figure 56: Comparison between the experimental tensile data and the model.

5.6.2 Effect of voids

To study the effects of voids on SLM 17-4 PH steel, SVEs of 1 mm x 1 mm were used. The mechanical properties for the simulations were taken from the prediction performed with the up-scaling scheme, shown in Figure 56. Figure 57 shows a simulation of a SVE containing voids. As can be seen, crack propagation occurs perpendicular to the loading direction. The location of the void plays a detrimental role on the ductility in AM materials [2,22]. Carlton et al. [22]

performed a tensile test with ct-tomography to understand the crack evolution in AM parts. They found that crack bridging forms voids, affirming that failure in AM part is defect driven. The influence of void location in the ductility of AM parts can be seen in Figure 57. Failure is driven by voids that are aligned perpendicular to the loading direction by facilitating the crack initiation and crack propagation. Figure 58 shows a comparison between the experimental data and the prediction performed using un-voided and voided RVE. As was previously discussed, voided RVE simulations show mechanical behavior with a significantly lower ductility and a reduction of 8%-15% in UTS.

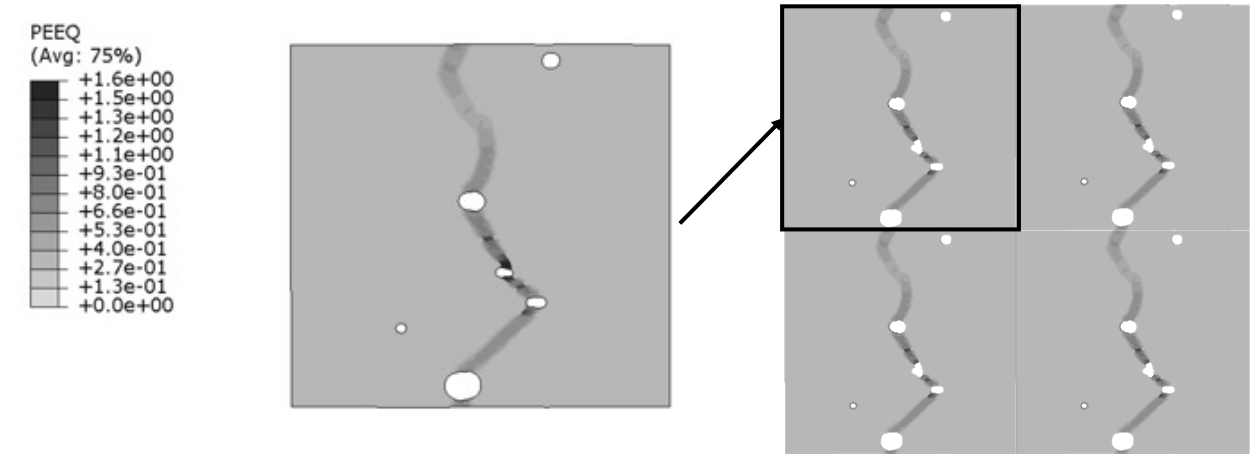

Figure 57: Screen shot of a voided SVE simulation.

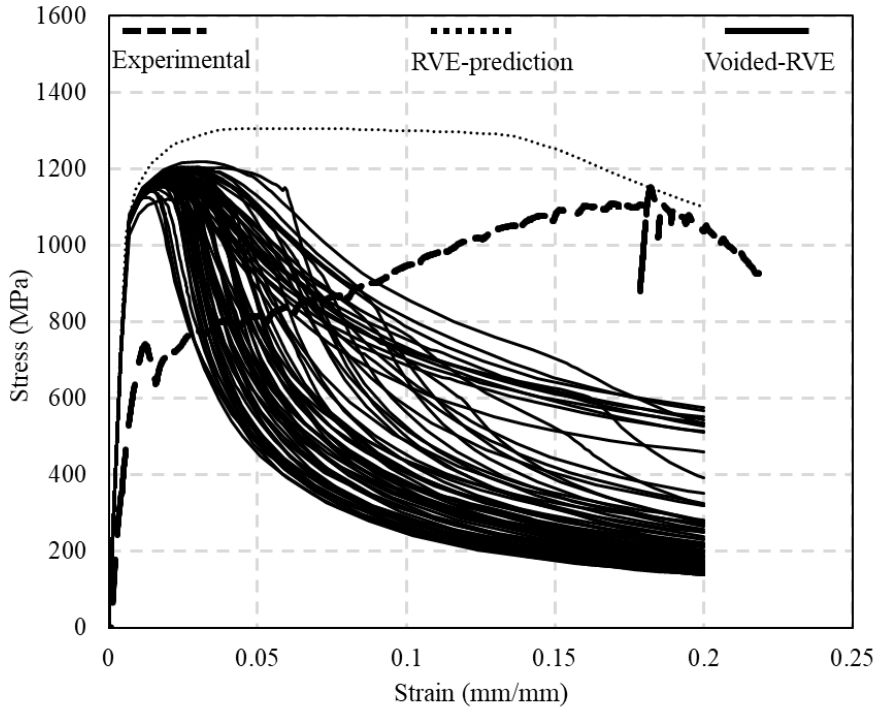

Figure 58: Comparison of experimental data and prediction using un-voided and voided RVE.

5.6.3 Micro-mechanical based RVE prediction challenges

At the current stage, this model overpredicts the performance of AM parts, as shown in Figure 56. One of the possible reasons for the performance overprediction is the size of the micro-tensile specimen. The development of small-scale mechanical testing has helped small scale application by providing mechanical properties at the scale of application, where usually it has been inferred from the bulk material [12]. It has been reported that materials could show improved mechanical behavior when its size is reduced [12,23–25], indicating a scale dependency of properties. Also, Kiener, D. et. al. [26], showed that aspect ratios of samples could influence mechanical behavior, where a low-aspect ratio 1:1 demonstrates a more pronounced hardening and stronger size effect compared to high aspect ratio (5:1 and higher) samples. These two facets of small-scale mechanical testing could be inflating mechanical property prediction.

A direct mechanical property translation can be also hindered by the differences in fracture mechanisms between micro-scale testing and macro-scale testing. Some fractures observed during micro-mechanical testing appear as shearing fractures along a slip plane, as shown in Figure 59, which is typical of ductile single crystals. The polycrystallinity of parts fabricated via SLM is well known. Also, during macro mechanical tensile testing, samples showed a cone-cup fracture, which is common in ductile metal. Ductile fracture at the macro-scale is associated with the nucleation and coalesce of voids; differing to the shear fracture associated to ductile single crystal behavior.

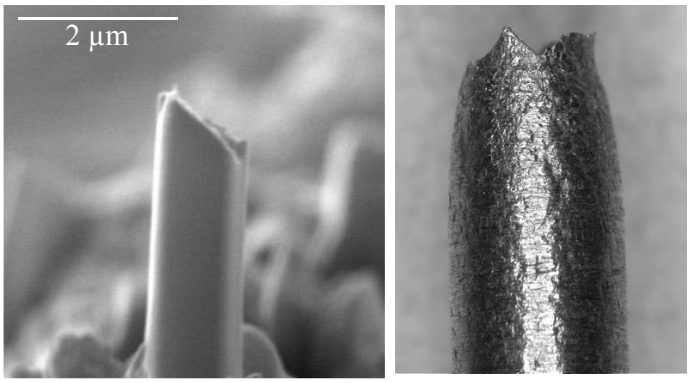

Figure 59: A fracture surface of a micro-tensile specimen showing a shear failure.

5.6.4 Suggestion for improvement

Testing at small scale provides unique material information. By fabricating samples with a gage cross sectional area of 1 µm x 1 µm, microstructural features, such as phase, can be isolated. The ratio of austenite and martensite phases in SLM 17-4 PH steel exerted an influence on the performance of this material [7,27]; higher martensite content provide higher UTS and Yield while austenite provides higher ductility. Micro-tensile tests along with electron backscattered diffraction (EBSD) would provide insightful information about the size of the crystal and the phase

to be tested. This combination could be helpful to study the difference in performance by having information on the crystallographic orientation and phase. Having the opportunity to test phases individually can open the possibility of not only learning about the mechanical performance of each phase, but also the influence of each phase on the macro mechanical behavior. The individual phase testing could be complemented by testing at the meso-scale.

Meso-scale testing can be helpful on linking the micro-scale mechanical behavior and the macro-scale. The advantage of testing at the meso-scale is that it can be small enough to keep the sample free of fabrication defects, such as voids, but also can be big enough to be polycrystalline or melting pool; similar microstructure to the bulk material instead of single or fraction of a crystal specimens that may show different behavior. These tests can provide information about the influence of crystal size or melting pool in the mechanical behavior at the macro-scale. Also, it may be possible to capture the upper-lower yield point that the SLM 17-4 PH showed at the macro-scale, but not during the micro-tensile test. Meso-scale mechanical testing can be useful to adjust and validate the upscale prediction on each scale.

5.7 Summary

The objective of this study is to introduce a framework to create a predictive model of the mechanical performance of AM parts, based on small scale mechanical testing. Two Python|Abaqus scripts are presented which were used to perform this study; one was used to upscale mechanical properties and the other to study the effect of voids. RVEs with a PBC were used as homogenization techniques to upscale mechanical properties obtained from micro-mechanical testing (cross-sectional gage area 1 μm x 1 μm) and predict bulk mechanical behavior. Also, the effect of voids in the performance was studied. Three different RVE scales were used (δ =10, 100, and 1000) to perform simulations. To study the effect of voids, a SVE of δ =20 was

chosen, as was done in [17]. At the end, recommendations were given to improve the predictive approach.

In general, during the upscaling of properties, homogenization was reached at RVE of δ = 100. Smaller RVEs resulted in SVEs, providing a distribution of results. The prediction made by the RVE resulted in an UTS and yield strength overestimation of 17% and 55% respectively, compared to experimental data. Also, the prediction fails to capture the strong strain hardening and upper-lower yield point that SLM 17-4 PH showed during testing. The model predicted that the UTS would be reached at a strain of 3%, while it was reached at 18% during the experimentation. Void simulations demonstrated that defects can significantly reduce the ductility and UTS of metals by facilitating the crack propagation, especially when voids are aligned perpendicular to the loading direction. Simulations with 1% porosity, a reduction of 8 – 15% in UTS was reached.

Although the present model did not accurately predict the bulk behavior, the approach of calibrating a predictive model using micro-tensile tests should not be discarded. This approach could provide a generalized prediction by isolating different microstructural features that can be attained to specific fabrication parameters. This methodology could be improved by incorporating other characterization techniques such as EBSD and meso- scale testing. Also, little to no micro-tensile data on AM metals is available in literature. While there is more information about micro-mechanical data of SLM metals, this predictive approach could be improved.

5.8 References

1. Yadollahi, A.; Shamsaei, N. Additive Manufacturing of Fatigue Resistant Materials: Challenges and Opportunities. *Int J Fatigue* **2017**, *98*, doi:10.1016/j.ijfatigue.2017.01.001.

2. Yadollahi, A.; Shamsaei, N.; Thompson, S.M.; Elwany, A.; Bian, L. Effects of Building Orientation and Heat Treatment on Fatigue Behavior of Selective Laser Melted 17-4 PH Stainless Steel. *Int J Fatigue* **2017**, *94*, doi:10.1016/j.ijfatigue.2016.03.014.

3. Karthik, G.M.; Kim, H.S. Heterogeneous Aspects of Additive Manufactured Metallic Parts: A Review. *Metals and Materials International* 2021, *27*.

4. Ben, D.D.; Ma, Y.R.; Yang, H.J.; Meng, L.X.; Shao, X.H.; Liu, H.Q.; Wang, S.G.; Duan, Q.Q.; Zhang, Z.F. Heterogeneous Microstructure and Voids Dependence of Tensile Deformation in a Selective Laser Melted AlSi10Mg Alloy. *Materials Science and Engineering: A* **2020**, *798*, 140109, doi:10.1016/J.MSEA.2020.140109.

5. Xiong, Z.H.; Liu, S.L.; Li, S.F.; Shi, Y.; Yang, Y.F.; Misra, R.D.K. Role of Melt Pool Boundary Condition in Determining the Mechanical Properties of Selective Laser Melting AlSi10Mg Alloy. *Materials Science and Engineering: A* **2019**, *740–741*, 148–156, doi:10.1016/J.MSEA.2018.10.083.

6. Shifeng, W.; Shuai, L.; Qingsong, W.; Yan, C.; Sheng, Z.; Yusheng, S. Effect of Molten Pool Boundaries on the Mechanical Properties of Selective Laser Melting Parts. *J Mater Process Technol* **2014**, *214*, 2660–2667, doi:10.1016/J.JMATPROTEC.2014.06.002.

7. Gonzalez-Nino, D.; Strasser, T.; Prinz, G.S. Ultra Low-Cycle Fatigue Behavior Comparison between Additively Manufactured and Rolled 17-4 Ph (Aisi 630) Stainless Steels. *Metals (Basel)* **2021**, *11*, doi:10.3390/met11111726.

8. Mahmoudi, M.; Elwany, A.; Yadollahi, A.; Thompson, S.M.; Bian, L.; Shamsaei, N. Mechanical Properties and Microstructural Characterization of Selective Laser Melted 17-4 PH Stainless Steel. *Rapid Prototyp J* **2017**, *23*, doi:10.1108/RPJ-12-2015-0192.

9. Yadollahi, A.; Shamsaei, N.; Hammi, Y.; Horstemeyer, M.F. Quantification of Tensile Damage Evolution in Additive Manufactured Austenitic Stainless Steels. *Materials Science and Engineering A* **2016**, *657*, 399–405, doi:10.1016/j.msea.2016.01.067.

10. Pei, C.; Zeng, W.; Yuan, H. A Damage Evolution Model Based on Micro-Structural Characteristics for an Additive Manufactured Superalloy under Monotonic and Cyclic Loading Conditions. *Int J Fatigue* **2020**, *131*, doi:10.1016/j.ijfatigue.2019.105279.

11. Torries, B.; Sterling, A.J.; Shamsaei, N.; Thompson, S.M.; Daniewicz, S.R. Utilization of a Microstructure Sensitive Fatigue Model for Additively Manufactured Ti-6Al-4V. In Proceedings of the Rapid Prototyping Journal; Emerald Group Publishing Ltd., 2016; Vol. 22, pp. 817–825.

12. Greer, J.R.; Kim, J.-Y.; Burek, M.J. The In-Situ Mechanical Testing of Nanoscale Single-Crystalline Nanopillars. *The Journal of The Minerals, Metals & Materials Society* **2009**, *61*, 19–25, doi:https://doi.org/10.1007/s11837-009-0174-8.

13. da Silva, W.R.L.; Němeček, J.; Štemberk, P. Methodology for Nanoindentation-Assisted Prediction of Macroscale Elastic Properties of High Performance Cementitious Composites. *Cem Concr Compos* **2014**, *45*, 57–68, doi:10.1016/j.cemconcomp.2013.09.013.

14. Shahzamanian, M.M.; Tadepalli, T.; Rajendran, A.M.; Hodo, W.D.; Mohan, R.; Valisetty, R.; Chung, P.W.; Ramsey, J.J. Representative Volume Element Based Modeling of Cementitious Materials. *J Eng Mater Technol* **2014**, *136*, doi:10.1115/1.4025916.

15. Weng, J.; Wen, W.; Cui, H.; Chen, B. Micromechanical Analysis of Composites with Fibers Distributed Randomly over the Transverse Cross-Section. *Acta Astronaut* **2018**, *147*, 133–140, doi:10.1016/j.actaastro.2018.03.056.

16. Shahzamanian, M.M.; Basirun, W.J. Modeling of Cementitious Representative Volume Element with Additives. *Journal of Multiscale Modelling* **2017**, *08*, 1750003, doi:10.1142/s1756973717500032.

17. Yin, X.; Chen, W.; To, A.; McVeigh, C.; Liu, W.K. Statistical Volume Element Method for Predicting Microstructure-Constitutive Property Relations. *Comput Methods Appl Mech Eng* **2008**, *197*, 3516–3529, doi:10.1016/j.cma.2008.01.008.

18. Gitman, I.M.; Askes, H.; Sluys, L.J. Representative Volume: Existence and Size Determination. *Eng Fract Mech* **2007**, *74*, 2518–2534, doi:10.1016/j.engfracmech.2006.12.021.

19. Ostoja-Starzewski, M. Material Spatial Randomness: From Statistical to Representative Volume Element. *Probabilistic Engineering Mechanics* **2006**, *21*, 112–132, doi:10.1016/j.probengmech.2005.07.007.

20. Okereke, M.; Keates, S. *Springer Tracts in Mechanical Engineering Finite Element Applications A Practical Guide to the FEM Process*;

21. Gonzalez-Nino, D.; Sonntag, S.; Afshar-Mohajer, M.; Goss, J.; Zou, M.; Prinz, G.S. Micromechanical Tension Testing of Additively Manufactured 17-4 Ph Stainless Steel Specimens. *Journal of Visualized Experiments* **2021**, *2021*, doi:10.3791/62433.

22. Carlton, H.D.; Haboub, A.; Gallegos, G.F.; Parkinson, D.Y.; MacDowell, A.A. Damage Evolution and Failure Mechanisms in Additively Manufactured Stainless Steel. *Materials Science and Engineering: A* **2016**, *651*, 406–414, doi:https://doi.org/10.1016/j.msea.2015.10.073.

23. Kim, J.Y.; Greer, J.R. Tensile and Compressive Behavior of Gold and Molybdenum Single Crystals at the Nano-Scale. *Acta Mater* **2009**, *57*, 5245–5253, doi:10.1016/J.ACTAMAT.2009.07.027.

24. Greer, J.R.; Kim, J.-Y.; Burek, M.J. The In-Situ Mechanical Testing of Nanoscale Single-Crystalline Nanopillars. *JOM* **2009**, *61*, 19–25, doi:10.1007/s11837-009-0174-8.

25. Kim, J.Y.; Jang, D.; Greer, J.R. Tensile and Compressive Behavior of Tungsten, Molybdenum, Tantalum and Niobium at the Nanoscale. *Acta Mater* **2010**, *58*, 2355–2363, doi:10.1016/j.actamat.2009.12.022.

26. Kiener, D.; Grosinger, W.; Dehm, G.; Pippan, R. A Further Step towards an Understanding of Size-Dependent Crystal Plasticity: In Situ Tension Experiments of Miniaturized Single-Crystal Copper Samples. *Acta Mater* **2008**, *56*, 580–592, doi:10.1016/J.ACTAMAT.2007.10.015.

27. LeBrun, T.; Nakamoto, T.; Horikawa, K.; Kobayashi, H. Effect of Retained Austenite on Subsequent Thermal Processing and Resultant Mechanical Properties of Selective Laser Melted 17–4 PH Stainless Steel. *Mater Des* **2015**, *81*, doi:10.1016/j.matdes.2015.05.026.

Chapter 6: Summary, Conclusions, Contribution and Future Work

Whereas AM technologies, such as SLM, have demonstrated the capability of building customizable and complex parts, the lack of a generalized and accurate predictive model hinders the full adoption of these technologies by the industry [1–3]. The heterogeneous and complex microstructure, resulted from the layer-to-layer melting process in SLM, contributes to the uncertainty of mechanical behavior in this technology [1]. Voids resulted from un-melted regions and/or gas entrapment have been named in numerous research as the major culprit of unexpected mechanical behavior or reduced strain to failure [1,2,4–11]. Hence, to contribute to a better understanding of the mechanical behavior of SLM 17-4 PH steel and thus, advance the massive introduction of AM in engineering industries, this research performed a characterization of SLM 17-4 PH steel at the bulk level by ultra-low cycle fatigue and at the micro-scale level by micro-compression, and micro-tension, and present a basic framework for a predictive model framework based on micro-mechanical testing. The following section summarizes the objectives of each chapter and presents the relevant conclusions.

6.1 Understanding the Ultra-Low Cycle Fatigue Behavior of Additively Manufactured 17-4 PH Stainless Steel

The first objective of this study was to characterize SLM 17-4 PH steel at macro-scale and understand its performance under ULCF. This objective considered mechanical testing, such as tensile and fatigue testing, and material characterization techniques, such as XRD, SEM, ct-tomography, and Vickers's hardness, to have a comprehensive understanding on the mechanical behavior and microstructure of SLM 17-4 PH steel. Two sets of AM parts, *as-built* and *heat treated*, were tested and compared with its wrought counterpart. All samples were subjected to

ULCF with a strain amplitude ($\Delta\varepsilon/2$) ranging from 2% up to 4%. Then, samples were subjected to a post-test fractography analysis with a SEM.

It was demonstrated that both SLM samples contained, at different ratio, martensite and austenite phases. Heat treatment resulted in an improvement in UTS in SLM sample, which outperformed its wrought counterpart during a tensile test. However, from the analysis it was shown that both sets of SLM 17-4 PH steel underperform its wrought counterpart when subjected to cyclic loading in the ULCF regime. A decrease of 62% and 65% in cyclic life was observed at strain amplitude of 3% and 4%. Nevertheless, within LCF regime ($N_f > 100$, resulting from strain amplitude of 2%), fatigue behavior of AM and wrought parts were similar. A microstructural analysis performed with ct-tomography and by a post-testing fractography with a SEM, showed the presence of voids, ranging on the order of 100 µm to 200 µm, in SLM parts. This suggests that the fatigue life of under ULCF regime of SLM 17-4 PH steel is driven by the fabrication defects. It is so, that Coffin-Manson universal slopes equation for LCF prediction overestimate the fatigue life of AM specimens by 119% and 213% for strain amplitude of 3% and 4% respectively. An empirical ULCF capacity equation was proposed for AM 17-4 PH steel, providing a fatigue-life estimation within 10% on average between the two additional verification tests.

6.2 Micromechanical Tension Testing of Additively Manufactured 17-4 PH Stainless Steel Specimens – Methodology

The second objective of this study was to develop a methodology to improve the throughput of micro-tensile specimen fabrication, which is hindered by the FIB milling process. Micro-tensile specimen fabrication process is a tedious and time-consuming procedure which can be economically expensive. Thus, a protocol was developed to speed up the micro-tensile specimen fabrication process which consists of the prefabrication of ~ 12 µm tall micro-columns

via patterning using photolithography and wet etching and later the use of FIB to etch the micro-tensile specimen. This methodology also provides a guide on how to customize a nanoindentation tip to be used as tensile test grip. Suggestions on how to perform micro-tensile testing and some of the possible difficulties were discussed.

The guided methodology for micro-tensile specimen fabrication and micro-tensile testing, serves as a reference for future researchers interested in performing similar testing. This protocol helps to reduce the FIB work required in micro-tensile specimen fabrication and ease the grip maneuverability during the testing, by etching unnecessary bulk material.

6.3 Micro-mechanical characterization of Selective Laser Melting 17-4 PH (AISI 630) Stainless Steels through *In-Situ* SEM experimentation

Small-scale mechanical testing allows determination of AM material performance without fabrication defects such as voids. Allowing the isolation of the influence that voids can have on the material mechanical performance. The motive of this study was to characterize SLM 17-4 PH stainless steel via small-scale testing such as nano-indentation, micro-compression and micro-tensile test and compare its behavior against a macro-specimen.

Micro-tensile specimens were fabricated from the grip and gage section of a previously tested sample. This allows the comparison of microstructure resulted from a post-tensile test, such as strain induced martensite, and its original microstructure (austenite and martensite). Micro-compressions and nanoindentations were performed just from the grip section, testing the original microstructure.

A modulus of elasticity of 187 GPa was measured, via nanoindentation. Micro-compression showed a yield strength of 759 ± 207 MPa, representing 40% reduction to the

obtained by micro-tensile test. Interestingly, the average yield strength obtained by micro-compression is comparable to the measured in macro-tensile, 720.5 MPa. On the other hand, a strengthen size effect was observed during micro-tensile tests. An average UTS of 1359 MPa and 1329 MPa, were seen for unstrained and pre-strained area respectively; representing an increase of 21% compared to macro-scale specimen. Also, an increase of 45% in yield strength was seen when grip section is compared to bulk-section. Another difference between micro- and macro-specimens includes the strain-hardening. During tensile test, micro-specimen reached UTS at ~5% strain, while macro-specimen reached at 18% strain. This difference could be related to different failure mechanisms, which could be inferred from fracture surface. Micro specimens showed failures that resemble a shear fracture, while macro-specimen showed a traditional cone and cup failure, linked to void growth and coalescence.

6.4 Framework for micromechanical based modeling of Selective Laser Melting 17-4 PH Stainless Steel using Statistical and Representative Volume Element

The aim of this chapter was to develop a micro-tensile test based RVE/SVE predictive model for SLM 17-4 PH steel that could upscale mechanical properties obtained from small-mechanical testing. A methodology for mechanical properties upscaling was presented, where three different RVEs size were tested (δ = 10, 100, and 1000) and compared to experimental data. To study the effect of voids in mechanical behavior of SLM 17-4 PH parts, voided RVE simulations were performed.

Using the mechanical properties upscaling methodology, the RVE modeling predicted a yield strength of 1115 MPa, 55% higher than the obtained experimentally (720 MPa). Also, an overprediction of 17% of the UTS was obtained via the RVE modeling, 1305 MPa versus 1115 MPa. This overprediction could be explained by two means: 1) the lack of incorporation of the

effects of fabrication induced defects in the modeling and 2) the strengthening size effect that the micro-tensile specimen exhibit and the RVE are based on.

The effects of voids in the mechanical behavior were studied using SVE of δ = 20 and assuming a 1% porosity. A reduction of 8 – 15 % in UTS was seen accompanied with a significant reduction in strain. The incorporation of voids in the micromechanical based RVE simulations, could improve the accuracy of results. However, a more difficult to incorporate is the significant strain hardening observed during the experimental test.

An advantage of SSMT is the ability to test materials by isolating fabrication induced defects. However, one of the biggest challenges is how to link the behavior from micro-scale and translate it to macro-scale. Strengthening size effects and different failure mechanisms are seen at the micro-scale, which are needed to be understood to incorporate their effect at the macro-scale. Characterization techniques, such as EBSD and ct-tomography, should be incorporated with SSMT, to have better understanding of the microstructure of SLM 17-4 PH steel.

6.5 Contributions

From the dissertation, the original contribution can be listed as following:

1) Experimentally measured cyclic life of SLM 17-4 PH steel under ULCF regime ($\Delta\varepsilon/2$ = 2%, 3% and 4%).
2) An empirical ULCF capacity equation was developed for SLM 17-4 PH steel.
3) Developed a methodology to improve micro-tensile specimen fabrication throughput.
4) Characterized SLM 17-4 PH steel at the micro-scale level via micro-tensile, micro-compression and nanoindentation, and provided comparisons to macro-scale behavior.

5) Developed a framework to model AM materials using RVE/SVE informed by micro-mechanical testing.
6) Developed a scheme to upscale mechanical properties obtained via micro-tensile test, using RVE.

6.6 Future Work

Micro-mechanical testing could be helpful to identify and isolate the influence of microstructural features in AM parts. However, small scale mechanical testing, such as micro-tensile testing, should be complemented by some characterization techniques such as EBSD and ct-tomography. The combination of these techniques will open the possibility of further improvement of microstructural based predictive models. As it was studied in this dissertation, SLM 17-4 PH, is sensitive to microstructure changes, as seen with the change in tensile test with heat treatment, and the presence of voids. Therefore, by combining micro-mechanical testing and characterization techniques, a further understanding on the influence that the microstructural can have on the mechanical performance of SLM parts.

Due to the heterogeneity and the microstructural randomness of SLM 17-4 PH steel, developing a universal predictive model can be challenging. The RVE/SVE predictive approach has been proved to be accurate with different heterogeneous materials such as cementitious paste and composite materials. Although this methodology was used in this study, with some success and challenge, it is recommended to implement this methodology with additional experimental testing. As for this study, just micro-mechanical testing was used to calibrate this model. The challenge of this approach resides on the lack of knowledge of other microstructural features such as melting pool, the crystal size and phase content. Therefore, the combination of micro-mechanical testing and other characterization techniques is recommended. Also, meso-scale

testing can be used to test material more similar microstructural wise to the macro-scale and to calibrate and adjust the mechanical property upscaling framework.

The RVE/SVE prediction approach based on micro-mechanical testing should be tested at larger scales using structural components fabricated through SLM processes.

6.7 References

1. Yadollahi, A.; Shamsaei, N. Additive Manufacturing of Fatigue Resistant Materials: Challenges and Opportunities. *Int J Fatigue* **2017**, *98*, doi:10.1016/j.ijfatigue.2017.01.001.
2. Shamsaei, N.; Yadollahi, A.; Bian, L.; Thompson, S.M. An Overview of Direct Laser Deposition for Additive Manufacturing; Part II: Mechanical Behavior, Process Parameter Optimization and Control. *Addit Manuf* 2015, *8*, 12–35.
3. Selcuk, C. Laser Metal Deposition for Powder Metallurgy Parts. *Powder Metallurgy* **2011**, *54*, 94–99, doi:10.1179/174329011X12977874589924.
4. Gonzalez-Nino, D.; Strasser, T.; Prinz, G.S. Ultra Low-Cycle Fatigue Behavior Comparison between Additively Manufactured and Rolled 17-4 Ph (Aisi 630) Stainless Steels. *Metals (Basel)* **2021**, *11*, doi:10.3390/met11111726.
5. Ben, D.D.; Ma, Y.R.; Yang, H.J.; Meng, L.X.; Shao, X.H.; Liu, H.Q.; Wang, S.G.; Duan, Q.Q.; Zhang, Z.F. Heterogeneous Microstructure and Voids Dependence of Tensile Deformation in a Selective Laser Melted AlSi10Mg Alloy. *Materials Science and Engineering: A* **2020**, *798*, 140109, doi:10.1016/J.MSEA.2020.140109.
6. Zhao, L.; Santos Macías, J.G.; Douillard, T.; Li, Z.; Simar, A. Unveiling Damage Sites and Fracture Path in Laser Powder Bed Fusion AlSi10Mg: Comparison between Horizontal and Vertical Loading Directions. *Materials Science and Engineering: A* **2021**, *807*, 140845, doi:10.1016/J.MSEA.2021.140845.
7. Mahmoudi, M.; Elwany, A.; Yadollahi, A.; Thompson, S.M.; Bian, L.; Shamsaei, N. Mechanical Properties and Microstructural Characterization of Selective Laser Melted 17-4 PH Stainless Steel. *Rapid Prototyp J* **2017**, *23*, doi:10.1108/RPJ-12-2015-0192.
8. Suryawanshi, J.; Prashanth, K.G.; Ramamurty, U. Mechanical Behavior of Selective Laser Melted 316L Stainless Steel. *Materials Science and Engineering A* **2017**, *696*, 113–121, doi:10.1016/j.msea.2017.04.058.
9. LeBrun, T.; Nakamoto, T.; Horikawa, K.; Kobayashi, H. Effect of Retained Austenite on Subsequent Thermal Processing and Resultant Mechanical Properties of Selective Laser Melted 17–4 PH Stainless Steel. *Mater Des* **2015**, *81*, doi:10.1016/j.matdes.2015.05.026.
10. Carlton, H.D.; Haboub, A.; Gallegos, G.F.; Parkinson, D.Y.; MacDowell, A.A. Damage Evolution and Failure Mechanisms in Additively Manufactured Stainless Steel. *Materials*

Science and Engineering: A **2016**, *651*, 406–414, doi:https://doi.org/10.1016/j.msea.2015.10.073.

11. Yadollahi, A.; Shamsaei, N.; Thompson, S.M.; Elwany, A.; Bian, L. Effects of Building Orientation and Heat Treatment on Fatigue Behavior of Selective Laser Melted 17-4 PH Stainless Steel. *Int J Fatigue* **2017**, *94*, doi:10.1016/j.ijfatigue.2016.03.014.

Appendix A: Matlab code for video strain correction

This appendix contains the Matlab code used to perform the video strain correction. To use this video the user needs to input the variables found in Table 8.

Table 8: Variables that need to be defined by the user in the video strain correction Matlab code.

Variable name	Input from user
maindir	Location of the video.
vidstring	Name of the video.
vid	Name of the video.
samplerate	Every how many frames do the user wants to take measurement.
fps	Frame per second that the video was recorded.
xtime	Factor which the video was accelerated.
Micronpixelratio	Measurement of pixel per micron. It is recommended to use Matlab's imtool function to measure this.
ims	Dimensions of the image in the video that will be used to take measurement. It is recommended to choose a rectangle aligned and with the width of the gage. The top of the rectangle should be something fixed along the video. The bottom part of the video should be the top of the micro-tensile specimen.

```
clc, close all, clear all

%% Video input
maindir='Location of the video'; %Copy paste the location of the video
vidstring='name of the video.m4v';
cd(maindir)

vid=VideoReader('name of the video.m4v');

frames = vid.NumFrames;
disp(frames)
samplerate = 2;      %Choosing a sample rate (Take measurement at each nth frame)
iter = floor(frames/samplerate);
fps = 151;      %Frames per second
micronpixelratio = 5/155.56; %using imtool, measure the number of pixel per micron.
xtime = 10; %factor which the video is accelerated
```

```
%%Video Loop
pickframe = 1;
count = 0;
topheightarray = zeros();
box1array = zeros();
box2array = zeros();
timearray = zeros();

for n = 1:iter
    frame=read(vid,pickframe);
    timepick = xtime*pickframe/fps; %Calculating time of image in seconds

    pickframe = 1 + (samplerate*count);
    %frame1=video(:,:,:,pickframe);
    ims = frame(170:281,909:949,:); %open image imtool and check dimensions
    count = count +1;
    %figure
    %imshow(ims)

    %% Image Processing
    I = rgb2gray(ims); %The Cropped image needs to be converted to 'bw'

    gmag = imgradient(I);
    %figure
    %imshow(gmag,[])
    %title('Gradient Magnitude')

    L = watershed(gmag);
    Lrgb = label2rgb(L);
    %figure
    %imshow(Lrgb)
    %title('Watershed Transform of Gradient Magnitude')

    %These operations will create flat maxima inside each object that can be located
using imregionalmax.
    se = strel('disk',2);
    Io = imopen(I,se);
    %figure
    %imshow(Io)
    %title('Opening')

    Ie = imerode(I,se);
    Iobr = imreconstruct(Ie,I);
    %figure
    %imshow(Iobr)
    %title('Opening-by-Reconstruction')

    Ioc = imclose(Io,se);
    %figure
    %imshow(Ioc)
    %title('Opening-Closing')

    Iobrd = imdilate(Iobr,se);
    Iobrcbr = imreconstruct(imcomplement(Iobrd),imcomplement(Iobr));
```

```
    Iobrcbr = imcomplement(Iobrcbr);
    %figure
    %imshow(Iobrcbr)
    %title('Opening-Closing by Reconstruction')

    Contrast1 = imadjust(Iobrcbr);
    Contrast2 = Contrast1 + 25;
    Watershed = imadjust(Contrast2);
    %figure
    %imshow(Watershed)
    %title('Contrast Adjustment');

    K1 = wiener2(Watershed,[5,5]);%Wiener Filter - Removes noise
    %figure
    %imshow(K1)
    %title('Image with Noise Removed by Wiener Filter');

    x2 = K1;
    x2_copy = x2;
    [a,b] = size(K1);
    glb_thr = 95;        %Defines Threshold setting (anything above is 0(white) below
is 255(black))
    for i = 1:a
        for j = 1:b
            if x2(i,j) > glb_thr
                x2_copy(i,j) = 0;
            else
                x2_copy(i,j) = 255;
            end
        end
    end
    %figure
    %imshow(x2_copy);
    %title('Globally Thresholded Image:');

    %Removing small areas
    bw1 = bwareaopen(x2_copy,70);

    %Infill hollow areas
    bw2 = imfill(bw1,'holes');

    %% Region Properties
    figure
    %imshow(bw2)
    bboxes = regionprops (bw2, 'BoundingBox', 'FilledImage');
    corners = regionprops(bw2,'Extrema','FilledImage');
    hold on
    for k = 1:length(bboxes)
        CurrBB = bboxes(k).BoundingBox;
        rectangle('Position',  [CurrBB(1),CurrBB(2),CurrBB(3),CurrBB(4)],'EdgeColor',
'r', 'LineWidth',2)
        x = CurrBB(1);
        y = CurrBB(2) - 15;
        str = sprintf("BBox_%d",k);
        text(x,y,str,'FontSize',14,'Color','r');
```

```
    end
    hold off
    close

    %%
    Box1 = bboxes(1).BoundingBox;
    Box1Height = Box1(4);
    box1array(n) = Box1Height;

    if length(bboxes) > 1;
        BoneBox = bboxes(2).BoundingBox;
        BoneTop = BoneBox(2);
        topheightarray(n) = BoneTop(1);
    else
        BoneBox = bboxes(1).BoundingBox;
        BoneTop = BoneBox(2);
        topheightarray(n) = BoneTop(1);
    end

    %% Corners with Extrema

    Corner1 = corners(1).Extrema;
    Corner1LeftTop = Corner1(8,2);
    Corner1RightTop = Corner1(3,2);
    corner1array_lt(n) = Corner1LeftTop;
    corner1array_rt(n) = Corner1RightTop;

    if length(corners) > 1;
        BoneCorner = corners(2).Extrema;
        BoneLeftTop = BoneCorner(8,2);
        BoneRightTop = BoneCorner(3,2);
        lefttopheightarray(n) = BoneLeftTop(1);
        righttopheightarray(n) = BoneRightTop(1);
    else
        BoneCorner = corners(1).Extrema;
        BoneLeftTop = BoneCorner(8,2);
        BoneRightTop = BoneCorner(3,2);
        lefttopheightarray(n) = BoneLeftTop(1);
        righttopheightarray(n) = BoneRightTop(1);
    end
    timearray(n) = timepick;

end

%% Analyzing Values
movementpixel = zeros();
movementbox1 = zeros();
for n = 1:iter
    movementpixel(n) = topheightarray(1) - topheightarray(n);
    movementbox1(n) = box1array(1) - box1array(n);
end
A = transpose(movementpixel);
B = transpose(movementbox1);

%% Analyzing Values Corners
```

```
movementpixel_clt = zeros();
movementpixel_crt = zeros();
movementbox1_clt = zeros();
movementbox1_crt = zeros();
for n = 1:iter
    movementpixel_clt(n) = lefttopheightarray(1) - lefttopheightarray(n);
    movementpixel_crt(n) = righttopheightarray(1) - righttopheightarray(n);
    movementbox1_clt(n) = corner1array_lt(1) - corner1array_lt(n);
    movementbox1_crt(n) = corner1array_rt(1) - corner1array_rt(n);
end
AA = transpose(movementpixel_clt);
BB = transpose(movementbox1_clt);
CC = transpose(movementpixel_crt);
DD = transpose(movementbox1_crt);
LL = (AA+CC)/2;
%%

timearray = transpose(timearray);

    %Needs to be measured outside of this code (microns/pixels)
LLmicron = LL*micronpixelratio;
LLstrain=LLmicron/4;

disp('DogBone Displacement (um)')
AMicron = A*micronpixelratio;
disp(AMicron)

disp('DogBone Strain (um)')
straindogbone = A*micronpixelratio/4;
disp(straindogbone)
%disp('Box 1 Displacement (um)')
%BMicron = B*micronpixelratio;
%disp(BMicron)

disp('Time Array (s)')
disp (timearray)
plot(timearray,straindogbone)

% rateofdisplacement = zeros();
% for n = 1:iter
%     rateofdisplacement(n) = AMicron(n)/timearray(n);
% end
% rateofdisplacement=transpose(rateofdisplacement);
% %disp('displacement rate (um/s)')
% %disp(rateofdisplacement)
%
%       displacementrate       =       (AMicron(iter)-AMicron(89))/(timearray(iter)-
timearray(89));%check the number 40
% disp('displacement rate (um/s)')
% disp(displacementrate)
plot(timearray,LLstrain)
```

Appendix B: Python|Abaqus script used for the mechanical propeties upscaling procedure

This Appendix contains the Abaqus script used to upscale mechanical properties of 3D printed steel. This script generates a RVE with 100 partitions, where each partitions is assigned a material randomly chosen from a previous scale or experimental data. Then, it applies a Periodic Boundary Condition to the RVE and performs a displacement controlled tensile load.

```
#!/usr/bin/env python3
# -*- coding: utf-8 -*-
""

import part
import material
import section
import assembly
import step
import interaction
import load
import mesh
import optimization
import job
import sketch
import visualization
from connectorBehavior import *
from regionToolset import*
import xyPlot
import displayGroupMdbToolset as dgm
import displayGroupOdbToolset as dgo
import random
from array import *
import math
import numpy
import os        # Operating system
import shutil    # copying or moving files
#import matplotlib.pyplot as plt
#%matplotlib inline

RVE_L = 1.0 #RVE x dimension in mm
RVE_W = 1.0 #RVE y dimension in mm
Sq = 10 #number of division
SqFac = RVE_L/Sq
phi = .6 #Distance factor
F = 1 #Distance borders factor
disfac = 0.2 #displacement = disfac*RVE_L
seedfac = 1.5 #seed = averagesize of voids/seedfac
avsize = SqFac*4
```

```
Max_iterations= 1    # Set number of iterations

for qq in range(1,Max_iterations+1):
    Vc = 0
    mdb.Model(modelType=STANDARD_EXPLICIT, name='Model-%d'%(qq))

    s1                    =                    mdb.models['Model-
%d'%(qq)].ConstrainedSketch(name='__profile__',
            sheetSize=RVE_L*2)
    g,  v,  d,  c  =  s1.geometry,  s1.vertices,  s1.dimensions,
s1.constraints
    s1.setPrimaryObject(option=STANDALONE)
    s1.rectangle(point1=(0.0, 0.0), point2=(RVE_L, RVE_W))

    p     =     mdb.models['Model-%d'%(qq)].Part(name='Part-1',
dimensionality=TWO_D_PLANAR,
        type=DEFORMABLE_BODY)
    p = mdb.models['Model-%d'%(qq)].parts['Part-1']
    p.BaseShell(sketch=s1)
    s1.unsetPrimaryObject()
    p = mdb.models['Model-%d'%(qq)].parts['Part-1']
    session.viewports['Viewport: 1'].setValues(displayedObject=p)
    del mdb.models['Model-%d'%(qq)].sketches['__profile__']

#============================================================
    #Partition

    p = mdb.models['Model-%d'%(qq)].parts['Part-1']
    f, e1, d2 = p.faces, p.edges, p.datums
    t          =          p.MakeSketchTransform(sketchPlane=f[0],
sketchPlaneSide=SIDE1, origin=(
            0.0, 0.0, 0.0))
    s                    =                    mdb.models['Model-
%d'%(qq)].ConstrainedSketch(name='__profile__',
            sheetSize=RVE_L*2, gridSpacing=14.14, transform=t)
    g,   v,   d,   c   =   s.geometry,   s.vertices,   s.dimensions,
s.constraints
    s.setPrimaryObject(option=SUPERIMPOSE)
    p = mdb.models['Model-%d'%(qq)].parts['Part-1']
    p.projectReferencesOntoSketch(sketch=s,
filter=COPLANAR_EDGES)
    Xc={}
    Yc={}
    v=1
    for i in range(1,Sq+1):
        for ii in range(1,Sq+1):
```

```
            s.rectangle(point1=((ii-1)*SqFac,       (i-1)*SqFac),
point2=(ii*SqFac, i*SqFac))
            Xc[v]=(0.5*(2*ii-1)*SqFac)
            Yc[v]=(0.5*(2*i-1)*SqFac)
            v = v + 1

    p = mdb.models['Model-%d'%(qq)].parts['Part-1']
    f = p.faces
    pickedFaces = f.getSequenceFromMask(mask=('[#1 ]', ), )
    e, d1 = p.edges, p.datums
    p.PartitionFaceBySketch(faces=pickedFaces, sketch=s)
    s.unsetPrimaryObject()
    del mdb.models['Model-%d'%(qq)].sketches['__profile__']


#============================================================
    #Material Properties
     #Assign Material Properties
    #MATRIX-------
    # mdb.models['Model-%d'%(qq)].Material(name='Steel')
    #                                          mdb.models['Model-
%d'%(qq)].materials['Steel'].Elastic(table=((1003.0,0.2), ))
    #                                          mdb.models['Model-
%d'%(qq)].HomogeneousSolidSection(name='Matrix',material='Steel'
, thickness=None)

    # p = mdb.models['Model-%d'%(qq)].parts['Part-1']
    # f = p.faces
    # faces = f.findAt((0,0,0))
    # q=faces.index
    # Fac = f[q:q+1]
    # region = p.Set(faces=Fac, name='Set-Matrix')
    # p = mdb.models['Model-%d'%(qq)].parts['Part-1']
    #  p.SectionAssignment(region=region,  sectionName='Matrix',
offset=0.0,      offsetType=MIDDLE_SURFACE,      offsetField='',
thicknessAssignment=FROM_SECTION)

    #SMALL SQUARES----
#------------------------------------------------------------
#Experimental DATA: 1 micron
#1 micron experimental data True Stress/Strain

    #strain = [[ 0, .0084, .02, .0294, .0357, .0436], [0, .0037,
.005, .007, .0079, .0087], [0, .001, .0014, .0019, .0037, .0042],
[0, .0036, .0072, .0109, .015, .02], [0, 0.0139, 0.0211, .0306,
.0394, .049], [0, 0.0046, 0.0055, 0.0135, 0.0203, 0.022], [0,
```

```
0.0081, 0.0166, 0.0255, 0.0336, 0.0396], [0, 0.0031, .0122,
0.0204, 0.0251, 0.0297]]

    #stress = [[945.75, 1121.63, 1346.87, 1378.21, 1406.3,
1443.03], [1231.16, 1249.42, 1260.62, 1276.62, 1301.2, 1308.9],
[1402.42, 1413.77, 1415.77, 1418.56, 1421.32, 1423.85], [995.61,
1058.33, 1107.03, 1126.7, 1151.97, 1179.36], [806.94, 1054.25,
1172.34, 1285.68, 1338.7, 1346.71], [1343.1, 1368.9, 1397.5,
1416.2, 1422.2, 1440.4], [840.3, 1021.79, 1136.44, 1199.90,
1256.63, 1273.39], [1273.48, 1338.3, 1369.77, 1414.42, 1429.78,
1457.82]]

#-------------------------------------------------------------

#-------------------------------------------------------------
#Data from Abaqus RVE of 10um
    #strain=[[0,   1.607107e-03,   4.982108e-03,   8.357107e-03,
1.341961e-02,  3.525164e-02],  [0,  1.592500e-03,  2.858125e-03,
4.756562e-03,  7.604219e-03,  2.649219e-02],  [0,  2.276377e-03,
5.124034e-03,  9.395518e-03,  1.580274e-02,  3.239646e-02],  [0,
2.266423e-03,    4.046208e-03,    8.050726e-03,    1.706089e-02,
3.340588e-02],  [0,  5.070819e-03,  8.445818e-03,  1.350832e-02,
1.857082e-02,  3.265090e-02],  [0,  1.596453e-03,  4.971454e-03,
8.346453e-03,  1.340895e-02,  2.643105e-02],  [0,  1.602001e-03,
4.977002e-03,  8.352001e-03,  1.341450e-02,  2.765278e-02],  [0,
2.268947e-03,    5.116604e-03,    9.388088e-03,    1.579531e-02,
2.540616e-02],  [0,  1.587946e-03,  4.962947e-03,  8.337946e-03,
1.340044e-02,  3.772417e-02],  [0,  1.587750e-03,  4.962751e-03,
8.337750e-03,  1.340025e-02,  3.523228e-02],  [0,  5.077015e-03,
8.452014e-03,  1.351451e-02,  2.110826e-02,  2.870201e-02],  [0,
1.590038e-03,    4.965039e-03,    8.340038e-03,    1.340254e-02,
2.764082e-02],  [0,  1.595114e-03,  4.970115e-03,  8.345114e-03,
1.340761e-02,  3.506167e-02],  [0,  2.265988e-03,  5.113645e-03,
9.385129e-03,  1.579235e-02,  2.517794e-02],  [0,  4.858050e-03,
7.705707e-03,  1.197719e-02,  1.838442e-02,  3.700542e-02],  [0,
1.592711e-03,    4.967712e-03,    8.342711e-03,    1.340521e-02,
3.523724e-02],  [0,  2.289261e-03,  5.136918e-03,  9.408402e-03,
1.581563e-02,  3.023189e-02],  [0,  2.755787e-03,  5.005788e-03,
8.380787e-03,  1.344329e-02,  3.242766e-02],  [0,  1.573630e-03,
4.948631e-03,  8.323630e-03,  1.169863e-02,  2.519863e-02],  [0,
2.276387e-03,    9.395528e-03,    1.820546e-02,    2.721563e-02,
3.937934e-02],  [0,  1.597543e-03,  4.972544e-03,  8.347543e-03,
1.172254e-02,  3.683729e-02],  [0,  1.580191e-03,  4.955192e-03,
8.330191e-03,  1.339269e-02,  2.810558e-02],  [0,  1.588041e-03,
4.963042e-03,  8.338041e-03,  1.171304e-02,  3.340170e-02],  [0,
5.054279e-03,    8.429278e-03,    1.349178e-02,    2.108553e-02,
3.220918e-02],  [0,  2.743093e-03,  6.118093e-03,  1.118059e-02,
```

```
1.624309e-02,  2.889934e-02],  [0,  1.608958e-03,  6.671458e-03,
1.426521e-02,  1.711286e-02,  2.538886e-02],  [0,  1.602452e-03,
4.977453e-03,  8.352452e-03,  1.172745e-02,  4.199698e-02],  [0,
1.600982e-03,    4.975983e-03,    8.350982e-03,    1.341348e-02,
3.809317e-02],  [0,  2.275690e-03,  5.123347e-03,  7.971004e-03,
1.081866e-02,  2.750415e-02],  [0,  1.609922e-03,  4.984923e-03,
8.359922e-03,  1.342242e-02,  3.114117e-02],  [0,  1.585430e-03,
4.960431e-03,  8.335430e-03,  1.171043e-02,  3.317002e-02],  [0,
2.773507e-03,    6.148507e-03,    1.121101e-02,    1.880476e-02,
3.304304e-02],  [0,  2.756546e-03,  5.006547e-03,  8.381546e-03,
1.344404e-02,  3.242842e-02],  [0,  1.589080e-03,  4.964081e-03,
8.339080e-03,  1.171408e-02,  2.659506e-02],  [0,  5.069215e-03,
1.181921e-02,  2.025671e-02,  2.974890e-02,  3.776535e-02],  [0,
2.289571e-03,    5.137228e-03,    9.408712e-03,    1.581594e-02,
3.240966e-02],  [0,  1.580123e-03,  4.955124e-03,  8.330123e-03,
1.339262e-02,  2.858012e-02],  [0,  2.947273e-04,  5.040821e-03,
1.571953e-02,  2.172631e-02,  2.700570e-02],  [0,  5.079202e-03,
8.454201e-03,  1.351670e-02,  1.541514e-02,  3.274580e-02],  [0,
1.595018e-03,    4.548143e-03,    6.802537e-03,    9.906038e-03,
3.371609e-02],  [0,  1.591367e-03,  3.278867e-03,  6.442930e-03,
1.356207e-02,  3.678827e-02],  [0,  1.606000e-03,  2.449750e-03,
3.293500e-03,  4.559125e-03,  3.440019e-02],  [0,  1.596100e-03,
4.971101e-03,  8.346100e-03,  1.172110e-02,  3.197110e-02],  [0,
2.284180e-03,    9.403321e-03,    1.821326e-02,    2.722342e-02,
3.685303e-02],  [0,  1.569041e-03,  4.944042e-03,  8.319041e-03,
1.169404e-02,  3.194404e-02],  [0,  2.274914e-03,  9.394055e-03,
1.339857e-02,  2.240874e-02,  3.374887e-02],  [0,  3.153225e-04,
2.213760e-03,  5.061417e-03,  9.332901e-03,  3.511198e-02],  [0,
1.608688e-03,    4.983689e-03,    8.358688e-03,    1.342119e-02,
3.004735e-02],  [0,  1.618066e-03,  4.993067e-03,  8.368066e-03,
1.343056e-02,  3.005672e-02],  [0,  1.587483e-03,  4.962484e-03,
8.337483e-03,  1.171248e-02,  3.820656e-02],  [0,  1.602921e-03,
6.665421e-03,  1.172792e-02,  1.679042e-02,  3.197792e-02],  [0,
1.605195e-03,    4.980196e-03,    8.355195e-03,    9.620820e-03,
3.165308e-02],  [0,  1.597737e-03,  4.972738e-03,  8.347737e-03,
1.341024e-02,  3.573171e-02],  [0,  1.601589e-03,  4.976590e-03,
8.351589e-03,  1.341409e-02,  2.323257e-02],  [0,  1.599124e-03,
4.974125e-03,  8.349124e-03,  1.341162e-02,  2.972632e-02],  [0,
1.622634e-03,    4.997635e-03,    5.841384e-03,    7.107009e-03,
2.893904e-02],  [0,  1.589279e-03,  4.964280e-03,  5.808029e-03,
7.073654e-03,  2.890569e-02],  [0,  2.282472e-03,  5.130129e-03,
9.401613e-03,  1.580884e-02,  3.262781e-02],  [0,  1.591355e-03,
4.966356e-03,  8.341355e-03,  1.171635e-02,  2.437260e-02],  [0,
1.572740e-03,    4.947741e-03,    8.322740e-03,    1.169774e-02,
3.206639e-02],  [0,  1.585550e-03,  6.648050e-03,  1.424180e-02,
2.183555e-02,  3.322617e-02],  [0,  1.575410e-03,  4.950411e-03,
8.325410e-03,  9.591035e-03,  2.621719e-02],  [0,  1.587313e-03,
```

```
4.962314e-03,  8.337313e-03,  1.171231e-02,  3.196231e-02],  [0,
2.310195e-03,    6.225723e-03,    1.023024e-02,    1.924040e-02,
3.545869e-02],  [0,  2.771740e-03,  7.271740e-03,  1.570924e-02,
2.045534e-02,  3.674037e-02],  [0,  1.599172e-03,  4.974173e-03,
8.349172e-03,  1.172417e-02,  3.149956e-02],  [0,  1.596368e-03,
4.971369e-03,  8.346368e-03,  1.172137e-02,  2.437762e-02],  [0,
1.594759e-03,    4.969760e-03,    8.344759e-03,    1.171976e-02,
2.437601e-02],  [0,  1.555853e-03,  6.301946e-03,  1.698066e-02,
2.899421e-02,  3.379963e-02],  [0,  1.598966e-03,  3.286466e-03,
5.026700e-03,  6.806485e-03,  3.116130e-02],  [0,  2.759300e-03,
6.134300e-03,  1.119680e-02,  1.879055e-02,  2.991421e-02],  [0,
1.589439e-03,    8.339439e-03,    1.677694e-02,    1.938729e-02,
2.491019e-02],  [0,  1.585236e-03,  3.272736e-03,  6.436799e-03,
8.216584e-03,  3.314157e-02],  [0,  1.589424e-03,  4.964425e-03,
8.339424e-03,  1.340192e-02,  3.191169e-02],  [0,  1.598229e-03,
4.973230e-03,  8.348229e-03,  1.341073e-02,  3.003689e-02],  [0,
4.417816e-04,    2.691782e-03,    6.066782e-03,    1.112928e-02,
3.224940e-02],  [0,  1.597373e-03,  6.659873e-03,  1.425362e-02,
2.184737e-02,  3.323800e-02],  [0,  1.590213e-03,  4.965214e-03,
8.340213e-03,  1.171521e-02,  3.576209e-02],  [0,  2.735709e-03,
1.117321e-02,  2.161461e-02,  2.748790e-02,  3.417044e-02],  [0,
1.605107e-03,    6.667607e-03,    1.173011e-02,    1.679261e-02,
4.431995e-02],  [0,  1.599835e-03,  8.349835e-03,  1.009007e-02,
1.186985e-02,  3.029063e-02],  [0,  1.610811e-03,  4.985812e-03,
8.360811e-03,  1.173581e-02,  3.462583e-02],  [0,  2.890222e-04,
7.636312e-04,  1.475545e-03,  2.543417e-03,  3.177639e-02],  [0,
7.501335e-03,    1.631127e-02,    2.532143e-02,    3.613363e-02,
4.153972e-02],  [0,  1.584785e-03,  4.959786e-03,  8.334785e-03,
1.170978e-02,  3.148517e-02],  [0,  1.594620e-03,  4.969621e-03,
8.344620e-03,  1.340712e-02,  2.812001e-02],  [0,  1.590880e-03,
4.965881e-03,  8.340880e-03,  1.340338e-02,  3.808307e-02],  [0,
1.591098e-03,    4.966099e-03,    8.341098e-03,    1.171610e-02,
2.690483e-02],  [0,  2.915876e-04,  2.190025e-03,  5.037682e-03,
9.309166e-03,  3.313604e-02],  [0,  2.749166e-03,  6.124166e-03,
1.118667e-02,  1.878042e-02,  3.551040e-02],  [0,  2.270566e-03,
5.118223e-03,  9.389707e-03,  1.579693e-02,  2.518252e-02],  [0,
2.270491e-03,    9.389632e-03,    1.819957e-02,    2.315516e-02,
3.107425e-02],  [0,  2.755537e-03,  6.130537e-03,  1.119304e-02,
1.878679e-02,  3.444890e-02],  [0,  2.754502e-03,  5.004503e-03,
8.379502e-03,  1.344200e-02,  3.052794e-02],  [0,  1.090754e-03,
5.095271e-03,  1.410543e-02,  2.424186e-02,  3.216095e-02],  [0,
1.608321e-03,    4.983322e-03,    8.358321e-03,    1.342082e-02,
2.955754e-02],  [0,  1.608508e-03,  4.983509e-03,  8.358508e-03,
1.342101e-02,  3.240538e-02],  [0,  2.271956e-03,  5.119613e-03,
9.391097e-03,  1.579832e-02,  3.261729e-02],  [0,  1.587734e-03,
3.275234e-03,  6.439297e-03,  1.355844e-02,  3.798599e-02],  [0,
```

```
1.605723e-03,    4.980724e-03,    8.355723e-03,    1.341822e-02,
3.240260e-02]]

    #stress=[[1.024607e+03,      1.096267e+03,      1.165604e+03,
1.211222e+03,    1.257807e+03,    1.315344e+03],    [1.031369e+03,
1.107647e+03,    1.141814e+03,    1.180566e+03,    1.221655e+03,
1.296579e+03],    [1.007946e+03,    1.094243e+03,    1.154154e+03,
1.211875e+03,    1.264925e+03,    1.313299e+03],    [1.027574e+03,
1.118539e+03,    1.157345e+03,    1.216913e+03,    1.285649e+03,
1.315044e+03],    [9.866211e+02,    1.144141e+03,    1.192309e+03,
1.240414e+03,    1.268301e+03,    1.289393e+03],    [1.043496e+03,
1.119482e+03,    1.187360e+03,    1.227468e+03,    1.263430e+03,
1.297929e+03],    [1.028053e+03,    1.101338e+03,    1.171958e+03,
1.215498e+03,    1.257476e+03,    1.296436e+03],    [1.048398e+03,
1.140411e+03,    1.196274e+03,    1.248038e+03,    1.291720e+03,
1.313974e+03],    [1.051043e+03,    1.130211e+03,    1.201150e+03,
1.245973e+03,    1.287166e+03,    1.332983e+03],    [1.024513e+03,
1.101744e+03,    1.177541e+03,    1.222936e+03,    1.266097e+03,
1.313040e+03],    [9.934249e+02,    1.149216e+03,    1.193756e+03,
1.238397e+03,    1.273666e+03,    1.287256e+03],    [1.037304e+03,
1.114779e+03,    1.183669e+03,    1.227292e+03,    1.268233e+03,
1.303344e+03],    [1.034840e+03,    1.110590e+03,    1.190878e+03,
1.240965e+03,    1.287126e+03,    1.340858e+03],    [1.044539e+03,
1.137144e+03,    1.194996e+03,    1.246917e+03,    1.286533e+03,
1.305553e+03],    [9.719936e+02,    1.121519e+03,    1.166959e+03,
1.215590e+03,    1.261264e+03,    1.296855e+03],    [1.046649e+03,
1.123992e+03,    1.190378e+03,    1.234501e+03,    1.278717e+03,
1.329672e+03],    [1.033704e+03,    1.118633e+03,    1.176384e+03,
1.230736e+03,    1.276165e+03,    1.294188e+03],    [9.971489e+02,
1.105664e+03,    1.150957e+03,    1.198610e+03,    1.245847e+03,
1.306984e+03],    [1.041143e+03,    1.124460e+03,    1.198433e+03,
1.241122e+03,    1.268502e+03,    1.304578e+03],    [1.016671e+03,
1.103712e+03,    1.222910e+03,    1.289679e+03,    1.318003e+03,
1.324186e+03],    [1.046746e+03,    1.122647e+03,    1.193657e+03,
1.237293e+03,    1.267902e+03,    1.335264e+03],    [1.017103e+03,
1.096222e+03,    1.176088e+03,    1.225297e+03,    1.270863e+03,
1.313420e+03],    [1.054186e+03,    1.133560e+03,    1.208662e+03,
1.252762e+03,    1.281211e+03,    1.332713e+03],    [9.941728e+02,
1.160980e+03,    1.212125e+03,    1.260741e+03,    1.299771e+03,
1.318161e+03],    [1.012085e+03,    1.127443e+03,    1.191413e+03,
1.249560e+03,    1.283299e+03,    1.316829e+03],    [1.010377e+03,
1.080563e+03,    1.180972e+03,    1.253825e+03,    1.269681e+03,
1.291931e+03],    [1.027088e+03,    1.100180e+03,    1.172926e+03,
1.220661e+03,    1.255053e+03,    1.329677e+03],    [1.029064e+03,
1.102705e+03,    1.180053e+03,    1.228736e+03,    1.274821e+03,
1.334035e+03],    [1.034011e+03,    1.122740e+03,    1.179710e+03,
1.218149e+03,    1.245279e+03,    1.302303e+03],    [1.013419e+03,
```

```
1.083570e+03,    1.164558e+03,    1.216032e+03,    1.267086e+03,
1.326108e+03],   [1.028531e+03,   1.106806e+03,   1.179208e+03,
1.224239e+03,   1.255729e+03,   1.322020e+03],   [1.012155e+03,
1.115830e+03,    1.175656e+03,    1.232502e+03,    1.276877e+03,
1.298056e+03],   [9.938242e+02,   1.101688e+03,   1.147350e+03,
1.196806e+03,   1.247503e+03,   1.306181e+03],   [1.038304e+03,
1.116154e+03,    1.187585e+03,    1.230768e+03,    1.259847e+03,
1.306450e+03],   [9.744245e+02,   1.130729e+03,   1.220703e+03,
1.280571e+03,   1.304850e+03,   1.308719e+03],   [1.022729e+03,
1.106675e+03,    1.164905e+03,    1.225397e+03,    1.281911e+03,
1.331415e+03],   [1.021348e+03,   1.100820e+03,   1.174581e+03,
1.221105e+03,   1.265916e+03,   1.306312e+03],   [1.033801e+03,
1.050405e+03,    1.178581e+03,    1.282264e+03,    1.302835e+03,
1.310547e+03],   [9.789324e+02,   1.131496e+03,   1.181570e+03,
1.231548e+03,   1.245455e+03,   1.295016e+03],   [1.034794e+03,
1.110569e+03,    1.180147e+03,    1.216224e+03,    1.252089e+03,
1.321569e+03],   [1.037167e+03,   1.114220e+03,   1.156223e+03,
1.210159e+03,   1.275708e+03,   1.325220e+03],   [9.992974e+02,
1.069474e+03,    1.092299e+03,    1.111998e+03,    1.137154e+03,
1.300284e+03],   [1.047567e+03,   1.123954e+03,   1.194437e+03,
1.236323e+03,   1.266120e+03,   1.321611e+03],   [1.017463e+03,
1.102406e+03,    1.216493e+03,    1.284956e+03,    1.310305e+03,
1.315610e+03],   [1.057421e+03,   1.143789e+03,   1.217052e+03,
1.258589e+03,   1.286762e+03,   1.329531e+03],   [1.007760e+03,
1.094458e+03,    1.217634e+03,    1.252801e+03,    1.289080e+03,
1.298505e+03],   [1.040474e+03,   1.056566e+03,   1.107961e+03,
1.159199e+03,   1.211628e+03,   1.299141e+03],   [1.017888e+03,
1.088666e+03,    1.159520e+03,    1.203299e+03,    1.246684e+03,
1.290657e+03],   [1.012575e+03,   1.080662e+03,   1.156173e+03,
1.203192e+03,   1.247713e+03,   1.295022e+03],   [1.004784e+03,
1.080611e+03,    1.160234e+03,    1.212015e+03,    1.249525e+03,
1.331568e+03],   [9.986410e+02,   1.069583e+03,   1.180454e+03,
1.241560e+03,   1.280871e+03,   1.321065e+03],   [1.030659e+03,
1.103255e+03,    1.178932e+03,    1.226489e+03,    1.240231e+03,
1.318891e+03],   [1.020003e+03,   1.093909e+03,   1.173209e+03,
1.224198e+03,   1.273096e+03,   1.330415e+03],   [1.035018e+03,
1.108915e+03,    1.181559e+03,    1.227818e+03,    1.270876e+03,
1.307729e+03],   [1.035142e+03,   1.109745e+03,   1.184246e+03,
1.230941e+03,   1.273838e+03,   1.314971e+03],   [1.003287e+03,
1.069692e+03,    1.142694e+03,    1.156189e+03,    1.174190e+03,
1.274887e+03],   [1.049414e+03,   1.128034e+03,   1.195827e+03,
1.208112e+03,   1.224080e+03,   1.309038e+03],   [1.024289e+03,
1.110269e+03,    1.167563e+03,    1.223089e+03,    1.270620e+03,
1.297113e+03],   [1.032577e+03,   1.109293e+03,   1.179429e+03,
1.223400e+03,   1.253315e+03,   1.292833e+03],   [1.043086e+03,
1.126886e+03,    1.200160e+03,    1.244466e+03,    1.274838e+03,
1.330456e+03],   [1.028098e+03,   1.106301e+03,   1.201375e+03,
```

```
1.267937e+03,    1.295321e+03,    1.303355e+03],    [1.038887e+03,
1.121379e+03,     1.202406e+03,     1.251024e+03,     1.264625e+03,
1.326880e+03],    [1.030181e+03,    1.107978e+03,     1.180822e+03,
1.225822e+03,    1.256242e+03,    1.305931e+03],    [1.003559e+03,
1.081005e+03,     1.158281e+03,     1.213174e+03,     1.278122e+03,
1.300865e+03],    [9.980535e+02,    1.100883e+03,     1.180839e+03,
1.259788e+03,    1.283694e+03,    1.307688e+03],    [1.023796e+03,
1.097568e+03,     1.170359e+03,     1.215616e+03,     1.246076e+03,
1.306972e+03],    [1.037688e+03,    1.113275e+03,     1.180011e+03,
1.221748e+03,    1.250833e+03,    1.279925e+03],    [1.021946e+03,
1.096856e+03,     1.170325e+03,     1.216775e+03,     1.249144e+03,
1.302424e+03],    [1.053261e+03,    1.104751e+03,     1.197313e+03,
1.290639e+03,    1.323019e+03,    1.326112e+03],    [1.016630e+03,
1.089943e+03,     1.135269e+03,     1.169734e+03,     1.198056e+03,
1.321270e+03],    [9.895543e+02,    1.095920e+03,     1.159550e+03,
1.222652e+03,    1.276342e+03,    1.306052e+03],    [1.027378e+03,
1.104297e+03,     1.223241e+03,     1.283379e+03,     1.293228e+03,
1.302686e+03],    [1.023308e+03,    1.101248e+03,     1.145824e+03,
1.200774e+03,    1.222987e+03,    1.312855e+03],    [1.040050e+03,
1.117922e+03,     1.191090e+03,     1.234098e+03,     1.273273e+03,
1.310400e+03],    [1.041486e+03,    1.116805e+03,     1.185236e+03,
1.227783e+03,    1.268583e+03,    1.305998e+03],    [1.059410e+03,
1.084061e+03,     1.146931e+03,     1.204180e+03,     1.253976e+03,
1.304734e+03],    [1.038879e+03,    1.114258e+03,     1.214082e+03,
1.282713e+03,    1.307785e+03,    1.313515e+03],    [1.028470e+03,
1.105231e+03,     1.182787e+03,     1.232207e+03,     1.267681e+03,
1.334355e+03],    [1.009476e+03,    1.127822e+03,     1.250859e+03,
1.307708e+03,    1.318826e+03,    1.322423e+03],    [1.020143e+03,
1.092022e+03,     1.203887e+03,     1.262764e+03,     1.299749e+03,
1.339248e+03],    [1.016699e+03,    1.089774e+03,     1.213113e+03,
1.231553e+03,    1.247049e+03,    1.301178e+03],    [1.015420e+03,
1.085483e+03,     1.160977e+03,     1.206845e+03,     1.238172e+03,
1.297520e+03],    [1.051522e+03,    1.068610e+03,     1.086964e+03,
1.110837e+03,    1.139810e+03,    1.320695e+03],    [1.028579e+03,
1.189686e+03,     1.274282e+03,     1.313868e+03,     1.327927e+03,
1.328219e+03],    [1.033661e+03,    1.112536e+03,     1.188083e+03,
1.233958e+03,    1.266788e+03,    1.330087e+03],    [1.028569e+03,
1.104006e+03,     1.179216e+03,     1.225050e+03,     1.270300e+03,
1.314120e+03],    [1.016227e+03,    1.091873e+03,     1.172120e+03,
1.220641e+03,    1.266677e+03,    1.318939e+03],    [1.055584e+03,
1.134090e+03,     1.201402e+03,     1.243980e+03,     1.272513e+03,
1.314777e+03],    [1.069691e+03,    1.086982e+03,     1.149057e+03,
1.201571e+03,    1.250634e+03,    1.308696e+03],    [1.035583e+03,
1.150998e+03,     1.209415e+03,     1.262688e+03,     1.306233e+03,
1.329657e+03],    [1.031368e+03,    1.121393e+03,     1.182319e+03,
1.238408e+03,    1.282716e+03,    1.300329e+03],    [1.010245e+03,
1.098449e+03,     1.218247e+03,     1.281269e+03,     1.295118e+03,
```

```
1.301015e+03],    [9.950558e+02,    1.103440e+03,    1.166877e+03,
1.230072e+03,    1.283141e+03,    1.309516e+03],    [1.030615e+03,
1.143286e+03,    1.179829e+03,    1.218659e+03,    1.256940e+03,
1.291174e+03],    [1.048517e+03,    1.085901e+03,    1.174823e+03,
1.268681e+03,    1.305724e+03,    1.313108e+03],    [1.032896e+03,
1.104815e+03,    1.169027e+03,    1.209961e+03,    1.248493e+03,
1.286657e+03],    [1.025529e+03,    1.096885e+03,    1.169351e+03,
1.215393e+03,    1.260193e+03,    1.302619e+03],    [1.029322e+03,
1.118751e+03,    1.179487e+03,    1.237897e+03,    1.284692e+03,
1.318586e+03],    [1.048592e+03,    1.127643e+03,    1.170736e+03,
1.226696e+03,    1.291563e+03,    1.328883e+03],    [1.034645e+03,
1.107379e+03,    1.175728e+03,    1.219214e+03,    1.261190e+03,
1.300918e+03]]

#-------------------------------------------------------------
#Data from abaqus 100 microns
    strain=[[0,    1.693476e-03,    6.755977e-03,    1.434973e-02,
2.574035e-02,  3.401635e-02],  [0,  1.674378e-03,  6.736879e-03,
1.433063e-02,  2.572125e-02,  3.159454e-02],  [0,  1.683763e-03,
6.746263e-03,  1.434001e-02,  2.573064e-02,  3.640935e-02],  [0,
1.713136e-03,    6.775636e-03,    1.436939e-02,    2.576001e-02,
3.163330e-02],  [0,  1.686866e-03,  6.749366e-03,  1.434312e-02,
2.573374e-02,  3.160703e-02],  [0,  7.740944e-03,  1.414817e-02,
2.375901e-02,  2.736308e-02,  3.276917e-02],  [0,  1.704474e-03,
6.766974e-03,  1.436072e-02,  2.575135e-02,  3.402735e-02],  [0,
1.672246e-03,    6.734746e-03,    1.432850e-02,    2.571912e-02,
3.319422e-02],  [0,  1.685425e-03,  6.747925e-03,  1.434168e-02,
2.573230e-02,  3.160559e-02],  [0,  1.697446e-03,  6.759946e-03,
1.435370e-02,  2.574432e-02,  3.321942e-02],  [0,  1.685899e-03,
6.748400e-03,  1.434215e-02,  2.573277e-02,  3.320787e-02],  [0,
1.681142e-03,    6.743642e-03,    1.433739e-02,    2.572802e-02,
3.160131e-02],  [0,  1.715710e-03,  6.778210e-03,  1.437196e-02,
2.576259e-02,  3.323768e-02],  [0,  1.717821e-03,  6.780322e-03,
1.437407e-02,  2.576470e-02,  3.163799e-02],  [0,  1.675804e-03,
6.738304e-03,  1.433205e-02,  2.572268e-02,  3.399868e-02],  [0,
5.034967e-04,    2.753497e-03,    6.128497e-03,    1.119100e-02,
3.444686e-02],  [0,  1.662132e-03,  6.724633e-03,  1.431838e-02,
2.570901e-02,  3.398501e-02],  [0,  1.715985e-03,  6.778485e-03,
1.437224e-02,  2.576286e-02,  3.403886e-02],  [0,  1.707878e-03,
6.770378e-03,  1.436413e-02,  2.575475e-02,  3.403076e-02],  [0,
1.709567e-03,    6.772068e-03,    1.436582e-02,    2.575644e-02,
3.403245e-02],  [0,  1.687692e-03,  6.750192e-03,  1.434394e-02,
2.573457e-02,  3.401057e-02],  [0,  1.660563e-03,  6.723063e-03,
1.431681e-02,  2.570744e-02,  3.158073e-02],  [0,  1.697363e-03,
6.759863e-03,  1.435361e-02,  2.574424e-02,  3.402024e-02],  [0,
1.673629e-03,    6.736129e-03,    1.432988e-02,    2.572050e-02,
3.159379e-02],  [0,  1.697795e-03,  6.760295e-03,  1.435405e-02,
```

```
2.574467e-02,  3.161796e-02],  [0,  1.705951e-03,  6.768451e-03,
1.436220e-02,  2.575283e-02,  3.402883e-02],  [0,  1.700083e-03,
6.762583e-03,  1.435633e-02,  2.574696e-02,  3.402296e-02],  [0,
1.722123e-03,    6.784623e-03,    1.437837e-02,    2.576900e-02,
3.464568e-02],  [0,  1.700654e-03,  6.763154e-03,  1.435690e-02,
2.574753e-02,  3.215475e-02],  [0,  1.691136e-03,  6.753636e-03,
1.434739e-02,  2.573801e-02,  3.161130e-02],  [0,  1.685649e-03,
6.748149e-03,  1.434190e-02,  2.573252e-02,  3.107188e-02],  [0,
1.689362e-03,    6.751862e-03,    1.434561e-02,    2.573624e-02,
3.491325e-02],  [0,  1.696076e-03,  6.758576e-03,  1.435233e-02,
2.574295e-02,  3.161624e-02],  [0,  1.691211e-03,  6.753711e-03,
1.434746e-02,  2.573809e-02,  3.321318e-02],  [0,  1.692235e-03,
6.754735e-03,  1.434849e-02,  2.573911e-02,  3.401511e-02],  [0,
1.696874e-03,    6.759375e-03,    1.435313e-02,    2.574375e-02,
3.396344e-02],  [0,  1.722374e-03,  6.784875e-03,  1.437863e-02,
2.576925e-02,  3.324435e-02],  [0,  1.685099e-03,  6.747599e-03,
1.434135e-02,  2.573197e-02,  3.400798e-02],  [0,  5.357893e-04,
2.785790e-03,  6.160790e-03,  1.122329e-02,  3.501309e-02],  [0,
1.685516e-03,    6.748016e-03,    1.434177e-02,    2.573239e-02,
3.520975e-02],  [0,  1.696763e-03,  6.759263e-03,  1.435301e-02,
2.574364e-02,  3.321874e-02],  [0,  1.706194e-03,  6.768694e-03,
1.436244e-02,  2.575307e-02,  3.748296e-02],  [0,  1.670748e-03,
6.733249e-03,  1.432700e-02,  2.571762e-02,  3.399363e-02],  [0,
1.702018e-03,    6.764518e-03,    1.435827e-02,    2.574889e-02,
3.162218e-02],  [0,  1.710392e-03,  6.772893e-03,  1.436664e-02,
2.575727e-02,  3.403327e-02],  [0,  1.690973e-03,  6.753473e-03,
1.434722e-02,  2.573785e-02,  3.401385e-02],  [0,  1.672929e-03,
6.735429e-03,  1.432918e-02,  2.571980e-02,  3.419603e-02],  [0,
1.730072e-03,    6.792572e-03,    1.438632e-02,    2.577695e-02,
3.365249e-02],  [0,  1.672402e-03,  6.734902e-03,  1.432865e-02,
2.571928e-02,  3.399528e-02],  [0,  1.680818e-03,  6.743318e-03,
1.433707e-02,  2.572769e-02,  3.520505e-02],  [0,  1.715931e-03,
6.778431e-03,  1.437218e-02,  2.576281e-02,  3.403881e-02],  [0,
1.698367e-03,    6.760867e-03,    1.435462e-02,    2.574524e-02,
3.678060e-02],  [0,  1.674072e-03,  6.736572e-03,  1.433032e-02,
2.572095e-02,  3.212817e-02],  [0,  1.695450e-03,  6.757950e-03,
1.435170e-02,  2.574232e-02,  3.481923e-02],  [0,  1.702990e-03,
6.765490e-03,  1.435924e-02,  2.574987e-02,  3.162316e-02],  [0,
1.659062e-03,    6.721562e-03,    1.431531e-02,    2.570594e-02,
3.398194e-02],  [0,  1.693961e-03,  6.756461e-03,  1.435021e-02,
2.574084e-02,  3.161413e-02],  [0,  1.700320e-03,  6.762820e-03,
1.435657e-02,  2.574719e-02,  3.162049e-02],  [0,  1.663446e-03,
6.725946e-03,  1.431970e-02,  2.571032e-02,  3.488734e-02],  [0,
1.680958e-03,    6.743458e-03,    1.433721e-02,    2.572783e-02,
3.520519e-02],  [0,  1.672146e-03,  6.734646e-03,  1.432840e-02,
2.571902e-02,  3.609739e-02],  [0,  1.669179e-03,  6.731679e-03,
1.432543e-02,  2.571605e-02,  3.319115e-02],  [0,  1.689666e-03,
```

```
6.752166e-03,  1.434592e-02,  2.573654e-02,  3.160983e-02],  [0,
1.665993e-03,    6.728493e-03,    1.432224e-02,    2.571287e-02,
3.519023e-02],  [0,  1.678119e-03,  6.740619e-03,  1.433437e-02,
2.572499e-02,  3.400100e-02],  [0,  1.676720e-03,  6.739220e-03,
1.433297e-02,  2.572359e-02,  3.399960e-02],  [0,  1.683510e-03,
6.746010e-03,  1.433976e-02,  2.573038e-02,  3.400639e-02],  [0,
1.671454e-03,    6.733954e-03,    1.432770e-02,    2.571833e-02,
3.159162e-02],  [0,  1.710247e-03,  6.772747e-03,  1.436650e-02,
2.575712e-02,  3.163041e-02],  [0,  1.694374e-03,  6.756874e-03,
1.435062e-02,  2.574125e-02,  3.401725e-02],  [0,  1.709348e-03,
6.771848e-03,  1.436560e-02,  2.575622e-02,  3.403223e-02],  [0,
1.692484e-03,    6.754984e-03,    1.434873e-02,    2.573936e-02,
3.401536e-02],  [0,  1.688821e-03,  6.751322e-03,  1.434507e-02,
2.573570e-02,  3.401170e-02],  [0,  1.694009e-03,  6.756509e-03,
1.435026e-02,  2.574088e-02,  3.321598e-02],  [0,  1.683140e-03,
6.745640e-03,  1.433939e-02,  2.573002e-02,  3.640873e-02],  [0,
1.684582e-03,    6.747083e-03,    1.434083e-02,    2.573146e-02,
3.400746e-02],  [0,  1.706803e-03,  6.769303e-03,  1.436305e-02,
2.575368e-02,  3.402968e-02],  [0,  1.707511e-03,  6.770011e-03,
1.436376e-02,  2.575439e-02,  3.403039e-02],  [0,  1.700582e-03,
6.763083e-03,  1.435683e-02,  2.574746e-02,  3.402346e-02],  [0,
1.703292e-03,    6.765792e-03,    1.435954e-02,    2.575017e-02,
3.402617e-02],  [0,  1.728517e-03,  6.791017e-03,  1.438477e-02,
2.577539e-02,  3.325049e-02],  [0,  1.725219e-03,  6.787719e-03,
1.438147e-02,  2.577209e-02,  3.404810e-02],  [0,  1.720416e-03,
6.782916e-03,  1.437667e-02,  2.576729e-02,  3.404329e-02],  [0,
1.684808e-03,    6.747309e-03,    1.434106e-02,    2.573168e-02,
3.160497e-02],  [0,  1.694432e-03,  6.756932e-03,  1.435068e-02,
2.574131e-02,  3.321640e-02],  [0,  1.692633e-03,  6.755133e-03,
1.434888e-02,  2.573951e-02,  3.401551e-02],  [0,  1.699549e-03,
6.762049e-03,  1.435580e-02,  2.574642e-02,  3.161971e-02],  [0,
1.706130e-03,    6.768630e-03,    1.436238e-02,    2.575300e-02,
3.402901e-02],  [0,  1.708769e-03,  6.771270e-03,  1.436502e-02,
2.575564e-02,  3.543323e-02],  [0,  1.655012e-03,  6.717512e-03,
1.431126e-02,  2.570189e-02,  3.157518e-02],  [0,  3.295786e-03,
7.567270e-03,  1.397450e-02,  2.358534e-02,  3.259550e-02],  [0,
1.707668e-03,    6.770168e-03,    1.436392e-02,    2.575454e-02,
3.448105e-02],  [0,  1.711711e-03,  6.774212e-03,  1.436796e-02,
2.575859e-02,  3.403459e-02],  [0,  1.739785e-03,  6.802285e-03,
1.439604e-02,  2.578666e-02,  3.406266e-02],  [0,  1.658188e-03,
6.720689e-03,  1.431444e-02,  2.570506e-02,  3.518242e-02],  [0,
1.711587e-03,    6.774087e-03,    1.436784e-02,    2.575846e-02,
3.313345e-02],  [0,  1.711303e-03,  6.773803e-03,  1.436755e-02,
2.575818e-02,  3.463486e-02],  [0,  1.699517e-03,  6.762017e-03,
1.435577e-02,  2.574639e-02,  3.402239e-02],  [0,  1.718601e-03,
6.781101e-03,  1.437485e-02,  2.576548e-02,  3.404148e-02],  [0,
```

```
1.690476e-03,    6.752976e-03,    1.434673e-02,    2.573735e-02,
3.461403e-02]]



    stress=[[1.072051e+03,       1.129633e+03,       1.207114e+03,
1.263359e+03,    1.296389e+03,    1.305412e+03],    [1.064373e+03,
1.124503e+03,    1.203808e+03,    1.262587e+03,    1.296433e+03,
1.305242e+03],    [1.075257e+03,    1.134486e+03,    1.211705e+03,
1.266294e+03,    1.297603e+03,    1.307135e+03],    [1.079030e+03,
1.134250e+03,    1.210330e+03,    1.264314e+03,    1.298347e+03,
1.305171e+03],    [1.070402e+03,    1.128884e+03,    1.206159e+03,
1.262340e+03,    1.296116e+03,    1.304278e+03],    [1.100273e+03,
1.219206e+03,    1.264256e+03,    1.293154e+03,    1.300060e+03,
1.302237e+03],    [1.076418e+03,    1.132667e+03,    1.209999e+03,
1.265630e+03,    1.298145e+03,    1.306385e+03],    [1.068181e+03,
1.128882e+03,    1.205477e+03,    1.262944e+03,    1.297092e+03,
1.305280e+03],    [1.071807e+03,    1.130588e+03,    1.209160e+03,
1.266460e+03,    1.298678e+03,    1.306523e+03],    [1.069178e+03,
1.126031e+03,    1.205216e+03,    1.262465e+03,    1.296534e+03,
1.304907e+03],    [1.068220e+03,    1.126730e+03,    1.204759e+03,
1.261016e+03,    1.295961e+03,    1.304086e+03],    [1.067540e+03,
1.126755e+03,    1.205072e+03,    1.262106e+03,    1.296251e+03,
1.303771e+03],    [1.076931e+03,    1.131710e+03,    1.209225e+03,
1.264966e+03,    1.298747e+03,    1.306725e+03],    [1.077855e+03,
1.132410e+03,    1.208930e+03,    1.264610e+03,    1.296352e+03,
1.304097e+03],    [1.067150e+03,    1.127203e+03,    1.205958e+03,
1.263368e+03,    1.296950e+03,    1.305487e+03],    [1.079835e+03,
1.101500e+03,    1.148438e+03,    1.198833e+03,    1.245604e+03,
1.306164e+03],    [1.063388e+03,    1.125567e+03,    1.205064e+03,
1.263687e+03,    1.296321e+03,    1.304799e+03],    [1.077805e+03,
1.132593e+03,    1.208964e+03,    1.265288e+03,    1.296879e+03,
1.306054e+03],    [1.074925e+03,    1.130632e+03,    1.207550e+03,
1.264198e+03,    1.297242e+03,    1.306367e+03],    [1.074518e+03,
1.129978e+03,    1.206081e+03,    1.262644e+03,    1.295854e+03,
1.304013e+03],    [1.068664e+03,    1.126926e+03,    1.205212e+03,
1.263303e+03,    1.296822e+03,    1.308839e+03],    [1.059806e+03,
1.122057e+03,    1.201215e+03,    1.260654e+03,    1.296610e+03,
1.304115e+03],    [1.070212e+03,    1.127132e+03,    1.205250e+03,
1.262506e+03,    1.295932e+03,    1.305361e+03],    [1.065264e+03,
1.125568e+03,    1.203546e+03,    1.261144e+03,    1.295825e+03,
1.304292e+03],    [1.070301e+03,    1.127164e+03,    1.205369e+03,
1.262913e+03,    1.297009e+03,    1.303757e+03],    [1.073996e+03,
1.129917e+03,    1.206592e+03,    1.263582e+03,    1.298159e+03,
1.305448e+03],    [1.070925e+03,    1.127497e+03,    1.205800e+03,
1.262564e+03,    1.295694e+03,    1.304791e+03],    [1.072340e+03,
1.126078e+03,    1.202687e+03,    1.261078e+03,    1.295396e+03,
```

```
1.305076e+03],    [1.072083e+03,    1.128636e+03,    1.206528e+03,
1.263245e+03,    1.295548e+03,    1.300611e+03],    [1.069163e+03,
1.126934e+03,    1.202386e+03,    1.259448e+03,    1.294621e+03,
1.303667e+03],    [1.068877e+03,    1.127463e+03,    1.205151e+03,
1.262938e+03,    1.296587e+03,    1.301941e+03],    [1.070894e+03,
1.129025e+03,    1.206878e+03,    1.263478e+03,    1.296460e+03,
1.307578e+03],    [1.071446e+03,    1.128617e+03,    1.205724e+03,
1.262974e+03,    1.296051e+03,    1.302764e+03],    [1.070179e+03,
1.127995e+03,    1.205345e+03,    1.259313e+03,    1.294161e+03,
1.302664e+03],    [1.069021e+03,    1.126622e+03,    1.204453e+03,
1.262525e+03,    1.295366e+03,    1.303646e+03],    [1.073633e+03,
1.130805e+03,    1.208478e+03,    1.264568e+03,    1.297672e+03,
1.306274e+03],    [1.075912e+03,    1.129798e+03,    1.205217e+03,
1.262161e+03,    1.296643e+03,    1.306221e+03],    [1.067735e+03,
1.126342e+03,    1.204726e+03,    1.263085e+03,    1.297033e+03,
1.306660e+03],    [1.081913e+03,    1.102402e+03,    1.149267e+03,
1.197897e+03,    1.243719e+03,    1.303545e+03],    [1.070229e+03,
1.128909e+03,    1.206475e+03,    1.264601e+03,    1.297904e+03,
1.308174e+03],    [1.071882e+03,    1.128977e+03,    1.206818e+03,
1.264215e+03,    1.297227e+03,    1.306210e+03],    [1.074912e+03,
1.130847e+03,    1.208052e+03,    1.264037e+03,    1.296487e+03,
1.308509e+03],    [1.066472e+03,    1.127328e+03,    1.206005e+03,
1.262683e+03,    1.295769e+03,    1.305149e+03],    [1.072596e+03,
1.128985e+03,    1.206186e+03,    1.263572e+03,    1.296368e+03,
1.304066e+03],    [1.074337e+03,    1.129678e+03,    1.207793e+03,
1.264576e+03,    1.296800e+03,    1.305712e+03],    [1.068376e+03,
1.126129e+03,    1.203089e+03,    1.259607e+03,    1.294809e+03,
1.305347e+03],    [1.068207e+03,    1.128794e+03,    1.207939e+03,
1.265679e+03,    1.298970e+03,    1.307964e+03],    [1.075866e+03,
1.128816e+03,    1.206863e+03,    1.264349e+03,    1.297457e+03,
1.306641e+03],    [1.065228e+03,    1.125735e+03,    1.205676e+03,
1.264674e+03,    1.296593e+03,    1.306480e+03],    [1.067000e+03,
1.126236e+03,    1.203609e+03,    1.261221e+03,    1.295804e+03,
1.307089e+03],    [1.075346e+03,    1.130016e+03,    1.206413e+03,
1.263740e+03,    1.297406e+03,    1.306441e+03],    [1.069614e+03,
1.126359e+03,    1.204215e+03,    1.261368e+03,    1.294163e+03,
1.303930e+03],    [1.064654e+03,    1.124851e+03,    1.203234e+03,
1.262331e+03,    1.298084e+03,    1.303823e+03],    [1.066793e+03,
1.123805e+03,    1.203992e+03,    1.263519e+03,    1.297799e+03,
1.306720e+03],    [1.072305e+03,    1.128544e+03,    1.205966e+03,
1.263645e+03,    1.297129e+03,    1.303851e+03],    [1.063702e+03,
1.126455e+03,    1.205574e+03,    1.262485e+03,    1.294987e+03,
1.302872e+03],    [1.067786e+03,    1.125068e+03,    1.203642e+03,
1.261825e+03,    1.295716e+03,    1.303388e+03],    [1.073262e+03,
1.129924e+03,    1.207553e+03,    1.263861e+03,    1.296926e+03,
1.303281e+03],    [1.065791e+03,    1.127875e+03,    1.206775e+03,
1.264112e+03,    1.298392e+03,    1.310098e+03],    [1.068855e+03,
```

```
1.128172e+03,    1.207435e+03,    1.264767e+03,    1.298889e+03,
1.309166e+03],    [1.066493e+03,    1.127115e+03,    1.205687e+03,
1.264291e+03,    1.297225e+03,    1.308481e+03],    [1.066137e+03,
1.127241e+03,    1.204599e+03,    1.262491e+03,    1.295305e+03,
1.303053e+03],    [1.069140e+03,    1.127129e+03,    1.204601e+03,
1.261051e+03,    1.295180e+03,    1.302480e+03],    [1.066109e+03,
1.127762e+03,    1.207187e+03,    1.264944e+03,    1.298760e+03,
1.309258e+03],    [1.070265e+03,    1.130115e+03,    1.208009e+03,
1.263642e+03,    1.297199e+03,    1.305581e+03],    [1.066352e+03,
1.126210e+03,    1.205891e+03,    1.265206e+03,    1.298467e+03,
1.308114e+03],    [1.070084e+03,    1.129067e+03,    1.207903e+03,
1.265294e+03,    1.296999e+03,    1.304574e+03],    [1.066364e+03,
1.127095e+03,    1.204184e+03,    1.261292e+03,    1.297035e+03,
1.305718e+03],    [1.075671e+03,    1.131101e+03,    1.208519e+03,
1.262893e+03,    1.296132e+03,    1.303895e+03],    [1.071400e+03,
1.128816e+03,    1.205116e+03,    1.261126e+03,    1.295958e+03,
1.306442e+03],    [1.072580e+03,    1.127969e+03,    1.204109e+03,
1.261765e+03,    1.296633e+03,    1.307454e+03],    [1.074873e+03,
1.132753e+03,    1.209145e+03,    1.265212e+03,    1.298189e+03,
1.307078e+03],    [1.067177e+03,    1.125187e+03,    1.205023e+03,
1.262733e+03,    1.296836e+03,    1.306293e+03],    [1.071851e+03,
1.129344e+03,    1.207303e+03,    1.265587e+03,    1.297863e+03,
1.305669e+03],    [1.068710e+03,    1.127676e+03,    1.207190e+03,
1.266576e+03,    1.299771e+03,    1.310213e+03],    [1.067260e+03,
1.125921e+03,    1.204460e+03,    1.261162e+03,    1.295345e+03,
1.304386e+03],    [1.070561e+03,    1.126188e+03,    1.205123e+03,
1.261925e+03,    1.295571e+03,    1.304974e+03],    [1.073102e+03,
1.128764e+03,    1.203790e+03,    1.259794e+03,    1.294277e+03,
1.302834e+03],    [1.076823e+03,    1.133635e+03,    1.211440e+03,
1.265088e+03,    1.298242e+03,    1.308865e+03],    [1.075967e+03,
1.132356e+03,    1.209020e+03,    1.265945e+03,    1.297926e+03,
1.306631e+03],    [1.080114e+03,    1.133459e+03,    1.207689e+03,
1.261862e+03,    1.295957e+03,    1.305169e+03],    [1.080494e+03,
1.134258e+03,    1.209956e+03,    1.263998e+03,    1.298139e+03,
1.307498e+03],    [1.076400e+03,    1.130554e+03,    1.206795e+03,
1.261201e+03,    1.295495e+03,    1.305259e+03],    [1.067005e+03,
1.125618e+03,    1.203552e+03,    1.262072e+03,    1.297002e+03,
1.306606e+03],    [1.072259e+03,    1.129712e+03,    1.207391e+03,
1.263446e+03,    1.297764e+03,    1.305991e+03],    [1.070795e+03,
1.128433e+03,    1.207085e+03,    1.263986e+03,    1.298532e+03,
1.307498e+03],    [1.071518e+03,    1.128197e+03,    1.207039e+03,
1.264463e+03,    1.297171e+03,    1.304920e+03],    [1.071636e+03,
1.127409e+03,    1.205469e+03,    1.263443e+03,    1.296963e+03,
1.305642e+03],    [1.075182e+03,    1.130783e+03,    1.208787e+03,
1.265735e+03,    1.297273e+03,    1.305969e+03],    [1.063762e+03,
1.127271e+03,    1.205588e+03,    1.263284e+03,    1.296956e+03,
1.305253e+03],    [1.092159e+03,    1.158303e+03,    1.213876e+03,
```

```
1.259933e+03,    1.290310e+03,    1.301122e+03],    [1.074828e+03,
1.130559e+03,     1.208259e+03,     1.264386e+03,     1.297085e+03,
1.305875e+03],    [1.073530e+03,    1.128655e+03,     1.205032e+03,
1.261897e+03,    1.296374e+03,    1.306054e+03],    [1.080316e+03,
1.132361e+03,     1.207599e+03,     1.262508e+03,     1.295588e+03,
1.304096e+03],    [1.061347e+03,    1.124121e+03,     1.204065e+03,
1.263500e+03,    1.296781e+03,    1.306608e+03],    [1.073423e+03,
1.128559e+03,     1.205646e+03,     1.262663e+03,     1.295190e+03,
1.303830e+03],    [1.073320e+03,    1.128489e+03,     1.206467e+03,
1.262219e+03,    1.297065e+03,    1.308496e+03],    [1.071044e+03,
1.127702e+03,     1.205618e+03,     1.262763e+03,     1.296780e+03,
1.305071e+03],    [1.075746e+03,    1.130095e+03,     1.205748e+03,
1.260957e+03,    1.294838e+03,    1.305897e+03],    [1.068199e+03,
1.126017e+03,     1.205594e+03,     1.263074e+03,     1.296302e+03,
1.306081e+03]]

#-----------------------------------------------------------------

#-----------------------------------------------------------------
    i = 1
    while i <= len(Xc):
        E= random.randrange(140, 240)
        EE= E*1000
        w= random.randint(0,99)

        mdb.models['Model-%d'%(qq)].Material(name='Small  Square-
%d'%(i))
        mdb.models['Model-%d'%(qq)].materials['Small      Square-
%d'%(i)].Elastic(table=((EE, 0.3), ))

        #mdb.models['Model-%d'%(qq)].materials['Small     Square-
%d'%(i)].Plastic(table=((stress[w][0],
strain[w][0]),(stress[w][5], strain[w][5])))

        #mdb.models['Model-%d'%(qq)].materials['Small     Square-
%d'%(i)].Plastic(table=((stress[w][0],
strain[w][0]),(stress[w][1],         strain[w][1]),(stress[w][2],
strain[w][2]),(stress[w][3],         strain[w][3]),(stress[w][4],
strain[w][4]),(stress[w][5],         strain[w][5]),(stress[w][6],
strain[w][6]),(stress[w][7],         strain[w][7]),(stress[w][8],
strain[w][8]),(stress[w][9], strain[w][9])))

        #mdb.models['Model-%d'%(qq)].materials['Small     Square-
%d'%(i)].Plastic(table=((stress[w][0],
strain[w][0]),(stress[w][1],         strain[w][1]),(stress[w][2],
strain[w][2]),(stress[w][3],         strain[w][3]),(stress[w][4],
strain[w][4]),(stress[w][5],         strain[w][5]),(stress[w][6],
```

```
strain[w][6]),(stress[w][7],         strain[w][7]),(stress[w][8],
strain[w][8])     ,(stress[w][9],   strain[w][9]),(stress[w][10],
strain[w][10]),(stress[w][11],     strain[w][11]),(stress[w][12],
strain[w][12])))

        mdb.models['Model-%d'%(qq)].materials['Small      Square-
%d'%(i)].Plastic(table=((stress[w][0],
strain[w][0]),(stress[w][1],         strain[w][1]),(stress[w][2],
strain[w][2]),(stress[w][3],         strain[w][3]),(stress[w][4],
strain[w][4]),(stress[w][5], strain[w][5])))

        mdb.models['Model-
%d'%(qq)].HomogeneousSolidSection(name='Small Square-%d'%(i),
        material='Small Square-%d'%(i), thickness=None)

        p = mdb.models['Model-%d'%(qq)].parts['Part-1']
        f = p.faces

        faces = f.findAt((Xc[i],Yc[i],0))
        q=faces.index
        Fac = f[q:q+1]
        region = p.Set(faces=Fac, name='Small Square-'+str(i))
# material assignment
        p.SectionAssignment(region=region,     sectionName='Small
Square-%d'%(i), offset=0.0,
        offsetType=MIDDLE_SURFACE, offsetField='',
        thicknessAssignment=FROM_SECTION)
        i=i+1

#==========================================================
    #Assembly
    a = mdb.models['Model-%d'%(qq)].rootAssembly
    p = mdb.models['Model-%d'%(qq)].parts['Part-1']
    a.Instance(name='Part-1-%d'%(qq), part=p, dependent=OFF)

#==========================================================
    #Step
    mdb.models['Model-%d'%(qq)].StaticStep(name='Step-1',
previous='Initial', maxNumInc=2000, minInc=1e-20, nlgeom=ON)
    mdb.models['Model-%d'%(qq)].steps['Step-
1'].setValues(maxNumInc=23000,
        initialInc=0.005, maxInc=0.1)


    #mdb.models['Model-%d'%(qq)].steps['Step-
1'].setValues(stabilizationMagnitude=0.0002,
stabilizationMethod=DISSIPATED_ENERGY_FRACTION,
```

```
continueDampingFactors=False,          adaptiveDampingRatio=0.05,
initialInc=0.01, matrixSolver=DIRECT, matrixStorage=UNSYMMETRIC)
#==========================================================
    #Meshing

    a = mdb.models['Model-%d'%(qq)].rootAssembly
    v1 = a.instances['Part-1-%d'%(qq)].vertices
    verts1      =      v1.findAt(((0,0,0),),      ((RVE_L,0,0),),
((0,RVE_W,0),), ((RVE_L,RVE_W,0),) )
    a.Set(vertices=verts1, name='Corners')

    a = mdb.models['Model-%d'%(qq)].rootAssembly
    e = a.instances['Part-1-%d'%(qq)].edges
#==========================================================
===
    #EdUp = e.getSequenceFromMask(mask=('[#4022002 ]', ), )
    #a.Set(edges=EdUp, name='Up')

    #EdLe = e.getSequenceFromMask(mask=('[#200124 ]', ), )
    #a.Set(edges=EdLe, name='Left')

    #EdDo = e.getSequenceFromMask(mask=('[#20040040 #4 ]', ), )
    #a.Set(edges=EdDo, name='Down')

    #EdRi = e.getSequenceFromMask(mask=('[#40010000 #82 ]', ), )
    #a.Set(edges=EdRi, name='Right')

#==========================================================
===
    EdUp    =    e.getSequenceFromMask(mask=('[#8020202    #200080
#88000020 #100000 ]', ), )
    a.Set(edges=EdUp, name='Up')

    EdLe = e.getSequenceFromMask(mask=('[#10040414 #400100 #480 #8
]', ), )
    a.Set(edges=EdLe, name='Left')

    EdDo   =   e.getSequenceFromMask(mask=('[#0:2   #100   #1000001
#40001000 #10004000 #420100 ]', ), )
    a.Set(edges=EdDo, name='Down')


    EdRi  =  e.getSequenceFromMask(mask=('[#0:2  #40000000  #800000
#20000800 #8002000 #8240080 ]', ), )
    a.Set(edges=EdRi, name='Right')
#==========================================================
===
```

```
    #a = mdb.models['Model-%d'%(qq)].rootAssembly
    #a.Set(edges=EdUp, name='Up')
    #a.Set(edges=EdDo, name='Down')
    #a.Set(edges=EdRi, name='Right')
    #a.Set(edges=EdLe, name='Left')

#=========================================================
    #Seed edges

    # Global Seed
    a = mdb.models['Model-%d'%(qq)].rootAssembly
    p = a.instances['Part-1-%d'%(qq)]
    EdgeMeshSize = avsize/2.0
    NumMeshRi = int (RVE_L/EdgeMeshSize)
    NumMeshUp = int (RVE_W/EdgeMeshSize)
    a.seedEdgeByNumber       (edges=EdRi,       number=NumMeshRi,
constraint=FIXED)
    a.seedEdgeByNumber       (edges=EdLe,       number=NumMeshRi,
constraint=FIXED)
    a.seedEdgeByNumber       (edges=EdUp,       number=NumMeshUp,
constraint=FIXED)
    a.seedEdgeByNumber       (edges=EdDo,       number=NumMeshUp,
constraint=FIXED)
    a = mdb.models['Model-%d'%(qq)].rootAssembly
    partInstances =(a.instances['Part-1-%d'%(qq)],)
    a.seedPartInstance(regions=partInstances,
size=avsize/seedfac, deviationFactor=0.1, minSizeFactor=0.1)

    elemType1           =           mesh.ElemType(elemCode=CPS4R,
elemLibrary=STANDARD,                    secondOrderAccuracy=OFF,
hourglassControl=ENHANCED, distortionControl=DEFAULT)

    elemType2           =            mesh.ElemType(elemCode=CPS3,
elemLibrary=STANDARD)

    a = mdb.models['Model-%d'%(qq)].rootAssembly
    f = a.instances['Part-1-%d'%(qq)].faces
    pickedRegions =(f, )
    a.setElementType(regions=pickedRegions, elemTypes=(elemType1,
elemType2))


    #a = mdb.models['Model-%d'%(qq)].rootAssembly
    #f1 = a.instances['Part-1-%d'%(qq)].faces
    #pickedRegions  =  f1.getSequenceFromMask(mask=('[#ffffffff:3
#f ]', ), )
    #a.setMeshControls(regions=pickedRegions, elemShape=TRI)
```

```
    a = mdb.models['Model-%d'%(qq)].rootAssembly
    partInstances =(a.instances['Part-1-%d'%(qq)], )
    a.generateMesh(regions=partInstances)

    session.viewports['Viewport: 1'].view.fitView()

#=============================================================
    # Finding the faces in the matrix
    #Storing the nodes of faces


    Upnodes = a.sets['Up'].nodes
    Downnodes = a.sets['Down'].nodes
    Rightnodes = a.sets['Right'].nodes
    Leftnodes = a.sets['Left'].nodes

    #Storing the coordinates and label of faces nodes
    UpCoord = []
    DownCoord = []
    RightCoord = []
    LeftCoord = []

    for node in Upnodes:
     UpCoord               =               UpCoord              +
[[node.coordinates[0],node.coordinates[1],node.label]]

    for node in Downnodes:
     DownCoord             =             DownCoord              +
[[node.coordinates[0],node.coordinates[1],node.label]]

    for node in Rightnodes:
     RightCoord            =            RightCoord              +
[[node.coordinates[0],node.coordinates[1],node.label]]

    for node in Leftnodes:
     LeftCoord             =             LeftCoord              +
[[node.coordinates[0],node.coordinates[1],node.label]]

    UpCoord.sort()
    DownCoord.sort()
    RightCoord.sort()
    LeftCoord.sort()

    #Degining sets for Up and Bottom faces
    NumUp = len(UpCoord)
```

```
    Node_Tol = 2
    for i in range(0,NumUp):
     if (abs(UpCoord[i][0]-DownCoord[i][0])<Node_Tol):

          NLable = DownCoord[i][2]
          a.Set(nodes=p.nodes[NLable-1:NLable],  name='DownNode_'
+str(i))
          NLable = UpCoord[i][2]
          a.Set(nodes=p.nodes[NLable-1:NLable],    name='UpNode_'
+str(i))
     else:
          print 'Distance between nodes are more than Tolerance'

    #Degining sets for Right and Left faces

    NumRi = len(RightCoord)
    for i in range(0,NumRi):
     if (abs(RightCoord[i][1]-LeftCoord[i][1])<Node_Tol):

          NLable = RightCoord[i][2]
          a.Set(nodes=p.nodes[NLable-1:NLable],
name='RightNode_'+str(i))
          NLable = LeftCoord[i][2]
          a.Set(nodes=p.nodes[NLable-1:NLable],  name='LeftNode_'
+str(i))
     else:
          print 'Distance between nodes are more than Tolerance'



#=========================================================
    #Defining constraints
    #Right and Left


    for i in range(1,NumRi):
     mdb.models['Model-%d'%(qq)].Equation(name='Const-LeRi-
x'+str(i),              terms=((-1.0,'LeftNode_'+str(i),1),(1.0,
'RightNode_'+str(i), 1), (-1.0, 'RightNode_0', 1)))

    for i in range(1,NumRi):
     mdb.models['Model-%d'%(qq)].Equation(name='Const-LeRi-
y'+str(i),              terms=((1.0,'LeftNode_'+str(i),2),(-1.0,
'RightNode_'+str(i), 2)))

    #Up and Down
    for i in range(1,NumUp-1):
```

```
     mdb.models['Model-%d'%(qq)].Equation(name='Const-UpDown-
y'+str(i),                terms=((-1.0,'DownNode_'+str(i),2),(1.0,
'UpNode_'+str(i), 2),(-1.0, 'UpNode_0', 2)))

    for i in range(1,NumUp-1):
     mdb.models['Model-%d'%(qq)].Equation(name='Const-UpDown-
x'+str(i),                terms=((1.0,'DownNode_'+str(i),1),(-1.0,
'UpNode_'+str(i), 1)))


#============================================================
    #Load
    #Fix Left Bottom corner along x and y
    a = mdb.models['Model-%d'%(qq)].rootAssembly
    v = a.instances['Part-1-%d'%(qq)].vertices
    ver = v.findAt((0.0,0.0,0.0))
    q = ver.index
    Fixver = v[q:q+1]
    region = a.Set(vertices=Fixver, name='Set-Fix')
    mdb.models['Model-%d'%(qq)].PinnedBC(name='Fix',
createStepName='Initial', region=region, localCsys=None)

    #Fix Left Up corner along x direction
    ver = v.findAt((0.0,RVE_W,0.0))
    q = ver.index
    Movever = v[q:q+1]
    region = a.Set(vertices=Movever, name='LeftX')
    mdb.models['Model-%d'%(qq)].DisplacementBC(name='LeftX',
createStepName='Step-1',    region=region,    u1=0.0,    u2=UNSET,
ur3=UNSET, amplitude=UNSET, fixed=OFF, distributionType=UNIFORM,
fieldName='', localCsys=None)

    #Fix Right Bottom corner along y direction
    ver = v.findAt((RVE_L,0.0,0.0))
    q = ver.index
    Movever = v[q:q+1]
    region = a.Set(vertices=Movever, name='Set-Move')
    mdb.models['Model-%d'%(qq)].DisplacementBC(name='Set-Move',
createStepName='Step-1', region=region, u1=disfac*RVE_L, u2=0.0,
ur3=UNSET, amplitude=UNSET, fixed=OFF, distributionType=UNIFORM,
fieldName='', localCsys=None)
#============================================================
    #History Output

    regionDef=mdb.models['Model-
%d'%(qq)].rootAssembly.sets['Corners']
```

```
    mdb.models['Model-%d'%(qq)].HistoryOutputRequest(name='H-
Output-2',
        createStepName='Step-1', variables=('RF1', 'RF2', 'U1',
'U2', 'COOR1',
        'COOR2',           'NFORC'),           region=regionDef,
sectionPoints=DEFAULT,
        rebar=EXCLUDE)

    #mdb.models['Model-%d'%(qq)].FieldOutputRequest(name='F-
Output-1',
      #  createStepName='Step-1', variables=('NFORC', ))


#==========================================================
    #JOB
    mdb.Job(name='RVExTension__%d'%(qq),   model='Model-%d'%(qq),
description='',   type=ANALYSIS,   atTime=None,   waitMinutes=0,
waitHours=0,   queue=None,   memory=90,   memoryUnits=PERCENTAGE,
getMemoryFromAnalysis=True,             explicitPrecision=SINGLE,
nodalOutputPrecision=SINGLE,    echoPrint=OFF,    modelPrint=OFF,
contactPrint=OFF,      historyPrint=OFF,      userSubroutine='',
scratch='',    resultsFormat=ODB,    multiprocessingMode=DEFAULT,
numCpus=1, numGPUs=0)
#==========================================================

    #SUBMIT JOB
    mdb.jobs['RVExTension__%d' %(qq)].writeInput()
    mdb.jobs['RVExTension__%d'
%(qq)].submit(consistencyChecking=OFF)
    mdb.jobs['RVExTension__%d' %(qq)].waitForCompletion()

#==========================================================

    session.mdbData.summary()
    o3                                                          =
session.openOdb(name='C:/Users/dg033/RVExTension__%d.odb'%(qq))
    session.viewports['Viewport:
1'].setValues(displayedObject=o3)
    odb    =    session.odbs['C:/Users/dg033/RVExTension__%d.odb'
%(qq)]
    xy1 = xyPlot.XYDataFromHistory(odb=odb,
        outputVariableName='Coordinates: COOR1 at Node 3 in NSET
CORNERS',
        steps=('Step-1', ), suppressQuery=True)
    c1 = session.Curve(xyData=xy1)
    xy2 = xyPlot.XYDataFromHistory(odb=odb,
```

```
        outputVariableName='Coordinates: COOR1 at Node 46 in NSET
CORNERS',
        steps=('Step-1', ), suppressQuery=True)
    c2 = session.Curve(xyData=xy2)
    xy3 = xyPlot.XYDataFromHistory(odb=odb,
        outputVariableName='Coordinates: COOR1 at Node 61 in NSET
CORNERS',
        steps=('Step-1', ), suppressQuery=True)
    c3 = session.Curve(xyData=xy3)
    xy4 = xyPlot.XYDataFromHistory(odb=odb,
        outputVariableName='Coordinates: COOR1 at Node 119 in NSET
CORNERS',
        steps=('Step-1', ), suppressQuery=True)
    c4 = session.Curve(xyData=xy4)
    xy5 = xyPlot.XYDataFromHistory(odb=odb,
        outputVariableName='Coordinates: COOR2 at Node 3 in NSET
CORNERS',
        steps=('Step-1', ), suppressQuery=True)
    c5 = session.Curve(xyData=xy5)
    xy6 = xyPlot.XYDataFromHistory(odb=odb,
        outputVariableName='Coordinates: COOR2 at Node 46 in NSET
CORNERS',
        steps=('Step-1', ), suppressQuery=True)
    c6 = session.Curve(xyData=xy6)
    xy7 = xyPlot.XYDataFromHistory(odb=odb,
        outputVariableName='Coordinates: COOR2 at Node 61 in NSET
CORNERS',
        steps=('Step-1', ), suppressQuery=True)
    c7 = session.Curve(xyData=xy7)
    xy8 = xyPlot.XYDataFromHistory(odb=odb,
        outputVariableName='Coordinates: COOR2 at Node 119 in NSET
CORNERS',
        steps=('Step-1', ), suppressQuery=True)
    c8 = session.Curve(xyData=xy8)
    xy9 = xyPlot.XYDataFromHistory(odb=odb,
        outputVariableName='Reaction force: RF1 at Node 3 in NSET
CORNERS',
        steps=('Step-1', ), suppressQuery=True)
    c9 = session.Curve(xyData=xy9)
    xy10 = xyPlot.XYDataFromHistory(odb=odb,
        outputVariableName='Reaction force: RF1 at Node 46 in NSET
CORNERS',
        steps=('Step-1', ), suppressQuery=True)
    c10 = session.Curve(xyData=xy10)
    xy11 = xyPlot.XYDataFromHistory(odb=odb,
        outputVariableName='Reaction force: RF1 at Node 61 in NSET
CORNERS',
```

```
        steps=('Step-1', ), suppressQuery=True)
    c11 = session.Curve(xyData=xy11)
    xy12 = xyPlot.XYDataFromHistory(odb=odb,
        outputVariableName='Reaction force: RF1 at Node 119 in
NSET CORNERS',
        steps=('Step-1', ), suppressQuery=True)
    c12 = session.Curve(xyData=xy12)
    xy13 = xyPlot.XYDataFromHistory(odb=odb,
        outputVariableName='Reaction force: RF2 at Node 3 in NSET
CORNERS',
        steps=('Step-1', ), suppressQuery=True)
    c13 = session.Curve(xyData=xy13)
    xy14 = xyPlot.XYDataFromHistory(odb=odb,
        outputVariableName='Reaction force: RF2 at Node 46 in NSET
CORNERS',
        steps=('Step-1', ), suppressQuery=True)
    c14 = session.Curve(xyData=xy14)
    xy15 = xyPlot.XYDataFromHistory(odb=odb,
        outputVariableName='Reaction force: RF2 at Node 61 in NSET
CORNERS',
        steps=('Step-1', ), suppressQuery=True)
    c15 = session.Curve(xyData=xy15)
    xy16 = xyPlot.XYDataFromHistory(odb=odb,
        outputVariableName='Reaction force: RF2 at Node 119 in
NSET CORNERS',
        steps=('Step-1', ), suppressQuery=True)
    c16 = session.Curve(xyData=xy16)
    xy17 = xyPlot.XYDataFromHistory(odb=odb,
        outputVariableName='Spatial displacement: U1 at Node 3 in
NSET CORNERS',
        steps=('Step-1', ), suppressQuery=True)
    c17 = session.Curve(xyData=xy17)
    xy18 = xyPlot.XYDataFromHistory(odb=odb,
        outputVariableName='Spatial displacement: U1 at Node 46 in
NSET CORNERS',
        steps=('Step-1', ), suppressQuery=True)
    c18 = session.Curve(xyData=xy18)
    xy19 = xyPlot.XYDataFromHistory(odb=odb,
        outputVariableName='Spatial displacement: U1 at Node 61 in
NSET CORNERS',
        steps=('Step-1', ), suppressQuery=True)
    c19 = session.Curve(xyData=xy19)
    xy20 = xyPlot.XYDataFromHistory(odb=odb,
        outputVariableName='Spatial displacement: U1 at Node 119
in NSET CORNERS',
        steps=('Step-1', ), suppressQuery=True)
    c20 = session.Curve(xyData=xy20)
```

```
    xy21 = xyPlot.XYDataFromHistory(odb=odb,
        outputVariableName='Spatial displacement: U2 at Node 3 in
NSET CORNERS',
        steps=('Step-1', ), suppressQuery=True)
    c21 = session.Curve(xyData=xy21)
    xy22 = xyPlot.XYDataFromHistory(odb=odb,
        outputVariableName='Spatial displacement: U2 at Node 46 in
NSET CORNERS',
        steps=('Step-1', ), suppressQuery=True)
    c22 = session.Curve(xyData=xy22)
    xy23 = xyPlot.XYDataFromHistory(odb=odb,
        outputVariableName='Spatial displacement: U2 at Node 61 in
NSET CORNERS',
        steps=('Step-1', ), suppressQuery=True)
    c23 = session.Curve(xyData=xy23)
    xy24 = xyPlot.XYDataFromHistory(odb=odb,
        outputVariableName='Spatial displacement: U2 at Node 119
in NSET CORNERS',
        steps=('Step-1', ), suppressQuery=False)
    c24 = session.Curve(xyData=xy24)
    xyp = session.xyPlots['XYPlot-1']
    chartName = xyp.charts.keys()[0]
    chart = xyp.charts[chartName]
    chart.setValues(curvesToPlot=(c1, c2, c3, c4, c5, c6, c7, c8,
c9, c10, c11,
        c12, c13, c14, c15, c16, c17, c18, c19, c20, c21, c22,
c23, c24, ), )
    session.viewports['Viewport:
1'].setValues(displayedObject=xyp)
    import sys
    sys.path.insert(34,
        r'c:/SIMULIA/Abaqus/6.14-
2/code/python2.7/lib/abaqus_plugins/excelUtilities')
    import abq_ExcelUtilities.excelUtilities


abq_ExcelUtilities.excelUtilities.XYtoExcel(xyDataNames='From
Current XY Plot',
        trueName='From Current XY Plot')
```

Appendix C: Python|Abaqus script used to study the effect of voids in SLM metals

This appendix contains the code used to generate RVE with voids in Abaqus. The code automatically applies PBC to the model. The user has to define the size of the RVE, the maximum and minimum size of the voids, and the volume fraction of the voids. The code is divided into section that describes what the code is does.

```
import part
import material
import section
import assembly
import step
import interaction
import load
import mesh
import optimization
import job
import sketch
import visualization
from connectorBehavior import *
from regionToolset import*
from xyPlot import*
import displayGroupMdbToolset as dgm
import displayGroupOdbToolset as dgo
import random
from array import *
import math
import numpy
import os        # Operating system
import shutil    # copying or moving files
#import matplotlib.pyplot as plt
#%matplotlib inline

RVE_W = .01 #RVE y dimension (m)
RVE_L = RVE_W #RVE x dimension (m)
#RVE_W = RVE_L/3 #RVE y dimension (m)
maxsize = 0.0001 #Max Void size (m)
minsize = 0.00002 #Min Void size (m)
Vf = .02  #desired Volume fraction
Vc = 0 #Volume fraction counter
#phi = .6 #Distance factor
```

```
F = 1.3 #Distance borders factor
disfac = .2 #displacement = disfac*RVE_L
seedfac = 3 #seed = averagesize of voids/seedfac
#dis=numpy.zeros(1000)
qq=1
volu_frac = {}
num_voids = {}
avdia = {}
Max_iterations= 1   # Set number of iterations

#=========================================================
#Creates RVE and Voids

for qq in range(1,Max_iterations+1):
    Vc = 0
    mdb.Model(modelType=STANDARD_EXPLICIT, name='Model-%d'%(qq))

    s1                    =                    mdb.models['Model-
%d'%(qq)].ConstrainedSketch(name='__profile__',
            sheetSize=RVE_L*2)
    g,  v,  d,  c  =  s1.geometry,  s1.vertices,  s1.dimensions,
s1.constraints
    s1.setPrimaryObject(option=STANDALONE)
    s1.rectangle(point1=(0.0, 0.0), point2=(RVE_L, RVE_W))


    x_coordinate = {}
    y_coordinate = {}
    D={}  # Diameter of Voids
    D[1]= 0
    Vi = 0
    while (D[1] < minsize) or Vi > Vf:
     D[1] = random.random()*maxsize

     Vi = 100*(3.14159*(D[1]**2))/(4*RVE_L*RVE_W)

    Vc = Vi
    x_coordinate[1]=0
    y_coordinate[1]=0

    dis={}
    disx = {}
    disxx = {}
    disy={}
    disyy = {}
```

```
    while      ((x_coordinate[1]-(D[1]/2)*F      <      0)      or
(x_coordinate[1]+(D[1]/2)*F > RVE_L)):
       x_coordinate[1]=(random.random()*RVE_L)
       disx[1]=x_coordinate[1]-(D[1]/2)
       disxx[1]=x_coordinate[1]+(D[1]/2)

    while      (y_coordinate[1]-(D[1]/2)*F      <      0      or
y_coordinate[1]+(D[1]/2)*F > RVE_W):
       y_coordinate[1]=(random.random()*RVE_W)
       disy[1]=y_coordinate[1]-(D[1]/2)
       disyy[1]=y_coordinate[1]+(D[1]/2)
    v=2

    while (Vc < Vf):
        D[v] = -1
        random_x = -1
        random_y = -1
        while (D[v] < minsize):
            D[v] = random.random()*maxsize
            i = Vc+100*(3.14159*(D[v]**2))/(4*RVE_L*RVE_W)
            if i > Vf*1.05:
                D[v] = 0

        #random_x=random.random()*RVE_L       #generate    random
x_coordinate within RVE

        while (random_x - (D[v]/2)*F) < 0 or (random_x + (D[v]/2)*F
> RVE_L):
                random_x = random.random()*RVE_L

        #random_y=random.random()*RVE_W       #generate    random
y_coordinate within RVE
        while (random_y - (D[v]/2)*F) < 0 or (random_y + (D[v]/2)*F
> RVE_W):
                random_y = random.random()*RVE_W

        isPointIntersecting = False


        # To check if new inclusion intersects with any existing
inclusions
        for j in range (1,len(x_coordinate)):


            dis=math.sqrt(((random_x-
x_coordinate[j])**2)+((random_y-y_coordinate[j])**2))*.7
```

```
            if dis < (D[v]+D[j]):

                isPointIntersecting = True
                break

        if (isPointIntersecting == False):
            x_coordinate[v]=(random_x)
            y_coordinate[v]=(random_y)
            Vc = Vc+100*(3.14159*(D[v]**2))/(4*RVE_L*RVE_W)
            v=v+1
            dis=0




    D_list = list(D.values())
    r_list = [a/2 for a in D_list]
    x_list = list(x_coordinate.values())
    y_list = list(y_coordinate.values())
    avsize = sum(D_list)/len(D_list)

    for i in range (0,len(D)):
        s1.CircleByCenterPerimeter(center=(x_list[i], y_list[i]),
point1=(x_list[i]-r_list[i], y_list[i]))
     p      =      mdb.models['Model-%d'%(qq)].Part(name='Part-1',
dimensionality=TWO_D_PLANAR,
        type=DEFORMABLE_BODY)
    p = mdb.models['Model-%d'%(qq)].parts['Part-1']
    p.BaseShell(sketch=s1)
    s1.unsetPrimaryObject()
    p = mdb.models['Model-%d'%(qq)].parts['Part-1']
    session.viewports['Viewport: 1'].setValues(displayedObject=p)
    del mdb.models['Model-%d'%(qq)].sketches['__profile__']

   # print("Number of Voids",len(D))
   # print("Average Diameter of Voids", avsize)
  #  print("Volume Fraction", Vc)

#============================================================
    # Material Properties
    # Randomize properties
    #E= random.randrange(140, 240)
    #EE= E*1000000000
    EE=187e9

#============================================================
```

```
#Data from upscaled RVE 100UM
    #strain=[[0,   1.693476e-03,   6.755977e-03,   1.434973e-02,
2.574035e-02,  3.401635e-02],  [0,  1.674378e-03,  6.736879e-03,
1.433063e-02,  2.572125e-02,  3.159454e-02],  [0,  1.683763e-03,
6.746263e-03,  1.434001e-02,  2.573064e-02,  3.640935e-02],  [0,
1.713136e-03,    6.775636e-03,    1.436939e-02,    2.576001e-02,
3.163330e-02],  [0,  1.686866e-03,  6.749366e-03,  1.434312e-02,
2.573374e-02,  3.160703e-02],  [0,  7.740944e-03,  1.414817e-02,
2.375901e-02,  2.736308e-02,  3.276917e-02],  [0,  1.704474e-03,
6.766974e-03,  1.436072e-02,  2.575135e-02,  3.402735e-02],  [0,
1.672246e-03,    6.734746e-03,    1.432850e-02,    2.571912e-02,
3.319422e-02],  [0,  1.685425e-03,  6.747925e-03,  1.434168e-02,
2.573230e-02,  3.160559e-02],  [0,  1.697446e-03,  6.759946e-03,
1.435370e-02,  2.574432e-02,  3.321942e-02],  [0,  1.685899e-03,
6.748400e-03,  1.434215e-02,  2.573277e-02,  3.320787e-02],  [0,
1.681142e-03,    6.743642e-03,    1.433739e-02,    2.572802e-02,
3.160131e-02],  [0,  1.715710e-03,  6.778210e-03,  1.437196e-02,
2.576259e-02,  3.323768e-02],  [0,  1.717821e-03,  6.780322e-03,
1.437407e-02,  2.576470e-02,  3.163799e-02],  [0,  1.675804e-03,
6.738304e-03,  1.433205e-02,  2.572268e-02,  3.399868e-02],  [0,
5.034967e-04,    2.753497e-03,    6.128497e-03,    1.119100e-02,
3.444686e-02],  [0,  1.662132e-03,  6.724633e-03,  1.431838e-02,
2.570901e-02,  3.398501e-02],  [0,  1.715985e-03,  6.778485e-03,
1.437224e-02,  2.576286e-02,  3.403886e-02],  [0,  1.707878e-03,
6.770378e-03,  1.436413e-02,  2.575475e-02,  3.403076e-02],  [0,
1.709567e-03,    6.772068e-03,    1.436582e-02,    2.575644e-02,
3.403245e-02],  [0,  1.687692e-03,  6.750192e-03,  1.434394e-02,
2.573457e-02,  3.401057e-02],  [0,  1.660563e-03,  6.723063e-03,
1.431681e-02,  2.570744e-02,  3.158073e-02],  [0,  1.697363e-03,
6.759863e-03,  1.435361e-02,  2.574424e-02,  3.402024e-02],  [0,
1.673629e-03,    6.736129e-03,    1.432988e-02,    2.572050e-02,
3.159379e-02],  [0,  1.697795e-03,  6.760295e-03,  1.435405e-02,
2.574467e-02,  3.161796e-02],  [0,  1.705951e-03,  6.768451e-03,
1.436220e-02,  2.575283e-02,  3.402883e-02],  [0,  1.700083e-03,
6.762583e-03,  1.435633e-02,  2.574696e-02,  3.402296e-02],  [0,
1.722123e-03,    6.784623e-03,    1.437837e-02,    2.576900e-02,
3.464568e-02],  [0,  1.700654e-03,  6.763154e-03,  1.435690e-02,
2.574753e-02,  3.215475e-02],  [0,  1.691136e-03,  6.753636e-03,
1.434739e-02,  2.573801e-02,  3.161130e-02],  [0,  1.685649e-03,
6.748149e-03,  1.434190e-02,  2.573252e-02,  3.107188e-02],  [0,
1.689362e-03,    6.751862e-03,    1.434561e-02,    2.573624e-02,
3.491325e-02],  [0,  1.696076e-03,  6.758576e-03,  1.435233e-02,
2.574295e-02,  3.161624e-02],  [0,  1.691211e-03,  6.753711e-03,
1.434746e-02,  2.573809e-02,  3.321318e-02],  [0,  1.692235e-03,
6.754735e-03,  1.434849e-02,  2.573911e-02,  3.401511e-02],  [0,
1.696874e-03,    6.759375e-03,    1.435313e-02,    2.574375e-02,
3.396344e-02],  [0,  1.722374e-03,  6.784875e-03,  1.437863e-02,
```

```
2.576925e-02,  3.324435e-02],  [0,  1.685099e-03,  6.747599e-03,
1.434135e-02,  2.573197e-02,  3.400798e-02],  [0,  5.357893e-04,
2.785790e-03,  6.160790e-03,  1.122329e-02,  3.501309e-02],  [0,
1.685516e-03,    6.748016e-03,    1.434177e-02,    2.573239e-02,
3.520975e-02],  [0,  1.696763e-03,  6.759263e-03,  1.435301e-02,
2.574364e-02,  3.321874e-02],  [0,  1.706194e-03,  6.768694e-03,
1.436244e-02,  2.575307e-02,  3.748296e-02],  [0,  1.670748e-03,
6.733249e-03,  1.432700e-02,  2.571762e-02,  3.399363e-02],  [0,
1.702018e-03,    6.764518e-03,    1.435827e-02,    2.574889e-02,
3.162218e-02],  [0,  1.710392e-03,  6.772893e-03,  1.436664e-02,
2.575727e-02,  3.403327e-02],  [0,  1.690973e-03,  6.753473e-03,
1.434722e-02,  2.573785e-02,  3.401385e-02],  [0,  1.672929e-03,
6.735429e-03,  1.432918e-02,  2.571980e-02,  3.419603e-02],  [0,
1.730072e-03,    6.792572e-03,    1.438632e-02,    2.577695e-02,
3.365249e-02],  [0,  1.672402e-03,  6.734902e-03,  1.432865e-02,
2.571928e-02,  3.399528e-02],  [0,  1.680818e-03,  6.743318e-03,
1.433707e-02,  2.572769e-02,  3.520505e-02],  [0,  1.715931e-03,
6.778431e-03,  1.437218e-02,  2.576281e-02,  3.403881e-02],  [0,
1.698367e-03,    6.760867e-03,    1.435462e-02,    2.574524e-02,
3.678060e-02],  [0,  1.674072e-03,  6.736572e-03,  1.433032e-02,
2.572095e-02,  3.212817e-02],  [0,  1.695450e-03,  6.757950e-03,
1.435170e-02,  2.574232e-02,  3.481923e-02],  [0,  1.702990e-03,
6.765490e-03,  1.435924e-02,  2.574987e-02,  3.162316e-02],  [0,
1.659062e-03,    6.721562e-03,    1.431531e-02,    2.570594e-02,
3.398194e-02],  [0,  1.693961e-03,  6.756461e-03,  1.435021e-02,
2.574084e-02,  3.161413e-02],  [0,  1.700320e-03,  6.762820e-03,
1.435657e-02,  2.574719e-02,  3.162049e-02],  [0,  1.663446e-03,
6.725946e-03,  1.431970e-02,  2.571032e-02,  3.488734e-02],  [0,
1.680958e-03,    6.743458e-03,    1.433721e-02,    2.572783e-02,
3.520519e-02],  [0,  1.672146e-03,  6.734646e-03,  1.432840e-02,
2.571902e-02,  3.609739e-02],  [0,  1.669179e-03,  6.731679e-03,
1.432543e-02,  2.571605e-02,  3.319115e-02],  [0,  1.689666e-03,
6.752166e-03,  1.434592e-02,  2.573654e-02,  3.160983e-02],  [0,
1.665993e-03,    6.728493e-03,    1.432224e-02,    2.571287e-02,
3.519023e-02],  [0,  1.678119e-03,  6.740619e-03,  1.433437e-02,
2.572499e-02,  3.400100e-02],  [0,  1.676720e-03,  6.739220e-03,
1.433297e-02,  2.572359e-02,  3.399960e-02],  [0,  1.683510e-03,
6.746010e-03,  1.433976e-02,  2.573038e-02,  3.400639e-02],  [0,
1.671454e-03,    6.733954e-03,    1.432770e-02,    2.571833e-02,
3.159162e-02],  [0,  1.710247e-03,  6.772747e-03,  1.436650e-02,
2.575712e-02,  3.163041e-02],  [0,  1.694374e-03,  6.756874e-03,
1.435062e-02,  2.574125e-02,  3.401725e-02],  [0,  1.709348e-03,
6.771848e-03,  1.436560e-02,  2.575622e-02,  3.403223e-02],  [0,
1.692484e-03,    6.754984e-03,    1.434873e-02,    2.573936e-02,
3.401536e-02],  [0,  1.688821e-03,  6.751322e-03,  1.434507e-02,
2.573570e-02,  3.401170e-02],  [0,  1.694009e-03,  6.756509e-03,
1.435026e-02,  2.574088e-02,  3.321598e-02],  [0,  1.683140e-03,
```

```
6.745640e-03,  1.433939e-02,  2.573002e-02,  3.640873e-02],  [0,
1.684582e-03,    6.747083e-03,    1.434083e-02,    2.573146e-02,
3.400746e-02],  [0,  1.706803e-03,  6.769303e-03,  1.436305e-02,
2.575368e-02,  3.402968e-02],  [0,  1.707511e-03,  6.770011e-03,
1.436376e-02,  2.575439e-02,  3.403039e-02],  [0,  1.700582e-03,
6.763083e-03,  1.435683e-02,  2.574746e-02,  3.402346e-02],  [0,
1.703292e-03,    6.765792e-03,    1.435954e-02,    2.575017e-02,
3.402617e-02],  [0,  1.728517e-03,  6.791017e-03,  1.438477e-02,
2.577539e-02,  3.325049e-02],  [0,  1.725219e-03,  6.787719e-03,
1.438147e-02,  2.577209e-02,  3.404810e-02],  [0,  1.720416e-03,
6.782916e-03,  1.437667e-02,  2.576729e-02,  3.404329e-02],  [0,
1.684808e-03,    6.747309e-03,    1.434106e-02,    2.573168e-02,
3.160497e-02],  [0,  1.694432e-03,  6.756932e-03,  1.435068e-02,
2.574131e-02,  3.321640e-02],  [0,  1.692633e-03,  6.755133e-03,
1.434888e-02,  2.573951e-02,  3.401551e-02],  [0,  1.699549e-03,
6.762049e-03,  1.435580e-02,  2.574642e-02,  3.161971e-02],  [0,
1.706130e-03,    6.768630e-03,    1.436238e-02,    2.575300e-02,
3.402901e-02],  [0,  1.708769e-03,  6.771270e-03,  1.436502e-02,
2.575564e-02,  3.543323e-02],  [0,  1.655012e-03,  6.717512e-03,
1.431126e-02,  2.570189e-02,  3.157518e-02],  [0,  3.295786e-03,
7.567270e-03,  1.397450e-02,  2.358534e-02,  3.259550e-02],  [0,
1.707668e-03,    6.770168e-03,    1.436392e-02,    2.575454e-02,
3.448105e-02],  [0,  1.711711e-03,  6.774212e-03,  1.436796e-02,
2.575859e-02,  3.403459e-02],  [0,  1.739785e-03,  6.802285e-03,
1.439604e-02,  2.578666e-02,  3.406266e-02],  [0,  1.658188e-03,
6.720689e-03,  1.431444e-02,  2.570506e-02,  3.518242e-02],  [0,
1.711587e-03,    6.774087e-03,    1.436784e-02,    2.575846e-02,
3.313345e-02],  [0,  1.711303e-03,  6.773803e-03,  1.436755e-02,
2.575818e-02,  3.463486e-02],  [0,  1.699517e-03,  6.762017e-03,
1.435577e-02,  2.574639e-02,  3.402239e-02],  [0,  1.718601e-03,
6.781101e-03,  1.437485e-02,  2.576548e-02,  3.404148e-02],  [0,
1.690476e-03,    6.752976e-03,    1.434673e-02,    2.573735e-02,
3.461403e-02]]


    #stress=[[1.072051e+09,      1.129633e+09,      1.207114e+09,
1.263359e+09,    1.296389e+09,    1.305412e+09],    [1.064373e+09,
1.124503e+09,    1.203808e+09,    1.262587e+09,    1.296433e+09,
1.305242e+09],    [1.075257e+09,    1.134486e+09,    1.211705e+09,
1.266294e+09,    1.297603e+09,    1.307135e+09],    [1.079030e+09,
1.134250e+09,    1.210330e+09,    1.264314e+09,    1.298347e+09,
1.305171e+09],    [1.070402e+09,    1.128884e+09,    1.206159e+09,
1.262340e+09,    1.296116e+09,    1.304278e+09],    [1.100273e+09,
1.219206e+09,    1.264256e+09,    1.293154e+09,    1.300060e+09,
1.302237e+09],    [1.076418e+09,    1.132667e+09,    1.209999e+09,
1.265630e+09,    1.298145e+09,    1.306385e+09],    [1.068181e+09,
1.128882e+09,    1.205477e+09,    1.262944e+09,    1.297092e+09,
```

```
1.305280e+09],    [1.071807e+09,    1.130588e+09,    1.209160e+09,
1.266460e+09,    1.298678e+09,    1.306523e+09],    [1.069178e+09,
1.126031e+09,    1.205216e+09,    1.262465e+09,    1.296534e+09,
1.304907e+09],    [1.068220e+09,    1.126730e+09,    1.204759e+09,
1.261016e+09,    1.295961e+09,    1.304086e+09],    [1.067540e+09,
1.126755e+09,    1.205072e+09,    1.262106e+09,    1.296251e+09,
1.303771e+09],    [1.076931e+09,    1.131710e+09,    1.209225e+09,
1.264966e+09,    1.298747e+09,    1.306725e+09],    [1.077855e+09,
1.132410e+09,    1.208930e+09,    1.264610e+09,    1.296352e+09,
1.304097e+09],    [1.067150e+09,    1.127203e+09,    1.205958e+09,
1.263368e+09,    1.296950e+09,    1.305487e+09],    [1.079835e+09,
1.101500e+09,    1.148438e+09,    1.198833e+09,    1.245604e+09,
1.306164e+09],    [1.063388e+09,    1.125567e+09,    1.205064e+09,
1.263687e+09,    1.296321e+09,    1.304799e+09],    [1.077805e+09,
1.132593e+09,    1.208964e+09,    1.265288e+09,    1.296879e+09,
1.306054e+09],    [1.074925e+09,    1.130632e+09,    1.207550e+09,
1.264198e+09,    1.297242e+09,    1.306367e+09],    [1.074518e+09,
1.129978e+09,    1.206081e+09,    1.262644e+09,    1.295854e+09,
1.304013e+09],    [1.068664e+09,    1.126926e+09,    1.205212e+09,
1.263303e+09,    1.296822e+09,    1.308839e+09],    [1.059806e+09,
1.122057e+09,    1.201215e+09,    1.260654e+09,    1.296610e+09,
1.304115e+09],    [1.070212e+09,    1.127132e+09,    1.205250e+09,
1.262506e+09,    1.295932e+09,    1.305361e+09],    [1.065264e+09,
1.125568e+09,    1.203546e+09,    1.261144e+09,    1.295825e+09,
1.304292e+09],    [1.070301e+09,    1.127164e+09,    1.205369e+09,
1.262913e+09,    1.297009e+09,    1.303757e+09],    [1.073996e+09,
1.129917e+09,    1.206592e+09,    1.263582e+09,    1.298159e+09,
1.305448e+09],    [1.070925e+09,    1.127497e+09,    1.205800e+09,
1.262564e+09,    1.295694e+09,    1.304791e+09],    [1.072340e+09,
1.126078e+09,    1.202687e+09,    1.261078e+09,    1.295396e+09,
1.305076e+09],    [1.072083e+09,    1.128636e+09,    1.206528e+09,
1.263245e+09,    1.295548e+09,    1.300611e+09],    [1.069163e+09,
1.126934e+09,    1.202386e+09,    1.259448e+09,    1.294621e+09,
1.303667e+09],    [1.068877e+09,    1.127463e+09,    1.205151e+09,
1.262938e+09,    1.296587e+09,    1.301941e+09],    [1.070894e+09,
1.129025e+09,    1.206878e+09,    1.263478e+09,    1.296460e+09,
1.307578e+09],    [1.071446e+09,    1.128617e+09,    1.205724e+09,
1.262974e+09,    1.296051e+09,    1.302764e+09],    [1.070179e+09,
1.127995e+09,    1.205345e+09,    1.259313e+09,    1.294161e+09,
1.302664e+09],    [1.069021e+09,    1.126622e+09,    1.204453e+09,
1.262525e+09,    1.295366e+09,    1.303646e+09],    [1.073633e+09,
1.130805e+09,    1.208478e+09,    1.264568e+09,    1.297672e+09,
1.306274e+09],    [1.075912e+09,    1.129798e+09,    1.205217e+09,
1.262161e+09,    1.296643e+09,    1.306221e+09],    [1.067735e+09,
1.126342e+09,    1.204726e+09,    1.263085e+09,    1.297033e+09,
1.306660e+09],    [1.081913e+09,    1.102402e+09,    1.149267e+09,
1.197897e+09,    1.243719e+09,    1.303545e+09],    [1.070229e+09,
```

```
1.128909e+09,    1.206475e+09,    1.264601e+09,    1.297904e+09,
1.308174e+09],    [1.071882e+09,    1.128977e+09,    1.206818e+09,
1.264215e+09,    1.297227e+09,    1.306210e+09],    [1.074912e+09,
1.130847e+09,    1.208052e+09,    1.264037e+09,    1.296487e+09,
1.308509e+09],    [1.066472e+09,    1.127328e+09,    1.206005e+09,
1.262683e+09,    1.295769e+09,    1.305149e+09],    [1.072596e+09,
1.128985e+09,    1.206186e+09,    1.263572e+09,    1.296368e+09,
1.304066e+09],    [1.074337e+09,    1.129678e+09,    1.207793e+09,
1.264576e+09,    1.296800e+09,    1.305712e+09],    [1.068376e+09,
1.126129e+09,    1.203089e+09,    1.259607e+09,    1.294809e+09,
1.305347e+09],    [1.068207e+09,    1.128794e+09,    1.207939e+09,
1.265679e+09,    1.298970e+09,    1.307964e+09],    [1.075866e+09,
1.128816e+09,    1.206863e+09,    1.264349e+09,    1.297457e+09,
1.306641e+09],    [1.065228e+09,    1.125735e+09,    1.205676e+09,
1.264674e+09,    1.296593e+09,    1.306480e+09],    [1.067000e+09,
1.126236e+09,    1.203609e+09,    1.261221e+09,    1.295804e+09,
1.307089e+09],    [1.075346e+09,    1.130016e+09,    1.206413e+09,
1.263740e+09,    1.297406e+09,    1.306441e+09],    [1.069614e+09,
1.126359e+09,    1.204215e+09,    1.261368e+09,    1.294163e+09,
1.303930e+09],    [1.064654e+09,    1.124851e+09,    1.203234e+09,
1.262331e+09,    1.298084e+09,    1.303823e+09],    [1.066793e+09,
1.123805e+09,    1.203992e+09,    1.263519e+09,    1.297799e+09,
1.306720e+09],    [1.072305e+09,    1.128544e+09,    1.205966e+09,
1.263645e+09,    1.297129e+09,    1.303851e+09],    [1.063702e+09,
1.126455e+09,    1.205574e+09,    1.262485e+09,    1.294987e+09,
1.302872e+09],    [1.067786e+09,    1.125068e+09,    1.203642e+09,
1.261825e+09,    1.295716e+09,    1.303388e+09],    [1.073262e+09,
1.129924e+09,    1.207553e+09,    1.263861e+09,    1.296926e+09,
1.303281e+09],    [1.065791e+09,    1.127875e+09,    1.206775e+09,
1.264112e+09,    1.298392e+09,    1.310098e+09],    [1.068855e+09,
1.128172e+09,    1.207435e+09,    1.264767e+09,    1.298889e+09,
1.309166e+09],    [1.066493e+09,    1.127115e+09,    1.205687e+09,
1.264291e+09,    1.297225e+09,    1.308481e+09],    [1.066137e+09,
1.127241e+09,    1.204599e+09,    1.262491e+09,    1.295305e+09,
1.303053e+09],    [1.069140e+09,    1.127129e+09,    1.204601e+09,
1.261051e+09,    1.295180e+09,    1.302480e+09],    [1.066109e+09,
1.127762e+09,    1.207187e+09,    1.264944e+09,    1.298760e+09,
1.309258e+09],    [1.070265e+09,    1.130115e+09,    1.208009e+09,
1.263642e+09,    1.297199e+09,    1.305581e+09],    [1.066352e+09,
1.126210e+09,    1.205891e+09,    1.265206e+09,    1.298467e+09,
1.308114e+09],    [1.070084e+09,    1.129067e+09,    1.207903e+09,
1.265294e+09,    1.296999e+09,    1.304574e+09],    [1.066364e+09,
1.127095e+09,    1.204184e+09,    1.261292e+09,    1.297035e+09,
1.305718e+09],    [1.075671e+09,    1.131101e+09,    1.208519e+09,
1.262893e+09,    1.296132e+09,    1.303895e+09],    [1.071400e+09,
1.128816e+09,    1.205116e+09,    1.261126e+09,    1.295958e+09,
1.306442e+09],    [1.072580e+09,    1.127969e+09,    1.204109e+09,
```

```
1.261765e+09,    1.296633e+09,    1.307454e+09],    [1.074873e+09,
1.132753e+09,     1.209145e+09,     1.265212e+09,     1.298189e+09,
1.307078e+09],    [1.067177e+09,    1.125187e+09,     1.205023e+09,
1.262733e+09,    1.296836e+09,    1.306293e+09],    [1.071851e+09,
1.129344e+09,     1.207303e+09,     1.265587e+09,     1.297863e+09,
1.305669e+09],    [1.068710e+09,    1.127676e+09,     1.207190e+09,
1.266576e+09,    1.299771e+09,    1.310213e+09],    [1.067260e+09,
1.125921e+09,     1.204460e+09,     1.261162e+09,     1.295345e+09,
1.304386e+09],    [1.070561e+09,    1.126188e+09,     1.205123e+09,
1.261925e+09,    1.295571e+09,    1.304974e+09],    [1.073102e+09,
1.128764e+09,     1.203790e+09,     1.259794e+09,     1.294277e+09,
1.302834e+09],    [1.076823e+09,    1.133635e+09,     1.211440e+09,
1.265088e+09,    1.298242e+09,    1.308865e+09],    [1.075967e+09,
1.132356e+09,     1.209020e+09,     1.265945e+09,     1.297926e+09,
1.306631e+09],    [1.080114e+09,    1.133459e+09,     1.207689e+09,
1.261862e+09,    1.295957e+09,    1.305169e+09],    [1.080494e+09,
1.134258e+09,     1.209956e+09,     1.263998e+09,     1.298139e+09,
1.307498e+09],    [1.076400e+09,    1.130554e+09,     1.206795e+09,
1.261201e+09,    1.295495e+09,    1.305259e+09],    [1.067005e+09,
1.125618e+09,     1.203552e+09,     1.262072e+09,     1.297002e+09,
1.306606e+09],    [1.072259e+09,    1.129712e+09,     1.207391e+09,
1.263446e+09,    1.297764e+09,    1.305991e+09],    [1.070795e+09,
1.128433e+09,     1.207085e+09,     1.263986e+09,     1.298532e+09,
1.307498e+09],    [1.071518e+09,    1.128197e+09,     1.207039e+09,
1.264463e+09,    1.297171e+09,    1.304920e+09],    [1.071636e+09,
1.127409e+09,     1.205469e+09,     1.263443e+09,     1.296963e+09,
1.305642e+09],    [1.075182e+09,    1.130783e+09,     1.208787e+09,
1.265735e+09,    1.297273e+09,    1.305969e+09],    [1.063762e+09,
1.127271e+09,     1.205588e+09,     1.263284e+09,     1.296956e+09,
1.305253e+09],    [1.092159e+09,    1.158303e+09,     1.213876e+09,
1.259933e+09,    1.290310e+09,    1.301122e+09],    [1.074828e+09,
1.130559e+09,     1.208259e+09,     1.264386e+09,     1.297085e+09,
1.305875e+09],    [1.073530e+09,    1.128655e+09,     1.205032e+09,
1.261897e+09,    1.296374e+09,    1.306054e+09],    [1.080316e+09,
1.132361e+09,     1.207599e+09,     1.262508e+09,     1.295588e+09,
1.304096e+09],    [1.061347e+09,    1.124121e+09,     1.204065e+09,
1.263500e+09,    1.296781e+09,    1.306608e+09],    [1.073423e+09,
1.128559e+09,     1.205646e+09,     1.262663e+09,     1.295190e+09,
1.303830e+09],    [1.073320e+09,    1.128489e+09,     1.206467e+09,
1.262219e+09,    1.297065e+09,    1.308496e+09],    [1.071044e+09,
1.127702e+09,     1.205618e+09,     1.262763e+09,     1.296780e+09,
1.305071e+09],    [1.075746e+09,    1.130095e+09,     1.205748e+09,
1.260957e+09,    1.294838e+09,    1.305897e+09],    [1.068199e+09,
1.126017e+09,     1.205594e+09,     1.263074e+09,     1.296302e+09,
1.306081e+09]]

#============================================================
```

```
#Data from 1mm RVE
    strain=[[0,    1.761166e-03,    6.823666e-03,    1.441742e-02,
2.580804e-02,  3.652430e-02],  [0,  1.737919e-03,  6.800419e-03,
1.439417e-02,  2.578479e-02,  4.247028e-02],  [0,  1.662920e-03,
6.725420e-03,  1.431917e-02,  2.570979e-02,  3.879122e-02],  [0,
1.725197e-03,    6.787697e-03,    1.438145e-02,    2.577207e-02,
4.245756e-02],  [0,  1.698622e-03,  6.761122e-03,  1.435487e-02,
2.574550e-02,  4.243098e-02],  [0,  1.672370e-03,  6.734870e-03,
1.432862e-02,  2.571924e-02,  4.240473e-02],  [0,  1.731560e-03,
6.794060e-03,  1.438781e-02,  2.577843e-02,  4.606799e-02],  [0,
1.682715e-03,    6.745215e-03,    1.433897e-02,    2.572959e-02,
4.241507e-02],  [0,  1.761293e-03,  6.823793e-03,  1.441754e-02,
2.580817e-02,  3.318315e-02],  [0,  1.750996e-03,  6.813496e-03,
1.440725e-02,  2.579787e-02,  4.248336e-02],  [0,  1.740180e-03,
6.802680e-03,  1.439643e-02,  2.578705e-02,  4.607660e-02],  [0,
1.687411e-03,    6.749911e-03,    1.434366e-02,    2.573428e-02,
4.241977e-02],  [0,  1.738184e-03,  6.800684e-03,  1.439443e-02,
2.578506e-02,  4.247054e-02],  [0,  1.710165e-03,  6.772665e-03,
1.436642e-02,  2.575704e-02,  4.244252e-02],  [0,  1.718003e-03,
6.780503e-03,  1.437425e-02,  2.576488e-02,  4.245036e-02],  [0,
1.779940e-03,    6.842440e-03,    1.443619e-02,    2.582681e-02,
4.611637e-02],  [0,  1.721582e-03,  6.784082e-03,  1.437783e-02,
2.576846e-02,  3.348132e-02],  [0,  1.686461e-03,  6.748961e-03,
1.434271e-02,  2.573334e-02,  4.241882e-02],  [0,  5.524212e-04,
2.802421e-03,  6.177420e-03,  1.123992e-02,  3.405779e-02],  [0,
1.665417e-03,    6.727917e-03,    1.432167e-02,    2.571229e-02,
4.239778e-02],  [0,  1.706292e-03,  6.768792e-03,  1.436254e-02,
2.575317e-02,  4.243865e-02],  [0,  1.722013e-03,  6.784513e-03,
1.437826e-02,  2.576889e-02,  4.605844e-02],  [0,  1.713362e-03,
6.775862e-03,  1.436961e-02,  2.576024e-02,  4.244572e-02],  [0,
1.722685e-03,    6.785185e-03,    1.437894e-02,    2.576956e-02,
4.605911e-02],  [0,  5.411196e-04,  2.791120e-03,  6.166119e-03,
1.122862e-02,  3.348335e-02],  [0,  1.694766e-03,  6.757266e-03,
1.435102e-02,  2.574164e-02,  4.242713e-02],  [0,  1.704814e-03,
6.767314e-03,  1.436106e-02,  2.575169e-02,  3.162498e-02],  [0,
1.727260e-03,    6.789760e-03,    1.438351e-02,    2.577413e-02,
4.245962e-02],  [0,  1.693262e-03,  6.755762e-03,  1.434951e-02,
2.574014e-02,  4.602969e-02],  [0,  1.723433e-03,  6.785933e-03,
1.437968e-02,  2.577031e-02,  4.245579e-02],  [0,  1.723433e-03,
6.785933e-03,  1.437968e-02,  2.577031e-02,  4.245579e-02],  [0,
1.744866e-03,    6.807366e-03,    1.440112e-02,    2.579174e-02,
4.247723e-02],  [0,  1.671377e-03,  6.733877e-03,  1.432763e-02,
2.571825e-02,  4.240374e-02],  [0,  1.669931e-03,  6.732431e-03,
1.432618e-02,  2.571680e-02,  3.399281e-02],  [0,  1.710173e-03,
6.772673e-03,  1.436642e-02,  2.575705e-02,  3.883847e-02],  [0,
1.683575e-03,    6.746075e-03,    1.433983e-02,    2.573045e-02,
4.241593e-02],  [0,  1.717667e-03,  6.780167e-03,  1.437392e-02,
```

```
2.576454e-02,  4.245003e-02],  [0,  1.695664e-03,  6.758164e-03,
1.435191e-02,  2.574254e-02,  4.302870e-02],  [0,  1.727323e-03,
6.789823e-03,  1.438357e-02,  2.577420e-02,  4.245968e-02],  [0,
1.745573e-03,    6.808073e-03,    1.440182e-02,    2.579245e-02,
4.247793e-02],  [0,  1.748090e-03,  6.810590e-03,  1.440434e-02,
2.579496e-02,  3.647368e-02],  [0,  1.710370e-03,  6.772870e-03,
1.436662e-02,  2.575724e-02,  4.784883e-02],  [0,  1.715072e-03,
6.777572e-03,  1.437132e-02,  2.576195e-02,  4.244743e-02],  [0,
1.737311e-03,    6.799811e-03,    1.439356e-02,    2.578418e-02,
4.246967e-02],  [0,  1.697187e-03,  6.759687e-03,  1.435344e-02,
2.574406e-02,  4.986293e-02],  [0,  1.701483e-03,  6.763983e-03,
1.435773e-02,  2.574836e-02,  4.243384e-02],  [0,  1.742116e-03,
6.804616e-03,  1.439837e-02,  2.578899e-02,  4.247448e-02],  [0,
1.725293e-03,    6.787793e-03,    1.438154e-02,    2.577217e-02,
4.245765e-02],  [0,  1.731886e-03,  6.794386e-03,  1.438814e-02,
2.577876e-02,  4.246425e-02],  [0,  1.713157e-03,  6.775657e-03,
1.436941e-02,  2.576003e-02,  4.244552e-02],  [0,  1.729985e-03,
6.792485e-03,  1.438624e-02,  2.577686e-02,  3.405286e-02],  [0,
1.704616e-03,    6.767116e-03,    1.436087e-02,    2.575149e-02,
4.243698e-02],  [0,  3.508044e-03,  7.779528e-03,  1.418675e-02,
2.379759e-02,  3.407481e-02],  [0,  1.713045e-03,  6.775545e-03,
1.436930e-02,  2.575992e-02,  4.244540e-02],  [0,  1.732379e-03,
6.794879e-03,  1.438863e-02,  2.577925e-02,  4.246474e-02],  [0,
1.715449e-03,    6.777949e-03,    1.437170e-02,    2.576232e-02,
4.244781e-02],  [0,  1.740082e-03,  6.802582e-03,  1.439633e-02,
2.578696e-02,  3.166025e-02],  [0,  1.667831e-03,  6.730331e-03,
1.432408e-02,  2.571470e-02,  4.240019e-02],  [0,  1.677586e-03,
6.740086e-03,  1.433384e-02,  2.572446e-02,  3.159775e-02],  [0,
1.719998e-03,    6.782498e-03,    1.437625e-02,    2.576687e-02,
4.245236e-02],  [0,  1.700482e-03,  6.762982e-03,  1.435673e-02,
2.574736e-02,  3.312234e-02],  [0,  1.755134e-03,  6.817634e-03,
1.441138e-02,  2.580201e-02,  4.248749e-02],  [0,  1.683311e-03,
6.745811e-03,  1.433956e-02,  2.573018e-02,  4.241567e-02],  [0,
1.715364e-03,    6.777864e-03,    1.437162e-02,    2.576224e-02,
4.244772e-02],  [0,  3.516733e-03,  1.419544e-02,  2.741035e-02,
3.383009e-02,  3.459032e-02],  [0,  1.709430e-03,  6.771930e-03,
1.436568e-02,  2.575630e-02,  3.883773e-02],  [0,  1.737373e-03,
6.799873e-03,  1.439362e-02,  2.578425e-02,  4.246973e-02],  [0,
1.674780e-03,    6.737280e-03,    1.433103e-02,    2.572165e-02,
4.781324e-02],  [0,  1.733597e-03,  6.796097e-03,  1.438985e-02,
2.578047e-02,  3.476039e-02],  [0,  1.736404e-03,  6.798904e-03,
1.439266e-02,  2.578328e-02,  3.648702e-02],  [0,  1.701623e-03,
6.764123e-03,  1.435787e-02,  2.574850e-02,  4.283444e-02],  [0,
1.710968e-03,    6.773468e-03,    1.436722e-02,    2.575784e-02,
4.244333e-02],  [0,  1.698333e-03,  6.760833e-03,  1.435458e-02,
2.574521e-02,  3.644895e-02],  [0,  1.746437e-03,  6.808937e-03,
1.440269e-02,  2.579331e-02,  3.406931e-02],  [0,  1.742870e-03,
```

```
6.805370e-03,  1.439912e-02,  2.578974e-02,  4.607930e-02],  [0,
1.666847e-03,    6.729347e-03,    1.432310e-02,    2.571372e-02,
4.600327e-02],  [0,  1.678780e-03,  6.741280e-03,  1.433503e-02,
2.572565e-02,  4.601520e-02],  [0,  1.731798e-03,  6.794298e-03,
1.438805e-02,  2.577867e-02,  4.246416e-02],  [0,  1.702073e-03,
6.764573e-03,  1.435832e-02,  2.574895e-02,  3.162224e-02],  [0,
1.704396e-03,    6.766896e-03,    1.436065e-02,    2.575127e-02,
3.642998e-02],  [0,  1.728241e-03,  6.790741e-03,  1.438449e-02,
2.577512e-02,  4.246060e-02],  [0,  1.709996e-03,  6.772496e-03,
1.436625e-02,  2.575687e-02,  3.643558e-02],  [0,  1.729651e-03,
6.792151e-03,  1.438590e-02,  2.577653e-02,  3.645524e-02],  [0,
1.706737e-03,    6.769237e-03,    1.436299e-02,    2.575361e-02,
4.243910e-02],  [0,  1.697961e-03,  6.760461e-03,  1.435421e-02,
2.574483e-02,  4.243032e-02],  [0,  1.740257e-03,  6.802757e-03,
1.439651e-02,  2.578713e-02,  4.247262e-02],  [0,  1.707559e-03,
6.770059e-03,  1.436381e-02,  2.575443e-02,  4.243992e-02],  [0,
1.733635e-03,    6.796135e-03,    1.438989e-02,    2.578051e-02,
4.246599e-02],  [0,  1.744788e-03,  6.807288e-03,  1.440104e-02,
2.579166e-02,  4.568076e-02],  [0,  1.696096e-03,  6.758596e-03,
1.435235e-02,  2.574297e-02,  4.242845e-02],  [0,  1.749144e-03,
6.811644e-03,  1.440539e-02,  2.579602e-02,  3.887744e-02],  [0,
1.739137e-03,    6.801637e-03,    1.439539e-02,    2.578601e-02,
3.886743e-02],  [0,  1.699189e-03,  6.761689e-03,  1.435544e-02,
2.574606e-02,  3.312105e-02],  [0,  1.714115e-03,  6.776615e-03,
1.437037e-02,  2.576099e-02,  4.605054e-02],  [0,  1.746859e-03,
6.809359e-03,  1.440311e-02,  2.579373e-02,  3.406973e-02],  [0,
1.740483e-03,    6.802983e-03,    1.439673e-02,    2.578736e-02,
4.247284e-02],  [0,  1.743680e-03,  6.806180e-03,  1.439993e-02,
2.579055e-02,  4.247604e-02],  [0,  1.702280e-03,  6.764780e-03,
1.435853e-02,  2.574915e-02,  3.402515e-02],  [0,  1.700830e-03,
6.763330e-03,  1.435708e-02,  2.574770e-02,  4.243319e-02],  [0,
1.715848e-03,    6.778348e-03,    1.437210e-02,    2.576272e-02,
4.244821e-02]]

    stress=[[1.098650e+09,      1.149262e+09,      1.213196e+09,
1.264330e+09,    1.296292e+09,    1.305258e+09],    [1.094604e+09,
1.147551e+09,    1.212219e+09,    1.263618e+09,    1.295882e+09,
1.305682e+09],    [1.081481e+09,    1.144574e+09,    1.210218e+09,
1.262528e+09,    1.295382e+09,    1.305109e+09],    [1.092506e+09,
1.146870e+09,    1.211944e+09,    1.263520e+09,    1.295799e+09,
1.305413e+09],    [1.088016e+09,    1.145700e+09,    1.211012e+09,
1.262800e+09,    1.295188e+09,    1.305332e+09],    [1.082919e+09,
1.144436e+09,    1.210350e+09,    1.262663e+09,    1.295316e+09,
1.305046e+09],    [1.092980e+09,    1.146594e+09,    1.211704e+09,
1.263461e+09,    1.295711e+09,    1.305344e+09],    [1.084849e+09,
1.144772e+09,    1.210640e+09,    1.262606e+09,    1.295114e+09,
1.305331e+09],    [1.098544e+09,    1.149138e+09,    1.213168e+09,
```

```
1.264130e+09,    1.295975e+09,    1.303945e+09],    [1.096427e+09,
1.148003e+09,     1.212525e+09,     1.263993e+09,     1.296176e+09,
1.305822e+09],    [1.095357e+09,    1.148081e+09,     1.212481e+09,
1.263788e+09,    1.295919e+09,    1.305751e+09],    [1.086443e+09,
1.145717e+09,     1.211050e+09,     1.263140e+09,     1.295578e+09,
1.305642e+09],    [1.095166e+09,    1.148109e+09,     1.212543e+09,
1.263505e+09,    1.295657e+09,    1.305468e+09],    [1.090259e+09,
1.146451e+09,     1.211347e+09,     1.263027e+09,     1.295522e+09,
1.305304e+09],    [1.091096e+09,    1.146298e+09,     1.211445e+09,
1.263083e+09,    1.295435e+09,    1.305471e+09],    [1.101090e+09,
1.149978e+09,     1.213563e+09,     1.264439e+09,     1.296259e+09,
1.305343e+09],    [1.092530e+09,    1.147348e+09,     1.211912e+09,
1.263275e+09,    1.295438e+09,    1.303742e+09],    [1.085868e+09,
1.145258e+09,     1.210918e+09,     1.263255e+09,     1.295774e+09,
1.305364e+09],    [1.108629e+09,    1.129085e+09,     1.162617e+09,
1.207106e+09,    1.244064e+09,    1.304879e+09],    [1.080765e+09,
1.143368e+09,     1.209601e+09,     1.262339e+09,     1.295226e+09,
1.305477e+09],    [1.089771e+09,    1.146466e+09,     1.211506e+09,
1.263234e+09,    1.295692e+09,    1.305551e+09],    [1.092420e+09,
1.147177e+09,     1.212097e+09,     1.263465e+09,     1.295545e+09,
1.305418e+09],    [1.090815e+09,    1.146609e+09,     1.211385e+09,
1.262958e+09,    1.295233e+09,    1.305191e+09],    [1.092899e+09,
1.147596e+09,     1.212073e+09,     1.263303e+09,     1.295610e+09,
1.305364e+09],    [1.108817e+09,    1.129636e+09,     1.163405e+09,
1.207335e+09,    1.244327e+09,    1.304132e+09],    [1.087007e+09,
1.145200e+09,     1.210835e+09,     1.262871e+09,     1.295525e+09,
1.305689e+09],    [1.096269e+09,    1.153508e+09,     1.218542e+09,
1.269726e+09,    1.301592e+09,    1.308697e+09],    [1.093473e+09,
1.147632e+09,     1.212292e+09,     1.263317e+09,     1.295460e+09,
1.305480e+09],    [1.087331e+09,    1.145765e+09,     1.211001e+09,
1.262885e+09,    1.295452e+09,    1.305312e+09],    [1.092226e+09,
1.146796e+09,     1.211815e+09,     1.263567e+09,     1.295791e+09,
1.305432e+09],    [1.092226e+09,    1.146796e+09,     1.211815e+09,
1.263567e+09,    1.295791e+09,    1.305432e+09],    [1.096210e+09,
1.148447e+09,     1.212721e+09,     1.263922e+09,     1.296036e+09,
1.305514e+09],    [1.082760e+09,    1.144437e+09,     1.210257e+09,
1.262435e+09,    1.295099e+09,    1.305342e+09],    [1.089316e+09,
1.151617e+09,     1.217317e+09,     1.269041e+09,     1.301413e+09,
1.309453e+09],    [1.090639e+09,    1.146850e+09,     1.211754e+09,
1.263422e+09,    1.295660e+09,    1.305265e+09],    [1.085976e+09,
1.145825e+09,     1.210946e+09,     1.262930e+09,     1.295620e+09,
1.305556e+09],    [1.091196e+09,    1.146446e+09,     1.211545e+09,
1.263315e+09,    1.295396e+09,    1.305410e+09],    [1.087616e+09,
1.145710e+09,     1.210985e+09,     1.262699e+09,     1.295236e+09,
1.305280e+09],    [1.092830e+09,    1.146949e+09,     1.211905e+09,
1.263574e+09,    1.295944e+09,    1.305622e+09],    [1.096260e+09,
1.148420e+09,     1.212774e+09,     1.263869e+09,     1.295809e+09,
```

```
1.305520e+09],    [1.096707e+09,    1.148611e+09,    1.212695e+09,
1.263765e+09,    1.295799e+09,    1.305221e+09],    [1.090577e+09,
1.146757e+09,    1.211525e+09,    1.262928e+09,    1.295227e+09,
1.305388e+09],    [1.091112e+09,    1.146695e+09,    1.211577e+09,
1.263215e+09,    1.295373e+09,    1.305184e+09],    [1.094168e+09,
1.147165e+09,    1.211789e+09,    1.263203e+09,    1.295531e+09,
1.305596e+09],    [1.088756e+09,    1.146687e+09,    1.211478e+09,
1.262439e+09,    1.294726e+09,    1.305499e+09],    [1.088944e+09,
1.146268e+09,    1.211255e+09,    1.262809e+09,    1.295421e+09,
1.305400e+09],    [1.096144e+09,    1.148686e+09,    1.212923e+09,
1.264058e+09,    1.296031e+09,    1.305520e+09],    [1.092797e+09,
1.147164e+09,    1.212027e+09,    1.263532e+09,    1.295710e+09,
1.305204e+09],    [1.093889e+09,    1.147509e+09,    1.212091e+09,
1.263360e+09,    1.295388e+09,    1.305244e+09],    [1.091089e+09,
1.146924e+09,    1.211735e+09,    1.263193e+09,    1.295427e+09,
1.305494e+09],    [1.092819e+09,    1.146614e+09,    1.211696e+09,
1.263355e+09,    1.295475e+09,    1.304122e+09],    [1.089518e+09,
1.146432e+09,    1.211522e+09,    1.263174e+09,    1.295553e+09,
1.305516e+09],    [1.119970e+09,    1.172055e+09,    1.219302e+09,
1.262675e+09,    1.290890e+09,    1.304551e+09],    [1.090380e+09,
1.146193e+09,    1.211444e+09,    1.263455e+09,    1.295953e+09,
1.305534e+09],    [1.093460e+09,    1.147000e+09,    1.211821e+09,
1.263367e+09,    1.295696e+09,    1.305576e+09],    [1.091755e+09,
1.147322e+09,    1.212099e+09,    1.263158e+09,    1.295308e+09,
1.305742e+09],    [1.103122e+09,    1.156231e+09,    1.220653e+09,
1.271418e+09,    1.302818e+09,    1.309146e+09],    [1.081803e+09,
1.144040e+09,    1.209838e+09,    1.262095e+09,    1.294822e+09,
1.305331e+09],    [1.091497e+09,    1.152623e+09,    1.217923e+09,
1.269440e+09,    1.301490e+09,    1.308226e+09],    [1.092478e+09,
1.147493e+09,    1.212116e+09,    1.263355e+09,    1.295490e+09,
1.305312e+09],    [1.095815e+09,    1.153644e+09,    1.218728e+09,
1.270142e+09,    1.302004e+09,    1.309333e+09],    [1.097258e+09,
1.148431e+09,    1.212869e+09,    1.264270e+09,    1.296273e+09,
1.305684e+09],    [1.085261e+09,    1.145112e+09,    1.210452e+09,
1.262330e+09,    1.294776e+09,    1.305136e+09],    [1.091132e+09,
1.146678e+09,    1.211648e+09,    1.263302e+09,    1.295773e+09,
1.305558e+09],    [1.120409e+09,    1.172054e+09,    1.262559e+09,
1.297883e+09,    1.304436e+09,    1.304529e+09],    [1.091082e+09,
1.147416e+09,    1.211959e+09,    1.263485e+09,    1.295704e+09,
1.305384e+09],    [1.095082e+09,    1.148115e+09,    1.212521e+09,
1.263787e+09,    1.295863e+09,    1.305390e+09],    [1.083730e+09,
1.144887e+09,    1.210495e+09,    1.262542e+09,    1.295092e+09,
1.305467e+09],    [1.093632e+09,    1.147036e+09,    1.211829e+09,
1.263472e+09,    1.295773e+09,    1.304379e+09],    [1.094045e+09,
1.147140e+09,    1.212053e+09,    1.263674e+09,    1.295877e+09,
1.305174e+09],    [1.089023e+09,    1.146332e+09,    1.211148e+09,
1.262601e+09,    1.295009e+09,    1.305242e+09],    [1.091142e+09,
```

```
1.147271e+09,    1.212315e+09,    1.263645e+09,    1.295718e+09,
1.306044e+09],    [1.088202e+09,    1.145938e+09,    1.211276e+09,
1.263219e+09,    1.295630e+09,    1.305344e+09],    [1.096071e+09,
1.148127e+09,    1.212536e+09,    1.263735e+09,    1.295786e+09,
1.303255e+09],    [1.095194e+09,    1.147605e+09,    1.212138e+09,
1.263545e+09,    1.295804e+09,    1.305327e+09],    [1.081920e+09,
1.144337e+09,    1.210101e+09,    1.262344e+09,    1.295217e+09,
1.305619e+09],    [1.084346e+09,    1.144876e+09,    1.210457e+09,
1.262663e+09,    1.295250e+09,    1.304796e+09],    [1.093689e+09,
1.147310e+09,    1.212171e+09,    1.263675e+09,    1.295885e+09,
1.305542e+09],    [1.095761e+09,    1.153360e+09,    1.218572e+09,
1.270193e+09,    1.302245e+09,    1.308916e+09],    [1.089670e+09,
1.146622e+09,    1.211709e+09,    1.263290e+09,    1.295654e+09,
1.305156e+09],    [1.093084e+09,    1.147103e+09,    1.212075e+09,
1.263742e+09,    1.296035e+09,    1.305544e+09],    [1.090325e+09,
1.146543e+09,    1.211392e+09,    1.262897e+09,    1.295285e+09,
1.305118e+09],    [1.093944e+09,    1.147835e+09,    1.212235e+09,
1.263023e+09,    1.295110e+09,    1.305260e+09],    [1.089488e+09,
1.146106e+09,    1.211150e+09,    1.263143e+09,    1.295724e+09,
1.305476e+09],    [1.088398e+09,    1.146198e+09,    1.211099e+09,
1.262945e+09,    1.295412e+09,    1.305398e+09],    [1.095006e+09,
1.147704e+09,    1.212312e+09,    1.263808e+09,    1.295886e+09,
1.305344e+09],    [1.089309e+09,    1.145806e+09,    1.211212e+09,
1.263168e+09,    1.295469e+09,    1.305304e+09],    [1.094253e+09,
1.147683e+09,    1.212269e+09,    1.263378e+09,    1.295329e+09,
1.305162e+09],    [1.096337e+09,    1.148589e+09,    1.212824e+09,
1.263874e+09,    1.295996e+09,    1.305558e+09],    [1.087878e+09,
1.145923e+09,    1.211106e+09,    1.262563e+09,    1.294987e+09,
1.305176e+09],    [1.096171e+09,    1.147935e+09,    1.212528e+09,
1.263809e+09,    1.295868e+09,    1.305420e+09],    [1.095352e+09,
1.148195e+09,    1.212641e+09,    1.263823e+09,    1.295919e+09,
1.305414e+09],    [1.087959e+09,    1.145559e+09,    1.211194e+09,
1.263190e+09,    1.295498e+09,    1.303797e+09],    [1.091041e+09,
1.146746e+09,    1.211666e+09,    1.263095e+09,    1.295174e+09,
1.305611e+09],    [1.096203e+09,    1.148219e+09,    1.212621e+09,
1.263924e+09,    1.296009e+09,    1.304100e+09],    [1.095071e+09,
1.147746e+09,    1.212448e+09,    1.263800e+09,    1.295930e+09,
1.305385e+09],    [1.096091e+09,    1.148455e+09,    1.212682e+09,
1.263656e+09,    1.295799e+09,    1.305373e+09],    [1.088526e+09,
1.145715e+09,    1.211101e+09,    1.262725e+09,    1.295184e+09,
1.303701e+09],    [1.089058e+09,    1.146481e+09,    1.211645e+09,
1.263077e+09,    1.294962e+09,    1.305200e+09],    [1.091180e+09,
1.146666e+09,    1.211463e+09,    1.262859e+09,    1.295207e+09,
1.305485e+09]]

#============================================================
```

```
    w = random.randint(0,99)

    mdb.models['Model-%d'%(qq)].Material(name='Steel')
    mdb.models['Model-
%d'%(qq)].materials['Steel'].Elastic(table=((EE,0.3), ))

    #mdb.models['Model-
%d'%(qq)].materials['Steel'].Plastic(table=((stress[w][0],
strain[w][0]),(stress[w][1], strain[w][1])))

    #mdb.models['Model-
%d'%(qq)].materials['Steel'].Plastic(table=((stress[w][0],
strain[w][0]),(stress[w][1],         strain[w][1]),(stress[w][2],
strain[w][2]),(stress[w][3],    strain[w][3]),    (stress[w][4],
strain[w][4]),   (stress[w][5],   strain[w][5]),   (stress[w][6],
strain[w][6]),   (stress[w][7],   strain[w][7]),   (stress[w][8],
strain[w][8]), (stress[w][9], strain[w][9])))


    mdb.models['Model-
%d'%(qq)].materials['Steel'].Plastic(table=((stress[w][0],
strain[w][0]),(stress[w][1],         strain[w][1]),(stress[w][2],
strain[w][2]),(stress[w][3],    strain[w][3]),    (stress[w][4],
strain[w][4]), (stress[w][5], strain[w][5])))

    mdb.models['Model-
%d'%(qq)].HomogeneousSolidSection(name='Matrix',material='Steel'
, thickness=None)

#============================================================
 #Assign material property
    p = mdb.models['Model-%d'%(qq)].parts['Part-1']
    f = p.faces
    faces = f.findAt((0,0,0))
    q=faces.index
    Fac = f[q:q+1]
    region = p.Set(faces=Fac, name='Set-Matrix')
    p = mdb.models['Model-%d'%(qq)].parts['Part-1']
    p.SectionAssignment(region=region,      sectionName='Matrix',
offset=0.0,      offsetType=MIDDLE_SURFACE,      offsetField='',
thicknessAssignment=FROM_SECTION)

#============================================================
    #Assembly
    a = mdb.models['Model-%d'%(qq)].rootAssembly
    p = mdb.models['Model-%d'%(qq)].parts['Part-1']
    a.Instance(name='Part-1-%d'%(qq), part=p, dependent=OFF)
```

```
#==========================================================
    #Step
    mdb.models['Model-%d'%(qq)].StaticStep(name='Step-1',
previous='Initial', maxNumInc=2000, minInc=1e-20, nlgeom=ON)

    mdb.models['Model-%d'%(qq)].steps['Step-
1'].setValues(stabilizationMagnitude=0.0002,
stabilizationMethod=DISSIPATED_ENERGY_FRACTION,
continueDampingFactors=False,          adaptiveDampingRatio=0.05,
initialInc=0.01, matrixSolver=DIRECT, matrixStorage=UNSYMMETRIC)

#==========================================================
    #Mesh

    a = mdb.models['Model-%d'%(qq)].rootAssembly
    v1 = a.instances['Part-1-%d'%(qq)].vertices
    verts1      =      v1.findAt(((0,0,0),),      ((RVE_L,0,0),),
((0,RVE_W,0),), ((RVE_L,RVE_W,0),) )
    a.Set(vertices=verts1, name='Corners')


    a = mdb.models['Model-%d'%(qq)].rootAssembly
    e = a.instances['Part-1-%d'%(qq)].edges

    EdgeUp=e.findAt ((RVE_L/2.0,RVE_W,0.0))
    EdgeDo=e.findAt((RVE_L/2.0,0.0,0.0))
    EdgeRi=e.findAt((RVE_L,RVE_W/2.0,0.0))
    EdgeLe=e.findAt((0.0,RVE_W/2.0,0.0))

    q1 = EdgeUp.index
    q2 = EdgeDo.index
    q3 = EdgeRi.index
    q4 = EdgeLe.index

    EdUp = e[q1:q1+1]
    EdDo = e[q2:q2+1]
    EdRi = e[q3:q3+1]
    EdLe = e[q4:q4+1]

    a.Set(edges=EdUp, name='Up')
    a.Set(edges=EdDo, name='Down')
    a.Set(edges=EdRi, name='Right')
    a.Set(edges=EdLe, name='Left')

#==========================================================
    #Seed edges
```

```
    # Global Seed
    a = mdb.models['Model-%d'%(qq)].rootAssembly
    p = a.instances['Part-1-%d'%(qq)]
    session.viewports['Viewport: 1'].setValues(displayedObject=a)
    session.viewports['Viewport:
1'].assemblyDisplay.setValues(mesh=OFF)
    session.viewports['Viewport:
1'].assemblyDisplay.meshOptions.setValues(meshTechnique=OFF)
    session.viewports['Viewport: 1'].view.fitView()
    session.viewports['Viewport:
1'].assemblyDisplay.setValues(mesh=ON)
    session.viewports['Viewport:
1'].assemblyDisplay.meshOptions.setValues(meshTechnique=ON)

    EdgeMeshSize = avsize/2.0
    NumMeshRi = int (RVE_L/EdgeMeshSize)
    NumMeshUp = int (RVE_W/EdgeMeshSize)

    a.seedEdgeByNumber       (edges=EdRi,       number=NumMeshRi,
constraint=FIXED)
    a.seedEdgeByNumber       (edges=EdLe,       number=NumMeshRi,
constraint=FIXED)
    a.seedEdgeByNumber       (edges=EdUp,       number=NumMeshUp,
constraint=FIXED)
    a.seedEdgeByNumber       (edges=EdDo,       number=NumMeshUp,
constraint=FIXED)

    a = mdb.models['Model-%d'%(qq)].rootAssembly
    partInstances =(a.instances['Part-1-%d'%(qq)],)
    a.seedPartInstance(regions=partInstances,
size=avsize/seedfac, deviationFactor=0.1, minSizeFactor=0.1)

    elemType1           =           mesh.ElemType(elemCode=CPS4R,
elemLibrary=STANDARD,                    secondOrderAccuracy=OFF,
hourglassControl=ENHANCED, distortionControl=DEFAULT)

    elemType2           =            mesh.ElemType(elemCode=CPS3,
elemLibrary=STANDARD)

    a = mdb.models['Model-%d'%(qq)].rootAssembly
    f = a.instances['Part-1-%d'%(qq)].faces
    pickedRegions =(f, )
    a.setElementType(regions=pickedRegions, elemTypes=(elemType1,
elemType2))
```

```
    a = mdb.models['Model-%d'%(qq)].rootAssembly
    f1 = a.instances['Part-1-%d'%(qq)].faces
    pickedRegions = f1.getSequenceFromMask(mask=('[#1 ]', ), )
    a.setMeshControls(regions=pickedRegions, elemShape=TRI)


    a = mdb.models['Model-%d'%(qq)].rootAssembly
    partInstances =(a.instances['Part-1-%d'%(qq)], )
    a.generateMesh(regions=partInstances)

    session.viewports['Viewport: 1'].view.fitView()

#=======================================================
    # Finding the faces in the matrix
    #Storing the nodes of faces


    Upnodes = a.sets['Up'].nodes
    Downnodes = a.sets['Down'].nodes
    Rightnodes = a.sets['Right'].nodes
    Leftnodes = a.sets['Left'].nodes

    #Storing the coordinates and label of faces nodes
    UpCoord = []
    DownCoord = []
    RightCoord = []
    LeftCoord = []

    for node in Upnodes:
     UpCoord               =               UpCoord              +
[[node.coordinates[0],node.coordinates[1],node.label]]

    for node in Downnodes:
     DownCoord             =             DownCoord              +
[[node.coordinates[0],node.coordinates[1],node.label]]

    for node in Rightnodes:
     RightCoord            =            RightCoord              +
[[node.coordinates[0],node.coordinates[1],node.label]]

    for node in Leftnodes:
     LeftCoord             =             LeftCoord              +
[[node.coordinates[0],node.coordinates[1],node.label]]

    UpCoord.sort()
    DownCoord.sort()
    RightCoord.sort()
```

```
    LeftCoord.sort()

    #Degining sets for Up and Bottom faces
    NumUp = len(UpCoord)
    Node_Tol = 2
    for i in range(0,NumUp):
     if (abs(UpCoord[i][0]-DownCoord[i][0])<Node_Tol):

          NLable = DownCoord[i][2]
          a.Set(nodes=p.nodes[NLable-1:NLable],  name='DownNode_'
+str(i))
          NLable = UpCoord[i][2]
          a.Set(nodes=p.nodes[NLable-1:NLable],    name='UpNode_'
+str(i))
     else:
          print 'Distance between nodes are more than Tolerance'

    #Degining sets for Right and Left faces

    NumRi = len(RightCoord)
    for i in range(0,NumRi):
     if (abs(RightCoord[i][1]-LeftCoord[i][1])<Node_Tol):

          NLable = RightCoord[i][2]
          a.Set(nodes=p.nodes[NLable-1:NLable],
name='RightNode_'+str(i))
          NLable = LeftCoord[i][2]
          a.Set(nodes=p.nodes[NLable-1:NLable],  name='LeftNode_'
+str(i))
     else:
          print 'Distance between nodes are more than Tolerance'



#=======================================================
    #Defining constraints
    #Right and Left


    for i in range(1,NumRi):
     mdb.models['Model-%d'%(qq)].Equation(name='Const-LeRi-
x'+str(i),               terms=((-1.0,'LeftNode_'+str(i),1),(1.0,
'RightNode_'+str(i), 1), (-1.0, 'RightNode_0', 1)))

    for i in range(1,NumRi):
```

```
     mdb.models['Model-%d'%(qq)].Equation(name='Const-LeRi-
y'+str(i),                terms=((1.0,'LeftNode_'+str(i),2),(-1.0,
'RightNode_'+str(i), 2)))

    #Up and Down
    for i in range(1,NumUp-1):
     mdb.models['Model-%d'%(qq)].Equation(name='Const-UpDown-
y'+str(i),                terms=((-1.0,'DownNode_'+str(i),2),(1.0,
'UpNode_'+str(i), 2),(-1.0, 'UpNode_0', 2)))

    for i in range(1,NumUp-1):
     mdb.models['Model-%d'%(qq)].Equation(name='Const-UpDown-
x'+str(i),                terms=((1.0,'DownNode_'+str(i),1),(-1.0,
'UpNode_'+str(i), 1)))
#=============================================================
    #Load
    #Fix Left Bottom corner along x and y
    a = mdb.models['Model-%d'%(qq)].rootAssembly
    v = a.instances['Part-1-%d'%(qq)].vertices
    ver = v.findAt((0.0,0.0,0.0))
    q = ver.index
    Fixver = v[q:q+1]
    region = a.Set(vertices=Fixver, name='Set-Fix')
    mdb.models['Model-%d'%(qq)].PinnedBC(name='Fix',
createStepName='Initial', region=region, localCsys=None)

    #Fix Left Up corner along x direction
    ver = v.findAt((0.0,RVE_W,0.0))
    q = ver.index
    Movever = v[q:q+1]
    region = a.Set(vertices=Movever, name='LeftX')
    mdb.models['Model-%d'%(qq)].DisplacementBC(name='LeftX',
createStepName='Step-1',    region=region,    u1=0.0,    u2=UNSET,
ur3=UNSET, amplitude=UNSET, fixed=OFF, distributionType=UNIFORM,
fieldName='', localCsys=None)

    #Fix Right Bottom corner along y direction
    ver = v.findAt((RVE_L,0.0,0.0))
    q = ver.index
    Movever = v[q:q+1]
    region = a.Set(vertices=Movever, name='Set-Move')
    mdb.models['Model-%d'%(qq)].DisplacementBC(name='Set-Move',
createStepName='Step-1', region=region, u1=disfac*RVE_L, u2=0.0,
ur3=UNSET, amplitude=UNSET, fixed=OFF, distributionType=UNIFORM,
fieldName='', localCsys=None)

#=============================================================
```

```
    #History Output

    regionDef=mdb.models['Model-
%d'%(qq)].rootAssembly.sets['Corners']
    mdb.models['Model-%d'%(qq)].HistoryOutputRequest(name='H-
Output-2',
        createStepName='Step-1', variables=('RF1', 'RF2', 'U1',
'U2', 'COOR1',
        'COOR2',           'NFORC'),           region=regionDef,
sectionPoints=DEFAULT,
        rebar=EXCLUDE)

    #mdb.models['Model-%d'%(qq)].FieldOutputRequest(name='F-
Output-1',
      #  createStepName='Step-1', variables=('NFORC', ))


#=========================================================
    #JOB
    mdb.Job(name='RVE--Tension_%d'%(qq),   model='Model-%d'%(qq),
description='',   type=ANALYSIS,   atTime=None,   waitMinutes=0,
waitHours=0,   queue=None,   memory=90,   memoryUnits=PERCENTAGE,
getMemoryFromAnalysis=True,             explicitPrecision=SINGLE,
nodalOutputPrecision=SINGLE,    echoPrint=OFF,    modelPrint=OFF,
contactPrint=OFF,      historyPrint=OFF,      userSubroutine='',
scratch='',    resultsFormat=ODB,    multiprocessingMode=DEFAULT,
numCpus=1, numGPUs=0)
#=========================================================
    #SUBMIT JOB
    mdb.jobs['RVE--Tension_%d' %(qq)].writeInput()
    mdb.jobs['RVE--Tension_%d'
%(qq)].submit(consistencyChecking=OFF)
    mdb.jobs['RVE--Tension_%d' %(qq)].waitForCompletion()

    session.mdbData.summary()
    o3        =        session.openOdb(name='C:/Users/dg033/RVE--
Tension_%d.odb'%(qq))
    session.viewports['Viewport:
1'].setValues(displayedObject=o3)
    odb    =    session.odbs['C:/Users/dg033/RVE--Tension_%d.odb'
%(qq)]

#=========================================================

  #INFO OF VOIDS

    #print("Model # ", qq)
```

```
    #print("Volume Fraction = ", Vc)
    #print("Number of Voids",len(D))
    volu_frac[qq] = Vc
    num_voids[qq] = len(D)
    avdia[qq] = sum(D_list)/len(D_list)
    #for i in range (1,len(D)+1):
     #print ()
     #print("Void #",i)
     #print("Diameter = ", D[i])
     #print("Area = ", 3.14159*(D[i]**2)/4)
     #print("X-coordinate = ", x_coordinate[i])
     #print("Y-Coordinate = ", y_coordinate[i])

for i in range (1, qq+1):
     print ()
     print 'Model', i
     print 'Number of Voids =', num_voids[i]
     print 'Average Diameter =', avdia[i]
     print 'Volume Fraction', volu_frac[i]
```

Appendix D: Matlab code for property upscaling simulation post-processing

This appendix is the Matlab code used to obtain the yield stress, ultimate tensile stress, and plasticity data from the result of the property upscaling simulation. The code extracts the strain and tensile stress from an excel file where each excel sheet contains the result of 10 simulations arranged in two columns (strain and stress) per run and then one column in blank (from column A up to column AC). After the data is extracted, the code organizes it in vectors and calculates the Young Modulus to estimate the Yield stress and strain. To store the plasticity data, as an input for Abaqus, the index of the UTS is obtained and then 5 points were taken between the Yield stress and UTS. At last, the code exports a text file with the plasticity data to be used as input in Abaqus.

```
clc, close all, clear all
%Process Data from Abaqus
%Code import data from excel
%Convert data from Engineering to True Stress/Strain
%Calculate Elastic Modulus
%Calculate Yield stress
maindir='C:\Users\dg033.GACL.001\Desktop\upscaled_data_10       microns(RVE       (1
um_experimental_data)\100 um RVE_Data fro 10 um RVE_abaqus';

%% Initialize Variables
rr = 100; %number of data exported to txt file
s1=zeros(1,100);
p=1;
r=1;
ss=1;
y1=zeros(71,100);
x1=zeros(71,100);
UTS=zeros(1,100);
E = zeros(1,100);
sy=zeros(1,100);
xp = zeros(6,100);
yp = zeros (6,100);
pp = zeros(1,100);
index = zeros(1,100);
x2= zeros(6,100);
y2=zeros (6,100);
xr=zeros(1,100);
xpp=zeros(6,100);
si=zeros(1,100);
sx=zeros(1,100);
sy=zeros(1,100);
%%
```

```
while r < 12
    if r==11;
        p=p+1;
        r=1;
    end
    if p > 10
        break
    end

    switch r
        case 1
        rx = 'A1:A2000';
        ry = 'B1:B2000';

        case 2
        rx = 'D1:D2000';
        ry = 'E1:E2000';

        case 3
        rx = 'G1:G2000';
        ry = 'H1:H2000';

        case 4
        rx = 'J1:J2000';
        ry = 'K1:K2000';

        case 5
        rx = 'M1:M2000';
        ry = 'N1:N2000';

        case 6
        rx = 'P1:P2000';
        ry = 'Q1:Q2000';

        case 7
        rx = 'S1:S2000';
        ry = 'T1:T2000';

        case 8
        rx = 'V1:V2000';
        ry = 'W1:W2000';

        case 9
        rx = 'Y1:Y2000';
        ry = 'Z1:Z2000';

        case 10
        rx = 'AB1:AB2000';
        ry = 'AC1:AC2000';
    end
%% Reads excel File
    x = xlsread('100 um RVE from 10 um RVE data.xlsx',p,rx);
    y = xlsread('100 um RVE from 10 um RVE data.xlsx',p,ry);

%% Stores Strain and Stress in a Matrix
```

```
    nn=size(x);
    for n =1:nn(1)
          x1(n,ss)=x(n);
          y1(n,ss)=y(n);
    end

%% Calculate Modulus of Elasticity

    E(ss)= (y1(4,ss)-y1(2,ss))/(x1(4,ss)-x1(2,ss));

%% Calculate Yield slope
    for n =1:6
        x2(n,ss)=x1(n,ss)+.002;
        y2(n,ss)=E(ss)*x1(n,ss);
    end
    if y2(6,ss)< y1(7,ss)
        x2(5,ss)=x1(7,ss)+.002;
        y2(5,ss)=E(ss)*x1(7,ss);
        x2(6,ss)=x1(8,ss)+.002;
        y2(6,ss)=E(ss)*x1(8,ss);
    end

%% Interpolate Yield Stress based on X position of Yield

D=0;
DN=0;
while D < y2(5,ss)
    D = y1(6+DN,ss);
    DN=DN+1;
end
DDN=0;
DD=0;
while DD < x2(5,ss)
   DD = x1(5+DDN,ss);
   DDN=DDN+1;
end

if DN > 2
   si(ss)=(((y1(6+DN-1,ss)-y1(5+DDN-2,ss))/(x1(6+DN-1,ss)-x1(5+DDN-2,ss)))*(x2(5,ss)-
x1(5+DDN-2,ss)))+y1(5+DDN-2,ss);
   sy(ss)=si(ss)-si(ss)*.01;
   sx(ss)=(((sy(ss)-y1(5+DDN-2,ss))*(x2(5,ss)-x1(5+DDN-2,ss)))/(si(ss)-y1(5+DDN-
2,ss)))+x1(5+DDN-2,ss);
else
   si(ss)=(((y1(6+DN-1,ss)-y1(5,ss))/(x1(6+DN-1,ss)-x1(5,ss)))*(x2(5,ss)-
x1(5,ss)))+y1(5,ss);
   sy(ss)=si(ss)-si(ss)*.01;
   sx(ss)=(((sy(ss)-y1(5,ss))*(x2(5,ss)-x1(5,ss)))/(si(ss)-y1(5,ss)))+x1(5,ss);
end

%% Obtain UTS
   UTS(ss)=max(y1(:,ss));

%% Find index of UTS
   [stress, index(ss)]=max(y1(:,ss));
```

```
%% Plasticity data list
   xp(1,ss) = sx(ss);
   xr(1,ss)= sx(ss);
   yp(1,ss) = sy(ss);
   pp(ss)= (index(ss) - 5)/6;
   i=floor(pp(ss));
   xp(2,ss) = x1(6+DN-1,ss);
   yp(2,ss) = y1(6+DN-1,ss);
   for n =1:3
       xp(2+n,ss)=x1(6+(DN-1)+n*i,ss);
       yp(2+n,ss)=y1(6+(DN-1)+n*i,ss);
   end
   xp(6,ss) = x1(index(ss),ss);
   yp(6,ss) = y1(index(ss),ss);

   for n =1:6
       xpp(n,ss)=xp(n,ss)-xr(1,ss);
   end
%% Counters
ss=ss+1;
 r=r+1;
end

%%Export text-file
yp=yp/1000;
plasticity_data = fopen('plasticity2.txt','w');
dd='strain=[';
fprintf(plasticity_data,'%c',dd)
for n=1:rr
%     j=randi(100);
    j=n;
    l(n)=j;
    dd='[0, ';
    fprintf(plasticity_data,'%c',dd)
    for nn=2:6
        ii=xpp(nn,j);
        fprintf(plasticity_data,'%c',ii);
        if nn == 6
            continue
        end
        dd=', ';
        fprintf(plasticity_data,'%c',dd);
    end
    if n == rr

        continue
    end
        dd='], ';
        fprintf(plasticity_data,'%c',dd);
end
dd=']]';
fprintf(plasticity_data,'%c',dd)
es='';
fprintf(plasticity_data,'%f\n\n',es)
```

```
dd='stress=[';
fprintf(plasticity_data,'%c',dd)
for n=1:rr
    dd='[';
    fprintf(plasticity_data,'%c',dd)
    for nn=1:6
        ii=yp(nn,n)*10^9;
        fprintf(plasticity_data,'%c',ii);
        if nn == 6
            continue
        end
        dd=', ';
        fprintf(plasticity_data,'%c',dd);
    end

    if n == rr
        dd=']';
        fprintf(plasticity_data,'%c',dd);
        continue

    end
        dd='], ';
        fprintf(plasticity_data,'%c',dd);
end
        dd='] ';
        fprintf(plasticity_data,'%c',dd);
```